Università degli Studi di Ferrara

DOCTORAL COURSE IN ENGINEERING SCIENCE

CYCLE XXXV

Director Prof. Stefano Trillo

Development of analytical-numerical methods for dynamic analysis of geared transmission systems

Scientific/Disciplinary Sector ING-IND/13

Candidate
Dott. Francesco Pizzolante

Supervisor
Prof. Emiliano Mucchi

Years 2019/2022

*A **Mamma e Papà**, per avermi permesso di realizzare i miei sogni*

ABSTRACT

The main objective of the present research activity is the study of geared transmission system dynamics, which is basically represented by a system of nonlinear differential equations. First of all, the different approaches to study the nonlinear dynamics of gears are qualitatively presented. Afterwards, the realization of a lumped parameter model is discussed by analyzing two different modeling strategies linked to two different numerical resolution techniques.

The first modeling strategy is based on time integration techniques and enhances the employment of a commercial software to speed-up the modeling set-up phase. The proposed method rely on a block diagram technique and it is developed in Simcenter AMESim, a commercial software widely used in industries. By starting from the single gear pair model, detailed guidelines are given to construct any type of ordinary transmission layout by connecting some pre-programmed devices between them. In order to demonstrate the reliability of the approach, an experimental validation on industrial use case is proposed with excellent outcomes.

The second modeling strategy rely on a frequency domain solution technique able to capture unstable solution branches in multi-valued frequency response regions. In particular, it proposes the Asymptotic Numerical Method combined to the Harmonic Balance Method as a valuable approach to solve the nonlinear dynamics of gear pairs. Thanks to a quadratic recast of the equation of motion, the Taylor and Fourier series can be computed in a very efficient way and each step produces a continuous representation of the solution branch making the continuation very robust. Effectiveness and reliability of the method are proved by comparing the numerical outcomes with that obtained from the Runge-Kutta time integration scheme. As a result, this technique provides for excellent computational performance despite additional time is needed for the quadratic recast of the equations system.

Once a detailed analysis on the modeling strategy has been conducted, rattle noise and whine noise occurrence are investigated.

Regarding the rattle noise, the research activity has conducted to the introduction of a new analytical parameter as a novelty to the current state of the art. A rattle index formulation is retrieved by starting from the classical 6-DOFs equation system defining

the nonlinear dynamics of a gear pair. The proposed formulation may be applied to single or multiple branch geartrain, both in idle or loaded condions. The reliability of the analytical formulation is proved by numerical experiments which demonstrate the capability of the proposed index to instantaneously describe the vibro-impacts events related to any gear pair of the driveline. In addition its magnitude may be a measure of the tooth impact severity and it is shown to be a proper indicator of the potential presence of mutual interactions between different gear pairs pertaining to the same driveline.

Finally, the investigation of whine noise occurrence addresses to an analytical formulation able to forecast the main overall direction and magnitude of bearing reaction forces on idler gear. By starting from the definition of meshing forces by means of Fourier series development, idler gear bearing forces are obtained under the hypothesis of quasi-static motion. This procedure demonstrates that the alternating component of bearing forces on idler gear describes an elliptical trajectory as the prime mover rotates over a pitch angle. The formulation directly links the bearing forces elliptical trajectory with the gear spatial position, the meshing phase and the amplitude of meshing forces. By properly setting the over-mentioned parameters one may be able to control the magnitude and direction of the overall idler bearing reaction forces. Numerical experiments were performed and the obtained results confirm the author intuition.

PREFACE

I graduated in Mechanical Engineering at the University of Ferrara in February 2019. During the last year of my Master's degree, I took part to the Double Degree exchange program with the Aix-Marseille Université where I received an additional Master in Mechanical Physical Engineering. After graduation, I worked as a research fellow at the University of Ferrara, Engineering Department with the Mechanics and Vibration Research Group. During this period, I worked on geartrain modeling based on a lumped parameter approach. In November 2019 I started my PhD program with the same research group.

My research activity deals with tools development for dynamic analysis of complex mechanical systems with a particular emphasis on power transmission. During the first year of my PhD program, I developed an effective tool to realize a nonlinear lumped parameter model of any ordinary transmission layout. The project was conducted in Simcenter AMESim environment. The tool has been used to study various driveline phenomena on real test case proposed by different companies. In this regard, a numerical vibro-acoustic methodology for the estimation of the overall vibratory and acoustic level of a gearbox employed on agricultural equipment has been presented to an international conference [1]:

[1] A. Gabrielli, F. Pizzolante, E. Soave, M. Battarra, C. Mazzeo, M. Tarabra, E. Fava, and E. Mucchi. "A numerical model for NVH analysis of gearboxes employed on agricultural equipment." In: *Proceedings of ISMA 2020 - International Conference on Noise and Vibration Engineering*. 2020.

During my second doctoral year, I kept working on geartrain dynamics by focusing the attention on gear rattle noise. The research activity has led to the introduction of a new parameter as a novelty to the current state of the art. The results were published on a relevant journal paper [2]:

[2] Francesco Pizzolante, Mattia Battarra, Gianluca D'Elia, and Emiliano Mucchi. "A rattle index formulation for single and multiple branch geartrains." In: *Mechanism and Machine Theory* 158 (2021).

Beside the gear dynamics I have worked on a lumped parameter model to describe the pressure dynamics of an axial piston pump. The numerical results were correlated with the experimental outcomes obtaining an high quality tool to forecast pressure ripple dynamics.

In addition, I focused on the study of friction condition in packaging industrial machinery. Within the framework of BI-REX project, I worked with the AETNA group in order to implement an algorithm able to analyze the wear condition of an industrial shrinkwrapper machine with a view to predictive maintenance.

In the first half of my third year, the main research activity has focused on gear whine noise control. This study have conducted to an analytical formulation able to forecast the main overall direction and magnitude of bearing reaction forces on idler gear when the geartrain works under quasi-static condition. The work has been published on a relevant journal [3] :

[3] Francesco Pizzolante, Mattia Battarra, and Emiliano Mucchi. "The role of gear layout and meshing phase for whine noise reduction in ordinary geartrains." In: *Mechanism and Machine Theory* (2022).

During the last part of my PhD, I spent six months at the Laboratory of Mechanics and Acoustic (LMA), a research unit of CNRS (Centre National de Recherche Scientifique) based in Marseille (France), where the development of new mathematical methods for engineering are coming to the fore. Under the supervision of Professor Bruno Cochelin, I applied a frequency domain numerical method for the resolution of nonlinear differential equations to the complex problem of geared system dynamics. This abroad experience, gave me the opportunity to deepen my knowledge on the resolution methods for nonlinear dynamic systems. In fact, bifurcations and unstable regions are not captured from resolution methods based on time integration scheme. The outcomes of this activity have been detailed in a scientific paper which is submitted for publication on a significant journal [4]:

[4] Francesco Pizzolante, Mattia Battarra, Emiliano Mucchi, and Bruno Cochelin. "A Taylor series-based continuation method for solution of non linear dynamics of spur gears." In: *Submitted to Mechanical System and Signal Processing* (2022).

This brief summary of the activities I committed during this last three years, leads me to express my appreciation and gratitude to all the people from the Mechanical and Vibration research group. Firstly, I would like to address

my sincere appreciation to my advisor, Professor Emiliano Mucchi, for the scientific technical support and its wise advice. Moreover, my sincere gratitude goes to Eng. Mattia Battarra, for the constant support, advice and lessons he gave me through the entire course of the PhD. A special thanks to Eng. Gianluca D'Elia, who made me passionate about engineering when I was a student. Finally, I thank Professor Giorgio Dalpiaz for the precious time he dedicated to me.

CONTENTS

LIST OF FIGURES

LIST OF TABLES

NOMENCLATURE

Latin symbols

a	parameter related to meshing forces amplitudes, phase shift Γ and mounting angle α
$\hat{a}$	real coefficient of x^2 term to define a generic conic section
$\hat{A}$	amplitude of acceleration excitation $\ddot{\theta}_p$
A_n	amplitude of the $n-th$ harmonic of meshing force $1-2$
b	parameter related to meshing force $2-3$ amplitude, phase shift Γ and mounting angle α
$\hat{b}$	real coefficient of xy term to define a generic conic section
$\hat{B}$	amplitude of external torque T_{e2}
B_n	amplitude of the $n-th$ harmonic of meshing force $2-3$
c	parameter related to meshing forces amplitudes, phase shift Γ and mounting angle α
C	amplitude of external torque T_{e10} and T_{e7}
$\hat{C}$	Rayleigh's overall proportional damping
$\hat{c}$	real coefficient of y^2 term to define a generic conic section
c_b	bearing damping coefficient
c_c	integral gain of controller
c_m	meshing damping coefficient
c_t	torsional spring damping coefficient

d	parameter related to meshing force $2-3$ amplitude, phase shift Γ and mounting angle α
$\hat{d}$	real coefficient of x term to define a generic conic section
$\hat{e}$	real coefficient of y term to define a generic conic section
$\hat{f}$	real coefficient to define a generic conic section
f_a	frequency of acceleration excitation $\ddot{\theta}_p$
F	dimensionless average force
F_e	external forces
f_{nl}	nonlinear contact function
$f_b^{x_i}$	bearing reaction force related to gear i along x direction
$f_b^{y_i}$	bearing reaction force related to gear i along y direction
$f_m^{x_i}$	gear mesh force related to gear i along x direction
$f_m^{y_i}$	gear mesh force related to gear i along y direction
$f_{m_{ij}}$	gear mesh force $i-j$ along line of action
$f_m^{x'}$	gear mesh force in x' direction
$f_m^{y'}$	gear mesh force in y' direction
f_t	frequency of external torque
h	meatus height
J	parameter related to d and c
J_i	inertia of gear i
K	parameter related to b and a
k_b	bearing stiffness
k_c	proportional gain of controller
k_m	meshing stiffness
k_{mc_k}	amplitude of the $k-th$ harmonic of meshing stiffness related to cosine

k_{ms_k}	amplitude of the $k-th$ harmonic of meshing stiffness related to sine
k_{m0}	mean value of meshing stiffness
k_t	torsional spring stiffness
m_i	mass of gear i
m_{eq}	equivalent gear pair mass
p	parameter related to K, J, δ and θ
q	parameter related to K, J, δ and θ
R_{eq}	equivalent radius of the approaching surfaces
R_i	base radius of gear i
r_{im}	mean curvature radius of the tooth profile of gear i
$\hat{t}$	tooth thickness
T_{ei}	external torque applied to gear i
ν	generic auxiliary variable
x	dimensionless transmission error for a single-degree-of-freedom-system
x_b	backlash clearance
x_i	radial displacement in x direction for gear i
x_r	dynamic transmission error
y_i	radial displacement in y direction for gear i
z	number of teeth

Greek symbols

α	half of the angle between the two lines of action
$\hat{\alpha}$	Rayleigh's damping mass proportionality coefficient
$\hat{\beta}$	Rayleigh's damping stiffness proportionality coefficient
γ	parameter related to d and c
$\hat{\gamma}$	angle between one line of action and y axis
Γ_n	phase shift between the two meshing force
$\hat{\delta}$	denominator of RI definition for loaded geartrains

δ	parameter related to φ and γ
ϵ	gear contact ratio
ζ	modal damping factor
η	smoothing parameter
θ	rotation angle of one of the ellipse semi-axis with respect to Ox_2y_2 frame
θ_i	rotation around z axis of gear i
ϑ_i	rotation of gear i divided for backlash
θ_{1kin}	mean angular velocity of driver gear
$\dot{\theta_{1m}}$	mean angular velocity of driver gear
$\ddot{\theta_p}$	acceleration excitation
μ	viscosity of the lubricant oil
τ	dimensionless time
φ	parameter related to b and a
$\hat{\phi}$	angle between one line of action and y axis
Φ_n	phase related to $n-th$ harmonic of meshing force $1-2$
χ_i	dimensionless displacement along x direction
χ_r	dimensionless dynamic transmission error
ψ	parameter related to excitation frequency and φ
ω_n	natural frequency of a single-degree-of-freedom system
ω_{ni}	natural frequency of $i-th$ mode
Ω	excitation frequency
Ω_m	meshing frequency
Ω_s	shaft frequency

Abbreviations

ODE	Ordinary differential equations
ANM	Asymptotic Numerical Method
HBM	Harmonic Balance Method

RI	rattle index
BLA	Back-side Line of Action
DLA	Direct Line of Action
SC	Supercomponent

1

INTRODUCTION

1.1 GEAR EXCITATION MECHANISM AND THEIR MODELING

Gears are essential elements in mechanical power transmission. Their dynamic behavior involves a great variety of phenomena introducing non-linear vibrations and generating an undesired noise emission. A typical gear, under operating conditions, is subjected to high dynamic forces which affect the surrounding components such as shafts, bearings and the gearbox case. In this regard, the time-depended bearing forces are transmitted to the gearbox case, which coupled with the whole system assembly provokes an undesired noise emission.

The vibration source in gear transmissions is originated by multiple factors. First of all, geared systems dynamics is characterized by an internal excitation, mainly caused by the static transmission error. In addition, a non-smooth nonlinearity is introduced, caused by the backlash clearance. In ideal conditions, the driveline motion must take place respecting the constancy of the transmission ratio. If gears were perfect involutes, absolutely rigid and correctly spaced, the transmission of rotational motion would take place with absolute regularity [5]. This means that a constant speed at the input shaft would result in a constant speed at the output shaft. In this regard, no time-varying forces would exist, hence, no vibrations would be generated. In real systems, obviously, gears are characterized by manufacturing errors, which may affect involute alignment deviations, involute form deviation, pitch errors, misalignment and so on. In addition, depending on gear contact ratio, there is a variable number of mating teeth in meshing area which are subjected to elastic deflection. Furthermore, gears are mounted on shaft by means of

rolling or journal bearing, which are featured by a certain compliance. With particular reference to rolling bearings only, these latter have variable nonlinear stiffness as a function of the local deformation of the rotating elements and therefore of the radial position of the gear body. Under the static condition, all the mentioned phenomena can be included in the definition of an overall kinematic function known as the static transmission error [6]. The vibration caused by the static transmission error lead to the emission of the so-called whine noise [7], [8], [9].

To summarize, the internal excitation represent the primary excitation source within geared power transmission. In addition, the presence of a certain amount of backlash introduce a non-smooth nonlinear contribution to the whole system dynamics. The presence of a backlash clearance is mandatory to allow better lubrication, limit interference due to geometrical manufacturing errors and reduce wear [6]. Despite these positive effects, it enhances torsional vibrations by allowing tooth detachment to take place. The contact loss due to the backlash clearance can be caused by the internal excitation, i.e. the static transmission error. When vibro-impacts are excited by the internal excitation, the geared system response function can be affected by instabilities regions and bifurcations. In fact, the domains of unstable motions can be expressed as a function of gear mesh damping and gear mesh stiffness excitation amplitudes, retaining the gear geometrical parameters [5]. The vibro-impacts between tooth flanks generate high dynamic forces leading to nonlinear vibrations and noise, known as rattle noise [6]. In addition, these strong dynamic load can provoke elevated tooth root and contact stresses, leading to a shorter gear fatigue live.

Tooth contact loss can also be caused from the external excitation source in lightly loaded geartrains. The external excitation can be originated by rotating mass unbalances, geometric eccentricities, and prime mover torque fluctuations [6]. Rattle of lightly loaded gears is one of the major problems facing the automotive sector, since cars transmission systems spend a lot of time idling in very light load [5]. As a matter of fact, a very common scenario is represented by the oscillating torque generated by the firing order of the internal combustion engine. The torque fluctuation causes impacts between the teeth of all the unloaded gears in manual transmission.

By taking into account all the elements briefly introduced, there is a clear need of a detailed mathematical model able to describe the complex nonlinear dynamic behavior of geared systems. The prediction of the dynamic forces

magnitude and the displacements suffered by the gear body is a necessary step for the design of quiet and reliable drivelines.

In the modeling of dynamic problems, a real engineering system is replaced by a numerical-analytical model which approximates its behavior. With reference to any mechanical system, the equations that govern its dynamic motion represent the physical-mathematical model. The use of numerical models and simulations is nowadays an extremely important aspect in modern industries. In fact, engineers use numerical-analytical models, supported by experimental correlation, in order to cut back the number of physical prototypes and reduce the quantity of performed experiments. In order to realize an effective and reliable model, different approaches are available. In fact, depending on the system under study, the choice of the modeling strategy constitutes a key point for the correct representation of its features. Within this framework, the Finite Element Modeling (FEM) represents the most accurate technique to describe the three-dimensional behavior of any mechanical system. It allows the user to properly account for an accurate representation of complex geometry and consider its real distributed properties. The FEM analysis is a powerful tool to study the dynamic response to a general time-varying load, it empower a comprehensive view of the structural integrity of the components and their assembly. By indicating the distribution of stresses and strains on the real object domain, this method permits a detailed visualization of the weakest point of a structure or system assembly. Despite these positive aspects, FEM models are characterized by a large number of degrees of freedom and their resolution requires an high computational effort. As a matter of fact, in certain application, a detailed FEM model may result very large for an efficient computation.

Depending on the object of study, FEM analysis can lead to an onerous computational effort which may result useless in practice. As an example let consider a simple mechanical transmission composed by a single gear pair. The realization of a FEM model can result very helpful for the determination of critical stressed spatial domain and failure analysis, but the calculation of dynamic forces transmitted to the gearbox case may be conducted by employing more suitable simulation tools. In this context, lumped parameter modeling represent an ever-increasing employed tool in modern industries for its high computational efficiency. The lumped parameter approach consists in the subdivision of the system into masses and inertias connected to each

other by means of elastic and damping elements. The distributed physical proprieties are replaced by lumped characteristics. This modeling technique can be applied at the earliest stages of the design process, when only the relevant design parameters are set and, therefore, several system configuration can be tested before to complete the design specifications. Within geared system dynamics, as proved in several scientific paper, lumped parameter modeling provides an excellent agreement between numerical and experimental test case.

In order to obtain a good correlation with real experiments, it is worth underlining that during the pre-processing stage different system parameters are still unknown. As an example, the calculation of bearing and meshing stiffness is not a straightforward task. One may account for analytical methods to compute bearing and tooth compliance both, unless this, different literature experiments have proved that numerical techniques are more suited to be used as they allow an excellent numerical-experimental correlation. In this regard, FEM analysis provides the optimum results for the computation of nonlinear bearing and meshing stiffness. As a matter of fact, the combination of these modeling strategies give rise to a mathematical model which is able to represent the real behavior of geared system with high fidelity. FEM analysis may be used to compute the nonlinear static response of the system, while the lumped parameter model allows the computation of its nonlinear dynamics in a very efficient way. Once the pre-processing stage is completed, the mathematical formulation of lumped parameter models is relatively simple and it can be easily implemented with coding software as Python, Matlab and Fortran. Coding software provides for the maximum of versatility and offers a complete customization of the system representation. Unless this, the lack of a graphical user interface makes their use cumbersome, especially in industrial environment where the engineers have to face tight schedule. In those framework where rapid and effective calculation tools are needed, lumped parameter model are obtained by using commercial software. The latter are characterized by an intuitive graphical user interface and are much more user friendly then coding interfaces. One of the most used software in industries is Simcenter AMESim (Advanced Modeling Environment for performing Simulation). It allows the simulation of physical multi-domain systems, empowers the resolution of linear and nonlinear systems by offering different time integration techniques. In addition, it is provided by editable devices which makes the

realization of a custom model a straightforward matter. This aspect can be very useful in industrial frameworks, where engineers have to achieve the results in the shortest time possible. Although commercial software are very intuitive and easy to use, they usually employ a numerical computation method based on time integration scheme. By dealing with nonlinear systems, one may be interested in the study of unstable solution branches, bifurcation analysis and multi-valued regions computation. These kind of analysis can result very onerous by using time integration technique and, even if bifurcation points may be clearly identified, the computation of unstable branches can not be performed. In this regard, the application of frequency domain methods which allow a complete nonlinear response function of a geared-rotor-bearing system may be adopted.

The present manuscript addresses two main subject. The first one is the investigation of numerical-analytical tools for the nonlinear dynamic analysis of geared systems. The second one regards the analytical study of gear whine noise and gear rattle noise occurrence. The analytical assumptions are provided by a numerical assessment in order to demonstrate their effectiveness and reliability.

1.2 OVERVIEW OF THE THESIS

On the basis of the various elements described in the previous section, the manuscript points out different tasks. Firstly, the realization of a lumped parameter model is discussed by analyzing two different modeling strategies for different purpose. The first one, is based on time integration technique and enhances the employment of commercial software to speed-up the modeling set-up phase. The second modeling strategy rely on a frequency domain solution technique able to describe the dynamic of those nonlinear systems which present unstable solution branches and multi-valued regions. Once a detailed analysis on the modeling strategy has been conducted, rattle noise and whine noise occurrence are investigated. The studies on rattle noise have conducted to the introduction of a new analytical parameter as a novelty to the current state of the art. In a similar manner, the investigation of whine noise occurrence addresses to an analytical formulation able to forecast the main overall direction and magnitude of bearing reaction forces on idler gear. The following is a brief overview of the chapters.

Chapter 2 is devoted to the geartrain nonlinear dynamics modeling. In particular, the nonlinear ordinary differential equations (ODE) governing the motion of a single gear pair are established. All the relevant phenomena within gear dynamics are deeply investigated and included in the equation of motion. The proposed modeling approach rely on a block diagram technique and is realized by employing Simcenter AMESim commercial software. Based on graphical software capabilities, the author propose detailed guidelines to build a complete geartrain model by connecting some programmable devices between them. This feature, make it possible the realization of a complete customized model. In a first instance, a complete nonlinear lumped parameter model of a single gear pair is realized. This is achieved by manually implementing the equation governing the motion of the system. Afterwards, a particular methodology is developed to obtain a modular architecture which offer the possibility to realize any kind of ordinary transmission layout. This modeling technique offers a great advantage in the model setup phase. In fact, once the model of a single gear pair is established, the realization of any geartrain is made by connecting the pre-programmed element between them. This approach allows the user to obtain a fully customized model and realize a driveline lumped parameter model with easy simple step. Based on this practical feature, the introduction of such tool in industrial environment may represent a key point to speed up the model setup phase. By focusing on ODE resolution methods, Simcenter AMESim solver is limited to the already built-in numerical computation techniques. For instance, the system of differential equations can be solved only with time integration techniques. Dealing with nonlinear systems, unstable solution branches and bifurcations can appear in the dynamic response. In this regard, the time integration techniques are not suited to perform these kind of analysis. Although bifurcation location can be clearly recognized, the computation of unstable branches can not be performed. In order to get further insight on the issue, an additional modeling strategy is developed in Chapter 3.

Chapter 3 is committed to the application of the Asymptotic Numerical Method for the resolution of the nonlinear dynamics of a gear pair. Firstly, a literature survey on the current methodologies is conducted. The Asymptotic Numerical Method stands out from the existing methods as it is a purely frequency domain method, characterized by an high efficiency in the computation of high-order Taylor series. In detail, the chapter provides a brief

explanation of the method itself and its effectiveness. In this regard, it is shown how the adoption of a quadratic formalism to recast the equation of motion is useful for the computation of high-order Taylor series. Afterwards, a single-degree-of-freedom nonlinear lumped parameter model of a spur gear pair with time-varying meshing stiffness and backlash is recalled. The equation of motion is recast in a quadratic form and implemented by means of a Matlab interface software. Results computed with the Asymptotic Numerical Method are compared with that obtained from the Runge-Kutta time integration scheme, demonstrating an excellent agreement. Finally, the complete model of a single gear pair is set. A comparison between the two solution methods in terms of computational performance is conducted. This methodology provide for a full nonlinear dynamic response of the geared rotor bearing system, where the computation of unstable solution branches is performed in very a short simulation time. Unless these positive aspects, the set-up of a geartrain model can be very time consuming. As a matter of fact, as the method needs a peculiar recast and dimensionless form of the initial ODE system, the model set-up time is drastically increased. In addition the user have to deal with coding interface, which may results less practical then user interface commercial software. On the other hand, once the model has been realized, the computational time is considerably reduced with respect to the time integration techniques.

Chapter 4 deals with the investigation of rattle noise occurrence in multimesh loaded geartrains. In detail, it proposes an analytical procedure for the generalization of the rattle index in any type of ordinary transmission layouts, single or multiple branch, both in idle and loaded conditions. In geartrain design, the introduction of an analytical parameter able to identify the contact loss occurrence may represents a powerful tool to detect rattle noise. By investigating the state of the art, it is clear that several studies have been focused on the identification of the rattle noise by using mathematical models and analytical parameters. However, the investigation has been exclusively focused on idle gear pairs, since this is an unavoidable working condition in multispeed gearboxes. Although the latter represents the most common situation, rattle noise may also appear in other driveline applications. As an example, in geared engine timing systems, the camshaft generate an oscillating torque at the output shaft which can lead to vibro-impact between teeth. In this chapter, the authors generalize the definition of the rattle index proposed by Sing et. al in [10] to

any kind of ordinary transmission, single or multiple branch. The proposed analytical parameter also includes the definition for loaded geartrains and it is related to gear inertial torque, viscous torque and external torque. By starting from the classical 6-DOFs equation system defining the nonlinear dynamics of a gear pair, a recursive analytical formulation of the rotational dynamics of gears is proposed. This mathematical expedient is adopted to deduce the generalization of the rattle index definition for any meshing pair pertaining to a multimesh geartrain. Firstly, the dissertation is conducted for a single branch, unloaded geartrain. Then, the definition is extended to single branch, loaded geartrain. In this regard, consideration on rattle index validity are made. In particular, in order to avoid numerical problems and erroneous indication of rattle occurrence some guideline are presented. Finally, the dissertation is applied to multiple branch, loaded geartrain. After the analytical formulation has been obtained, numerical experiments are conducted. Several geartrain layout are investigated by employing the AMESim modeling strategy described in Chapter 2. In this regard, single and multiple branch geartrains lumped parameter models were realized, both in idle and loaded conditions. The simulation results demonstrate the accuracy of the outlined parameter. The rattle index will remain under a certain threshold when gears are in contact on the drive side; on the other hand, when teeth detachment takes place it will respond with a peak, overcoming threshold value. The proposed analytical parameter instantaneously describes the vibro-impacts events related to any gear pair of the driveline. For instance, one may be able identify the exact meshing pair who undergoes rattling events. In addition, the introduced parameter may lead to a quantitative estimation of vibro-impact severity. Numerical assessment have been performed by using different oscillating torque amplitudes. The results proved that as the oscillating torque amplitude increases, the impact between teeth become more severe.

In Chapter 5, gear whine noise occurrence is investigated. In particular, the chapter proposes an analytical formulation able to forecast the main overall direction and magnitude of bearing reaction forces on idler gear when the geartrain works under quasi-static condition. Firstly, a literature survey is conducted in order to identify the main phenomena linked to whine noise emission. The primary excitation source of this kind of noise is represented by the time-varying mesh stiffness and the static transmission error. In this regard, the time-varying meshing forces are transferred to the bearing housing

and the vibration is transmitted along the entire system assembly. For instance, a detailed investigation of bearing forces transmission mechanism is an essential step to understand the relationship between system design parameters and noise emission. This study allowed the authors to obtain a mathematical relationship between the overall magnitude and direction of idler gear bearing reaction forces and some generic geartrain design parameters. In detail, the analytical formulation describes the trajectory drawn by the oscillating components of bearing forces on idler gear in multi-mesh geartrains when the latter work under quasi-static condition. By starting from the definition of meshing forces by means of Fourier series development, idler gear bearing forces are obtained under the hypothesis of quasi-static motion. This procedure demonstrates that the alternating component of bearing forces on idler gear describes an elliptical trajectory as the prime mover rotates over a pitch angle. This formulation directly links the bearing forces elliptical trajectory with the gear spatial position, the meshing phase and the amplitude of meshing forces. By properly setting the over-mentioned parameters one may be able to control the magnitude and direction of the overall idler bearing reaction forces. Finally, numerical experiments are carried out to investigate if the proposed analytical dissertation is suitable in dynamic conditions, when the internal excitation frequency is close to one system eigenvalue. In order to fulfill this purpose, a lumped parameter model is set and numerical analyses are conducted at various shaft rotational speeds. The model is realized by employing the AMESim modeling strategy described in Chapter 2. Numerical experiments were extremely useful to understand the ellipse modification when the dynamic effects become relevant. The obtained results confirm that under the hypothesis of quasi-static motion the analytical dissertation is an effective and reliable tool to forecast the main overall direction of pulsating bearing forces. Unless this, not all the parameters governing the ellipse can be set to a specific value. The gears spatial position and the phase shift between two consecutive meshing can be chosen during the gear design concept phase, on the other hand, estimating the amplitude of meshing forces is not a direct matter. In fact, the latter represent the limit of the analytical dissertation. The meshing force magnitude can be controlled by adopting gear micro-geometry modification but it can not be determined unequivocally without solving the gear equation of motion, as it is the result of internal excitation.

Chapter 6 is dedicated to conluding remarks.

2

A LUMPED PARAMETER MODEL FOR GEARED SYSTEMS

The Chapter is devoted to gear dynamics modeling. In particular, a nonlinear dynamic model of a single gear pair is established. The model accounts for time-varying mesh stiffness, backlash and lubricant squeeze force when vibro-impacts occur. In addition a nonlinear contribution of load-depended bearing and meshing stiffness is considered. The proposed modeling strategy rely a block diagram technique and it is realized in Simcenter AMESim, a commercial software widely used in industries. By starting from the single gear pair model, detailed guidelines are given to construct any type of ordinary transmission layout by connecting some pre-programmed devices between them. Finally an experimental validation on industrial use case is proposed in order to demonstrate the reliability of the dynamic model.

2.1 INTRODUCTION

Geared transmission systems are fundamental elements in powertrain applications. As depicted in the previous chapter, they act as self-excited mechanism as a results of static transmission error and time-varying mesh stiffness. In addition their dynamic behavior is strongly affected by a non-smooth non linearity due to the backlash clearance. Beside the contact non linearity, the meshing and bearing stiffness may be characterized by a nonlinear dependence on the applied load. As geartrains work under multiple load conditions, this aspect may lead to an additional complication in the realization of a dynamic model capable to forecast the forces acting on the gearbox case.

Apart from the elastic effects, an other important role is played by the lubricant. In fact, it is responsible for the forces and torque acting on gear teeth and body when contact loss occurs. Based on these assumption, the

realization of a complete model which account for all the described phenomena represent an essential instrument to investigate geartrain dynamics. The very first proposed dynamic models were essentially linear, as reviewed by Ozguven and Houser [11], however, the non-linear behaviour of the geared systems suddenly came out in several experimental analyses [12, 13, 14]. One of the first non-linear mathematical models was introduced by Kahraman and Singh, who formerly defined a single-degree-of-freedom torsional model considering backlash clearance [15]. Later, the same authors proposed a three-degrees-of-freedom model assuming bearings and shaft compliance [16]. Finally, the model was replaced with a three-degrees-of-freedom nonlinear model, taking into account time-varying mesh stiffness, backlash and bearing clearance. The last model developed by Kahraman and Singh constitutes an effective and reliable tool to predict nonlinear dynamics of a gear pair. As a matter of fact, it allows to highlight the interaction between the internal excitation and the contact non linearity [6].

Within this framework, the variation of mesh stiffness and the static transmission error, represent the main cause of vibration and noise in geared system applications. Different experimental studies ([17], [18], [19], [20], [21]) have clearly demonstrated that mesh stiffness fluctuation as well as backlash clearance must be included in spur gear pair modeling as it acts as a self-excitation mechanism. Based on this assumption, the mesh stiffness computation is considered a crucial phase during the pre-processing modeling stage. In this regard, experimental and numerical-analytical methods have been investigated in literature in order to evaluate meshing stiffness. Experimental methods require a dedicated test-rig and are based on transmission error measurements. According to the literature review proposed in [22], the meshing stiffness calculation methods can be divided into three main categories: analytical methods, pure finite element method and hybrid methods. By focusing on the analytical methods, Kuang and Yang [23] proposed an analytical formula based on the angular position, the contact ratio and the average stiffness of the gear pair. A similar procedure has been proposed by Cai and Hayashi [24]. In [25], the authors developed an analytical method to consider varying-load condition. Despite the analytical approach gives reasonable results in a low computational time, they lead to qualitative outcomes, useful in a first stage of the dynamic analysis. On the other hand, pure finite element analysis give an accurate description of the meshing stiffness, accounting for both tooth deflections and

gear body compliance. Based on nonlinear finite element analyses, different authors proposed various methodologies [26], [27], [28], [29], [30], [31]. One of the most efficient approach is based on the work of Cooley et. al in [30], where the mesh stiffness is calculated as the results of the relative difference between gear rotation. This methodology can be applied for various mean torque load giving the meshing stiffness value in varying-load condition. These kind of methods are characterized by an high computational effort, as they need very refined mesh in the contact area. As a matter of fact, hybrid methods [32], [33], [34] have been developed to speed-up the finite element analysis. The overall gear deformation is divided into two different terms: a linear global deformation term and local contact nonlinear deformation term. By adopting this expedient, one may be able to compute the nonlinear local contact deformation term by means of analytical formulation in order to lighten the finite element analysis computation.

Besides gear mesh stiffness, rolling bearings elements cover an important role in vibrations transmission as they provides for the dynamic coupling with the gearbox case. Based on this assumption, a large amount of literature on their static and dynamic behavior is available. In order to describe the real motion of a geared-rotor-bearing system, an accurate description of radial stiffness represent a crucial input parameter. Radial stiffness is not a constant value, on the contrary its magnitude has a nonlinear relation with respect to the applied load and the position of rolling elements. In fact, as underlined in [35], many authors focus their attention on the estimation of radial stiffness by means of experimental, analytical, and numerical approaches. Experimental approaches are based on direct displacement measurements [36] and indirect methods as modal analysis [37]. Analytical ones may be derived from Hertz contact theory [38, 39, 40] or obtained empirically as [41, 42]. The most effective and reliable numerical approach counts on finite elements modeling. As for meshing stiffness computation, radial stiffness estimation by means of finite element analysis, may represent a large computational effort. In this regard, many authors proposed various approach in order to simplify the problem. The most common techniques consists in take advantage of symmetries [43, 44, 45, 46, 47, 48, 49, 50], remove the unloaded roller elements [43] and consider an equivalent 2D problem [43, 51, 52].

Bearing and meshing stiffness dependence from the applied load, is a fundamental quantity in the modeling of a geared system. Apart from stiffness

determination, it is worth to underline that gearboxes work under lubricated conditions. Hence, another cardinal role is played by the lubricant. In fact, during the contact loss, it is the only element that can attenuate fluctuation and impacts between teeth [53]. When teeth detachment occurs, the elastic force due to meshing is zero. On the other hand, an oil squeeze effect between the approaching tooth flanks may act as as a nonlinear spring-damper system [54, 55]. The modeling of the lubricant role in rattle conditions has been the primary subjects of numerous studies [56, 57, 58, 59].

On the basis of the proposed literature survey, an effective dynamic model of a geared system may include all the introduced elements. In the present chapter a nonlinear lumped parameter model of a geared system is presented. The model accounts for backlash non linearity, time-varying and load-depended mesh stiffness, load-depended bearing stiffness and squeeze force due to lubricant between the approaching teeth. It is realized by means of Simcenter AMESim, a commercial software based on a block diagram technique. By taking advantage of graphical user interface, detailed guidelines are given to realize a complete geartrain model. Firstly, the nonlinear lumped parameter model of a single gear pair is realized. The equations governing the motion of the system are implemented manually by means of editable block devices. Then, a modular architecture is built. This expedient allows to define any kind of ordinary transmission layout by connecting some pre-programmed elements between them. In addition, this procedure permits a full customization of the dynamic model as it is implemented by the user. This approach gives a great advantage in terms of time schedule, in fact it speeds up the model setup phase as a complete driveline can be modeled with easy simple operations. In those framework where engineers have to face tight schedule, the introduction of such architecture may represent a relevant tool to expedite the model setup phase.

The chapter is structured as follows. Firstly, the analytic model of a single gear pair is recalled. Afterwards, the AMESim modeling strategy is deeply explained. The realization of the dynamic model is shown step by step. Finally a numerical assessment on industrial use case is depicted.

2.2 NONLINEAR MODELING OF A SPUR GEAR PAIR

A discrete model of a gear pair is shown in Figure 1. Three degrees of freedom

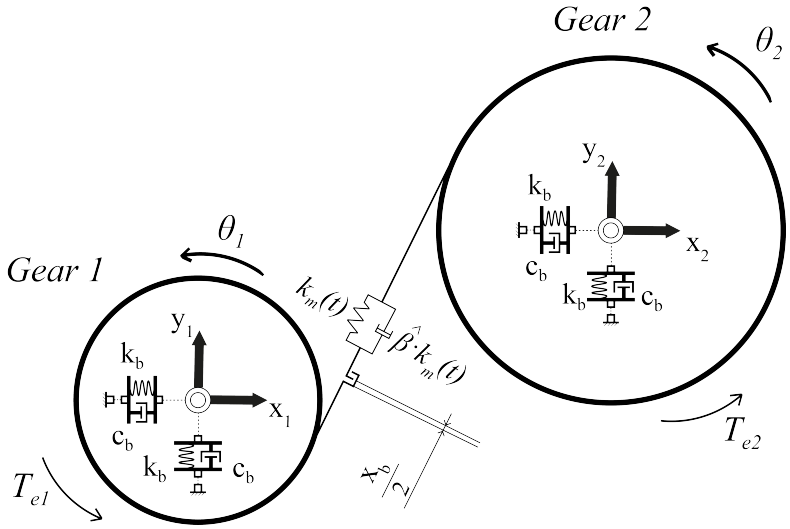

Figure 1: Lumped parameter model of a gear pair, x_b is the backlash clearance, k_b and c_b represent the bearing stiffness and damping, respectively.

are associated to each gear, namely θ_i, x_i, y_i. θ_i is the rotation around z axis, according to the reference frame, it is positive in counterclockwise direction, while x_i and y_i are the radial displacement in x and y directions. The motion of gear pair is described by the following 6-DOFs equation system:

$$\begin{cases} J_1\ddot{\theta_1} + \hat{\alpha}J_1\dot{\theta_1} + R_1 f_m = T_{e_1} \\ J_2\ddot{\theta_2} + \hat{\alpha}J_2\dot{\theta_2} + R_2 f_m = T_{e_2} \\ m_1\ddot{x_1} + \hat{\alpha}m_1\dot{x_1} + f_m^{x_1} + f_b^{x_1} = 0 \\ m_2\ddot{x_2} + \hat{\alpha}m_2\dot{x_2} + f_m^{x_2} + f_b^{x_2} = 0 \\ m_1\ddot{y_1} + \hat{\alpha}m_1\dot{y_1} + f_m^{y_1} + f_b^{y_1} = 0 \\ m_2\ddot{y_2} + \hat{\alpha}m_2\dot{y_2} + f_m^{y_2} + f_b^{y_2} = 0 \end{cases} \tag{1}$$

where J_i, m_i, R_i denote polar mass moment of inertia, mass, and the base radius of gear i, respectively. $\hat{\alpha}$ is the Rayleigh's damping mass proportionality coefficient. T_{e_i} is the external torque applied to gear i. $f_b^{x_i}$ and $f_b^{y_i}$ are the bearing reaction forces, respectively in x and y directions. f_m represents the gear mesh force along the line of action, that is modeled by taking into account backlash non-linearity as defined in [15]. $f_m^{x_i}$ and $f_m^{y_i}$ denote the components of gear mesh force in x and y directions. The Rayleigh's damping model

was adopted, i.e. $\hat{C} = \hat{\alpha}M + \hat{\beta}K$, and for the sake of clarity, damping terms proportional to stiffness are included in f_m definition as described in Eq. 2.

$$f_m(t) = \begin{cases} k_m(t)\left[(x_r - x_b/2) + \hat{\beta}\dot{x_r}\right] & \text{if } x_r > x_b/2 \\ 0 & \text{if } -x_b/2 \leqslant x_r \leqslant x_b/2 \\ k_m(t)\left[(x_r + x_b/2) + \hat{\beta}\dot{x_r}\right] & \text{if } x_r < -x_b/2 \end{cases} \tag{2}$$

where $k_m(t)$ denotes the time-varying gear mesh stiffness, x_r the dynamic transmission error and x_b the backlash clearance. $\hat{\beta}$ represents the Rayleigh's damping mass proportionality coefficient. The definition of the dynamic transmission error depends on which side of the tooth is actually in mesh at each time instant. When contact is occurring on the tooth working flank, transmission error x_r is defined on the *Direct Line of Action*

$$x_r = R_1\theta_1 + R_2\theta_2 - x_1 sin\hat{\varphi} - y_1 cos\hat{\varphi} + x_2 sin\hat{\varphi} + y_2 cos\hat{\varphi} \tag{3}$$

where $\hat{\varphi}$ is the angle between y axis and the *Direct Line of Action*. This condition satisfies the inequality $x_r \geqslant x_b/2$. On the other hand, when contact takes place on the tooth back flank, i.e. when $x_r \leqslant -x_b/2$, x_r is defined on the *Back-side Line of Action*:

$$x_r = -R_1\theta_1 - R_2\theta_2 - x_1 sin\hat{\gamma} + y_1 cos\hat{\gamma} + x_2 sin\hat{\gamma} - y_2 cos\hat{\gamma} \tag{4}$$

where $\hat{\gamma}$ is the angle between y axis and the *Back-side Line of Action*. The time-varying mesh stiffness is a periodic function

2.2.1 *Squeeze force*

When contact loss occurs, the meshing and proportional viscous force are zero. On the other hand, if tooth profiles are approaching, the lubricant trapped between teeth gives rise to an additional viscous force. The damping coefficient in this case is given by the formulation proposed in [60] :

$$C_{squeeze} = 12\pi\mu\hat{t}[R_{eq}/(2h)]^{3/2} \tag{5}$$

where μ is the lubricant dynamic viscosity, $\hat{t}$ is tooth thickness, h is the instantaneous meatus height computed along the line of action and R_{eq} is the equivalent radius of the approaching surfaces. It is calculated as $1/R_{eq} = 1/r_{1m} + 1/r_{2m}$, where r_{1m} and r_{2m} are the mean curvature radii of the tooth profile. The squeeze force along the line of action is:

$$F_{Squeeze}(t) = \begin{cases} C_{squeeze}\, \dot{x_{r_{DLA}}} & \text{if} \quad |x_r| < x_b/2 \ \wedge \ \dot{x_{r_{DLA}}} > 0 \\ \\ C_{squeeze}\, \dot{x_{r_{BLA}}} & \text{if} \quad |x_r| < x_b/2 \ \wedge \ \dot{x_{r_{DLA}}} < 0 \end{cases} \tag{6}$$

where $\dot{x_{r_{DLA}}}$ and $\dot{x_{r_{BLA}}}$ denote the time derivative of dynamic transmission error along the *Direct Line of Action* and *Back-side Line of Action* respectively. With reference to eq. 5 the meatus height is defined as follow:

$$h = \begin{cases} |x_r| & \text{if} \quad |x_r| \geqslant 10^{-6} \\ \\ 10^{-6} & \text{if} \quad |x_r| < 10^{-6} \end{cases} \tag{7}$$

2.3 THE BLOCK DIAGRAM MODELING STRATEGY

Simcenter Amesim (Advanced Modeling Environment for performing Simulation) is an advanced software based on an intuitive graphical interface. It allows the simulation of physical multi-domain systems. Steady state and transient simulations are performed by solving the nonlinear time-depended analytical equations that describe the system mechanical, thermal, electrical or hydraulic behavior. The realization of complex engineering systems is made thanks to the use of different Libraries. Each Library is characterized by a physical domain and contains various devices, namely sub-models, which are based on an input/output functioning. In this regard, a complete engineering system is realized by connecting different sub-models together. Each device is pre-programmed to execute a particular expression based on the inputs, to compute the outputs. Besides the existing programmed tools, thanks to the use of the elements pertaining Signal, Control Library, the user can program a specific device able to realize a custom expression based on input signals. In detail, the input variables can be combined between them or with constant

parameters. This aspect makes the user able to consider any feature inside the model. As a matter of fact, different authors combined AMESim fully editable devices with already programmed sub-models in order to realize full customized models [61, 62].

In this section, the authors combines elements belonging to 1D Mechanical and Signal, Control libraries to build a complete 2D nonlinear model of a spur gear pair. This choice has been made in order to realize a complete dynamical model were all the main features within gear dynamics are considered. Once the model of a spur gear pair is well established, a modular architecture is built in order to realize any type of ordinary transmission layout, single or multiple branch by connecting the gear pair models between them. This procedure allows the user to realize any kind of driveline with easy simple step, making the modeling of a geartrain a straightforward task. Moreover, the choice of a modular architecture, constitutes a manner to study the interaction between the geartrain and any kind of device whose dynamics is linked to the driveline one. The AMESim environment provides for the dynamical coupling among all the elements linked to the transmission system as electrical motor, combustion engines or hydraulic pumps.

2.3.1 *The gear pair model*

The nonlinear model introduced in the previous section is implemented by means of sub-models pertaining to the Signal, Control Library. The Signal, Control Library contains editable block components and makes it possible to construct block diagram models. For instance, the equation of motion are written manually by using the described sub-models. The gear characteristics and the other constant parameters are set by means of the Global Parameters interface. The Global parameter tab allow the user to define constant parameters and combine them together. The gear mass and inertia are represented by a planar rigid body sub-model pertaining to 2D Mechanical Library. Figure 2 depicts the entire spur gear pair AMESim model. At first sight the model seem to be very intricate, a detailed focus on each module will clarify its working principle. Basically, the gear pair model sketch can be divided into six relevant part: the Planar Body Module, the Equation Block Module, the Contact Module, the Meshing Stiffness Module, the Bearing Stiffness Module and the Squeeze Force Module. Moreover, there is an additional module useful

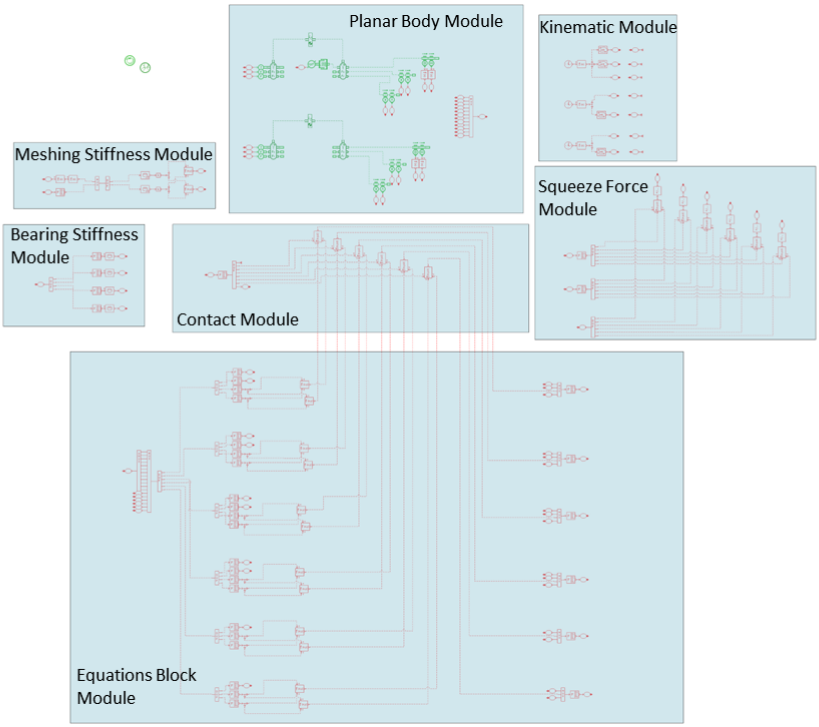

Figure 2: Block diagram of a single gear pair model

to define kinematic characteristics of the gear pair motion, i.e. the Kinematic Module. The Planar Body Module is the only module which contains 1D Mechanical and 2D Mechanical sub-models, in all the other modules only Signal, Control sub-models are employed. By focusing on the Planar Body Module, figure 3, the gear bodies are represented by the green devices, denoted as "Gear 1" and "Gear 2" in the sketch. These sub-models, represent a planar rigid body in a generic reference frame Oxy. The planar body takes as input variables the forces and torque provided by the junctions at ports and gives as output the displacements, velocities and accelerations suffered by the body. In this regard, an additional device is needed in order to handle the input/output quantities separately. The 2D-1D converter, is a connector that enables 1D mechanical components to be connected to 2D mechanical bodies. In particular, it allows the extraction of displacements and velocities along x and y direction, as well as the rotation and angular speed. In the same manner the forces and torque are transferred from the 1D mechanical ports to the planar rigid body. The coordinates and velocities of the gear body are monitored by means of

sensor devices as shown in figure 3. This is an important step of the model realization as the displacements and velocities represent the input quantities for the Equations Block Module. In detail, these signals are channeled by means of wireless devices to a specific sub-model, the dynamic multiplexer. It combines the variables of its multiple input ports into a single output port. The number of input ports is dynamic because it is set by the user when the icon is selected. Afterwards, all the variable are conveyed to a single wireless device. This expedient permits to group all the variable in a single channel and then duplicate it for various purpose. The wireless transmitter device contains twelve signals which correspond to displacements and velocities along x and y direction, as well as the rotation and angular speed for each gear. The Planar Body Module provides for the application of dynamic forces to the gear body and monitor all the degrees of freedom of the system. Coordinates and velocities of each gear body are then transferred to the different modules in order to accomplish several tasks. The Equation Block Module, figure 4, represent

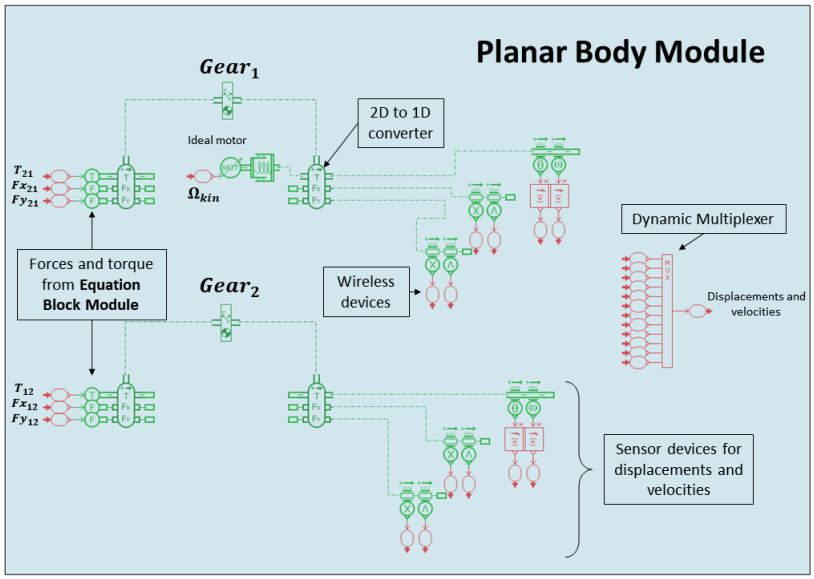

Figure 3: Planar Body Module: it is devoted to the monitoring of displacement and velocities and to the application of forces for each gear

the most important part of the model as it provides for the implementation of the equations of motion. The coordinate and velocities coming from the Planar Body Module are combined with bearing and meshing stiffness signals

in order to implement the system of equation 1. The equations are written by means of DYNFUNCoo sub-models, figure 5. The latter are widely used in

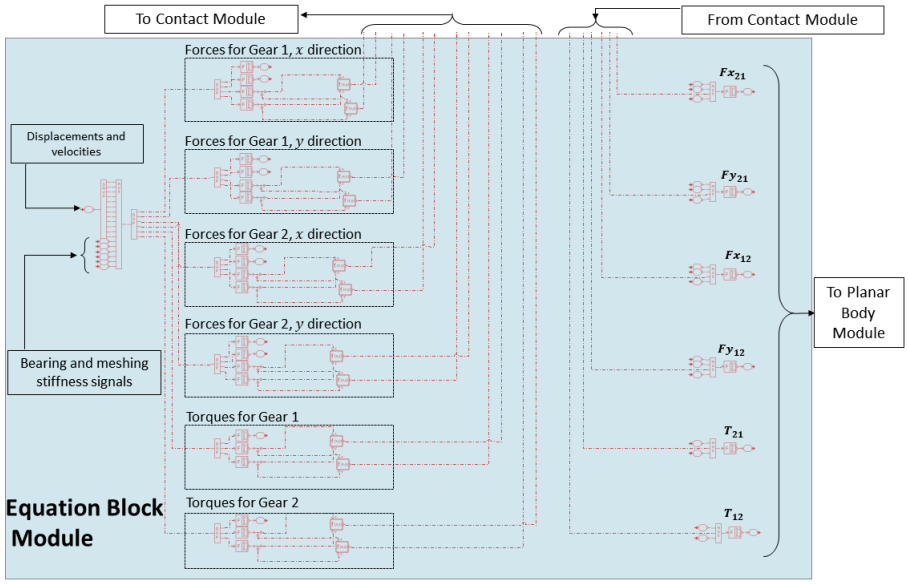

Figure 4: Equation Block Module: provides for the implementation of the equations of motion

the present model as they allow the output to be expressed as a combination of multiple input variables and constant parameters. As depicted in figure 4, the forces contribution is expressed for each gear and direction. In addition, the overall force/torque is further divided in three different part: the viscous contribution, the bearing contribution and the meshing contribution, see figure 5. As the proportional damping model is adopted, the viscous contribution accounts only for the viscous force due to the rotating inertia or translating mass. The bearing and meshing contribution includes for both elastic force and proportional viscous force. As it can be noticed from figure 5, the meshing contribution, is defined by means of two separated devices. As underlined in the previous section, the definition of the meshing force depends on which side of the tooth the contact occurs. In geared transmission system, the *Direct Line of Action* is recognized by the prime mover rotation direction which is assigned in relation to the system layout. In this regard, when modeling a geartrain, the position of *Direct Line of Action* is known a-priori. Based on this assumption, a user-defined parameter works as discriminant to select the line

of action to be considered as direct. This operation is made by two logic blocks linked to the meshing force definition sub-model. Successively, viscous and bearing contribution are sent to the Planar Body Module while meshing forces signals are transmitted to the Contact Module. The definition of dynamic transmission error is the basis of the Contact Module, figure 6. As for meshing

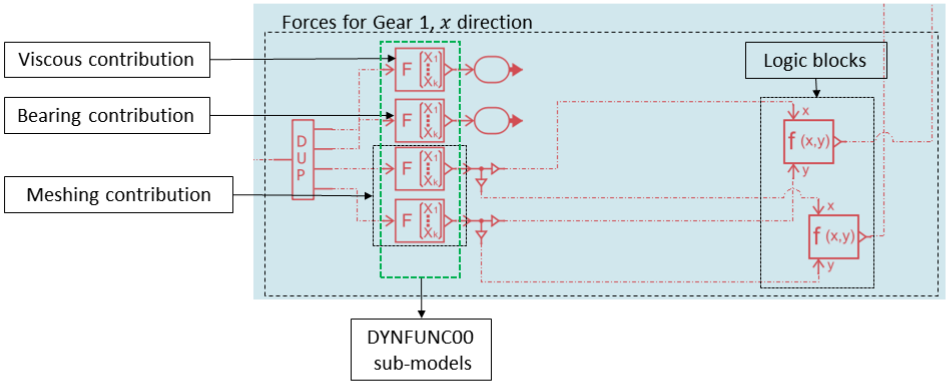

Figure 5: Detail of Equation Block Module

forces contribution, dynamic transmission error is defined by employing eq. 3 and 4 both. This assignment is performed by the x_r writer, see figure 6, which encompasses the logic operation to select the correct *Direct Line of Action*. After the computation of dynamic transmission error, the signal is sent to the logic blocks which determine the tooth side of contact by applying eq. 2. This operation is done for each gear and each direction. Once the meshing force has been selected, it is sent to the Equation Block Module which provides for the sum between viscous, bearing and meshing contribution. Let focus the attention now on meshing stiffness module, figure 7. As highlighted in the previous section, meshing stiffness is a periodic function whose periodicity is assigned by the gear mesh. In addition, it is characterized by a load-depended

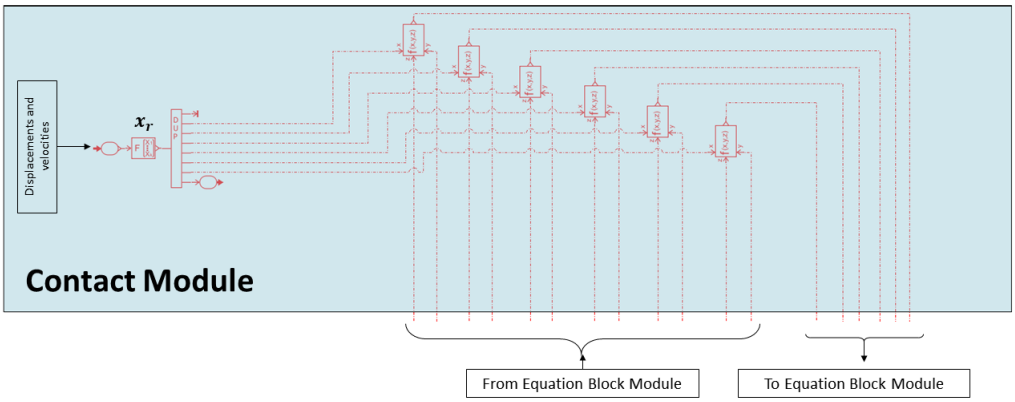

Figure 6: Contact Module: it provides for the selection of the correct line of action and tghe detection of free flight motion

non linearity, therefore, its value depends on the overall relative compression between teeth. In order to represent this feature, the meshing stiffness map is inserted by means of a dynamic 2D interpolation table. Then, the sub-model extracts the correct value depending on two input variables: the dynamic transmission error and the kinematic position of prime mover. In particular, the kinematics of prime mover rotation is computed by the Kinematic Module. The angular displacement is then converted into a sawtooth waveform clock signal by simple mathematical operations. The clock signal represents a rotation over a pitch angle. This is done in order to select the appropriate meshing stiffness over a pitch angle rotation. When back contact occurs, the corresponding phase of meshing stiffness is consequently chosen. For instance, an additional 2D interpolation table is employed to opportunely consider the gear mesh back contact phase. As for the gear mesh force definition, a user-defined parameter works as discriminant to select the mesh stiffness to be used. This operation is made by the logic block depicted in figure 7. The Bearing Stiffness Module, figure 8, provides for the selection of bearing stiffness. In particular the nonlinear stiffness is defined by means of a 1D interpolation table. This sub-model takes as input variables the displacement along each direction, and gives as

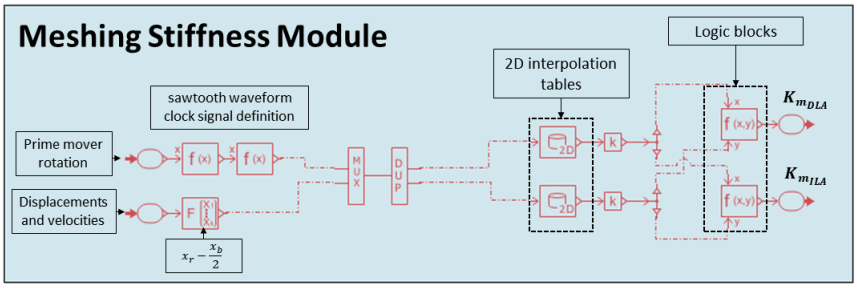

Figure 7: Meshing Stiffness Module: it selects the meshing stiffness to be used at each time step

output the bearing stiffness to be used. The squeeze force module, figure 9 is responsible for the squeeze viscous force computation when two teeth are approaching. Time derivative of dynamic transmission error along *Direct Line of Action* and *Back-side Line of Action* are computed in a similar manner as for dynamic transmission error definition. Successively, these signals are sent to the squeeze writer devices which execute the operations depicted in eq. 5, 6, 7. The squeeze force signal is then added to viscous, bearing and meshing contribution provided by Equations Block Module. The modeling strategy used to describe the nonlinear dynamics of a single gear pair can be easily extended to an arbitrary number of gears.

2.3.2 *The geartrain model*

By starting from the model shown in figure 2, it is worth noticing that the non linear dynamic computation modules are suited to work by taking as input variables the displacements and velocities from the gear bodies and giving as output the forces exchanged between them. In addition, the kinematic position of prime mover is needed for the correct selection of meshing stiffness.

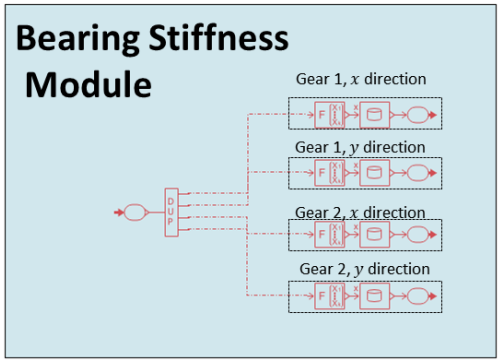

Figure 8: Bearing Stiffness Module: it selects the bearing stiffness to be used at each time step

In this regard the Meshing and Bearing Stiffness Modules, Equation Block Module, Contact Module and Squeeze Force Module can be collected in a black box in order to handle a unique device which performs the nonlinear dynamic computation of the system. In order to accomplish this task, the Simcenter AMESim software is provided of an appropriate facility, i.e. the Supercomponent Facility. The Supercomponent (SC) realization allows the user to organize a model from a functional point of view, especially when its usage is spreading. In particular, the user can manually choose the sub-models to be included in the SC and then create ports to make it communicate with other devices. By focusing on the complete model depicted in figure 2, one may select the devices to be included in the SC facility. Figure 10 depicts the same model shown in figure 2 where the different modules are included into a unique black box denoted as SC_{12}. By adopting this expedient, the user can simplify the visual appearance of the whole numerical model.

To summarize, the described procedure has led to the definition of a black box, the SC_{12}, able to describe the nonlinear motion of a single gear pair. Based

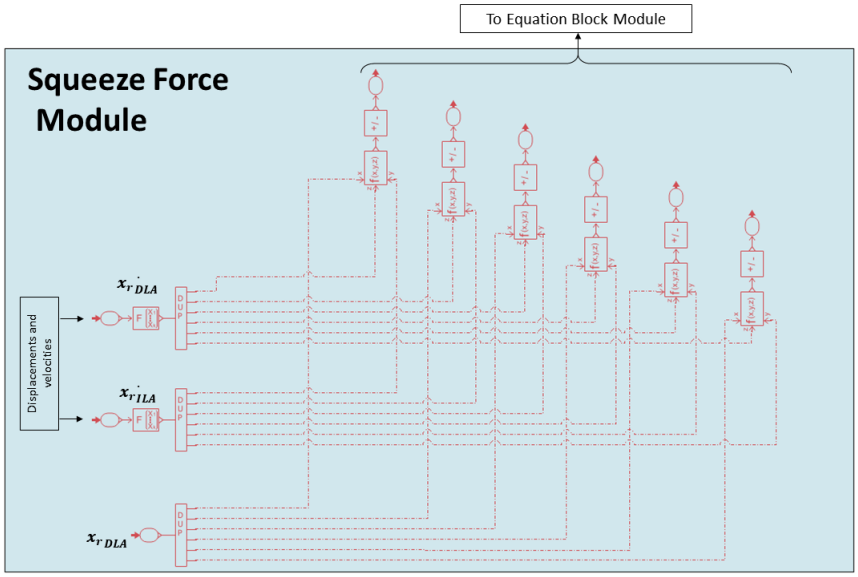

Figure 9: Squeeze Force Module: it provides for the implementation of the lubricant squeeze force between the approaching teeth

on this assumption, this tool can be used to model additional meshing in a multi mesh geartrain. By focusing on figure 2, the same architecture of meshing 1-2 can be reproduced to define meshing 2-3. In order to accomplish this task, one may adopt the same modeling strategy as for meshing 1-2, providing the adjustment of some technical features. In fact, the model of a single gear pair accounts for bearing and viscous contribution on gear 1 and gear 2 both, when adding a third gear to the driveline only meshing contribution for gear 2 may be considered. As a matter of fact, the modeling of meshing 2-3 would present the same architecture as for meshing 1-2, providing the deletion of viscous and bearing contribution from the Equation Block Module and Bearing Stiffness Module. As a final step, the Equation Block Module and Bearing stiffness Module would be re-programmed as shown in figure 11 and 12 respectively. This procedure will lead to the generation of a different device, the SC_{23}, able to define the nonlinear dynamics within the meshing 2-3. The final geartrain model is depicted in figure 13. It is worth to underline that the "Gear 2" receive forces from "Gear 1" and "Gear 3" both, allowing the dynamic coupling of the whole system. The supercomponent SC_{23} can be used to model any additional gear in ordinary transmissions. In fact, providing the

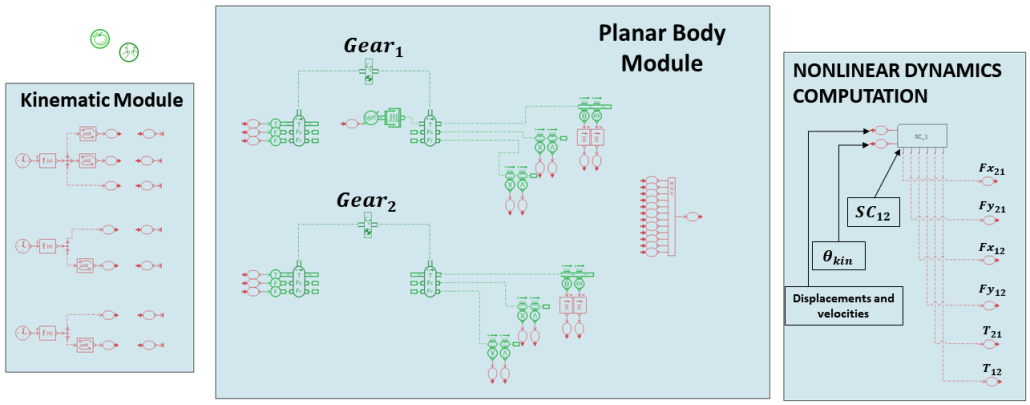

Figure 10: Gear pair block diagram complete model. The present figure depicts the same sistem in fig. 2 where the different modules have been collected into a unique black box, the SC_{12}

selection of correct gear parameters, it can be employed as a general device describing the nonlinear dynamic behavior of a generic meshing. For instance the SC_{23} can be renamed as $SC_{n-1/n}$ as it computes the dynamic response of a generic meshing $n-1/n$. The proposed modeling strategy is a powerful tool to realize any kind of ordinary transmission layout. In fact by employing SC_{12} and $SC_{n-1/n}$ the realization of a complete transmission system is made by connecting the supercomponents between them. This approach can be very useful in industrial environment were the model time setup represent an important aspect. In addition, the graphical user interface permits an user-friendly management of the model realization. Once the SC_{12} and $SC_{n-1/n}$ are established the realization of a geartrain may become a straightforward task. The next section provides a numerical experimental correlation on industrial use case.

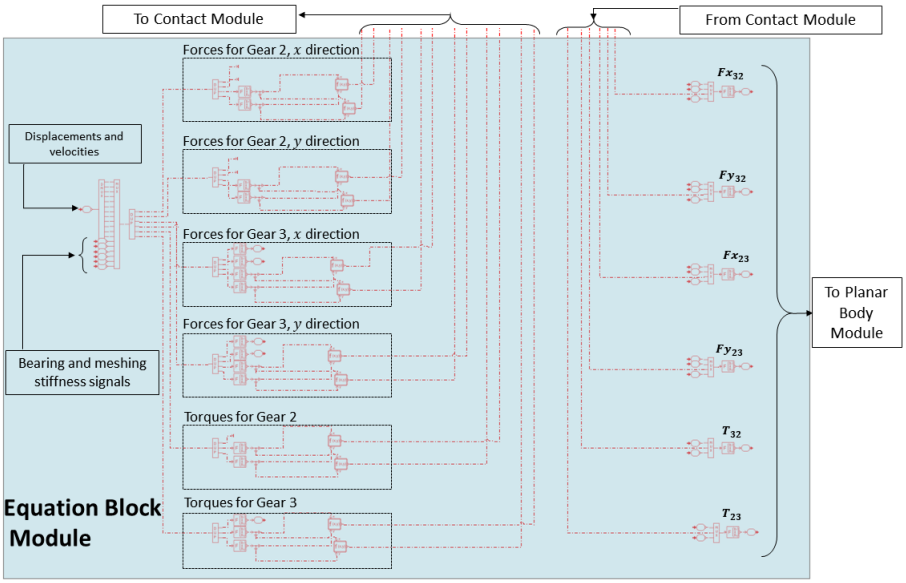

Figure 11: Equation block for an additional gear. It is worth noticing how the viscous and bearing contribution for the previous mesh are erased.

2.4 NUMERICAL ASSESSMENT

In this section a numerical experimental correlation on industrial use case is proposed. Unfortunately, obliged by confidentiality term, the author cannot give any kind of information of the real system specifications. The purpose of this section is to give proof of the accuracy of the model. The system under study is a timing geared system composed of 17 spur gears. The experimental setup is composed of the driveline with a dedicated test rig designed to reproduce the actual working condition. The geared-rotor-bearing system is accelerated in a certain speed range and torsional oscillations for different gears are monitored by means of optical encoders. The geartrain is subjected to a low mean value oscillating torque at its output, while it is driven by an electrical motor. The same system is then reproduced in Simcenter AMESim environment. The test rig is modeled by employing sub-models pertaining to 1D Mechanical and Powertrain Libraries. The geartrain is then constructed by following the methodology described in the previous section. The gear mesh stiffness is calculated by employing the method described by Cooley et al. in [30]. The methodology is applied for various mean torque load, in

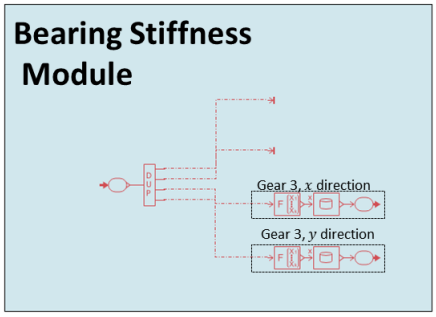

Figure 12: Bearing Stiffness Module for an additional gear. It is worth noticing how the bearing stiffness for the previous gear is erased.

order obtain the stiffness value in varying-load conditions. In the same manner, the load-depended bearing stiffness is computed by means of finite element analysis as depicted in [35]. Damping proportionality coefficients are set on the basis of the author experience. Results are computed by employing a time integration technique based on Runge Kutta method of order 4 and a fixed time step integrator of 10^{-7}s.

The numerical validation is made by matching the combustion engine orders amplitude in terms of angular displacement. In order to accomplish the confidentiality terms, the amplitude and frequency of the acquired signals are both normalized. Figure 14 shows a generic engine order N and its multiple 2N. The comparison is made for nine gears pertaining to the driveline. The experimental outcomes show an excellent agreement with numerical forecasts demonstrating the effectiveness and reliability of the model. As it may be clearly recognized from figure 14, the 2N order amplitude raises considerably by moving from Gear 1 to Gear 9 up to exceed the N order trend. The first gear is closer to the electric motor, while the ninth one is next to the output shaft. The oscillating torque on the lightly loaded transmission provokes vibro-impacts between gear teeth. This dynamic phenomenon occurring during the

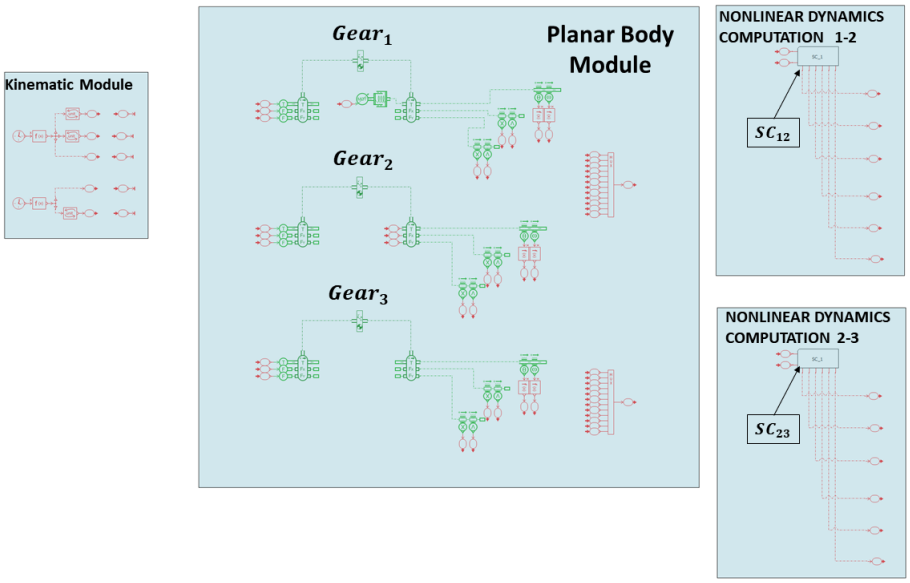

Figure 13: Geartrain model composed by three gears.

experimental test represent an important element captured by the numerical model. In fact, bifurcations appears in the neighborhood of 0.82 normalized frequency. By focusing on Gear 8 and Gear 9 diagrams in figure 14, it is clear the presence of a jump phenomenon, hence, the existence of an unstable solution branch. In particular, by approaching a resonance frequency range, the system dynamics undergoes through an unstable region, characterized by multiple solutions for the same frequency range. For instance, the system would assume a different stable behavior depending on the initial working condition. In fact, figure 14 depicts the dynamic behavior of the geared system when it is accelerated in a certain speed range. The numerical model approximates the real behavior of the transmission system with high fidelity, catching the main nonlinear dynamics phenomena.

In geared transmission systems, their dynamic motion during an increasing velocity condition may be different from the one in deceleration. In order to obtain a complete response function and get the exact position of the bifurcation points, the dynamic motion of the system must be investigated during run up and run down velocity regime. In this regard, run down simulation is performed and results are compared in figure 15. As it may be noticed from figure 15, the jump phenomenon is still present but its location

is changed. This aspect indicates the frequency range which is affected from the multi-valued solution. It is worth to underline that not all the gears are affected from the same instability regions wideness. In fact by focusing the attention on Gear 8 diagram in figure 15, it is possible to notice that the unstable region lasts through the normalized frequency range $0.72 - 0.81$. On the other hand, Gear 4 present a wider frequency range: $0.61 - 0.83$. Unless the run down simulation goes beyond the main purpose of model validation, it was extremely useful to locate the exact position of bifurcation points and the wideness of unstable regions. This aspect is also related to varying load condition. The load depended stiffness may have a significant role in unstable regions determination and the location of the jump phenomenon.

Numerically speaking, to obtain a complete response dynamic function by using Runge Kutta time integration scheme, several simulation may be performed in each working condition. This aspect makes the study of a nonlinear system a very onerous task from a computational point of view. In fact, in order to get a complete scenario of the possible solution for a generic nonlinear system, more suitable numerical techniques may be used. This aspect is deep investigated in the next Chapter. Beside these negative effects, the proposed solution permits an excellent approximation of the system dynamics for a single working condition.

2.5 CONCLUDING REMARKS

The present Chapter proposes a block diagram approach as an effective tool to realize geared transmission system models. By taking advantage from graphical software capabilities, the author gives detailed guidelines to realize any kind of ordinary transmission layout. Firstly, the nonlinear lumped parameter model of a single gear pair is established. The model accounts for backlash non linearity, time-varying and load depended meshing stiffness, load depended bearing stiffness and lubricant squeeze force when teeth detachment occurs. Once the model of a single gear pair is established, a modular architecture is developed in order to construct any geartrain by connecting the pre-programmed element between them. This methodology enhances the use of a modular architecture. In fact, the introduction of such tool in industrial environment may represent a key point to speed up the model setup phase. The model was realized with Simcenter AMESim commercial software. By fo-

cusing on numerical resolution methods, the software is limited to the already implemented numerical computation techniques. For instance, the system of differential equations can be solved only with time integration techniques. This may represent the main limit of the proposed approach. In fact, by studying nonlinear systems, one may be interested in the investigation of unstable regions and bifurcation tracking. Time integration techniques are not suited to perform these kind of analysis as the stable solution of a generic nonlinear system is strongly related to its initial conditions as depicted in the previous section. In this regard, an additional modeling strategy is investigated in the next Chapter.

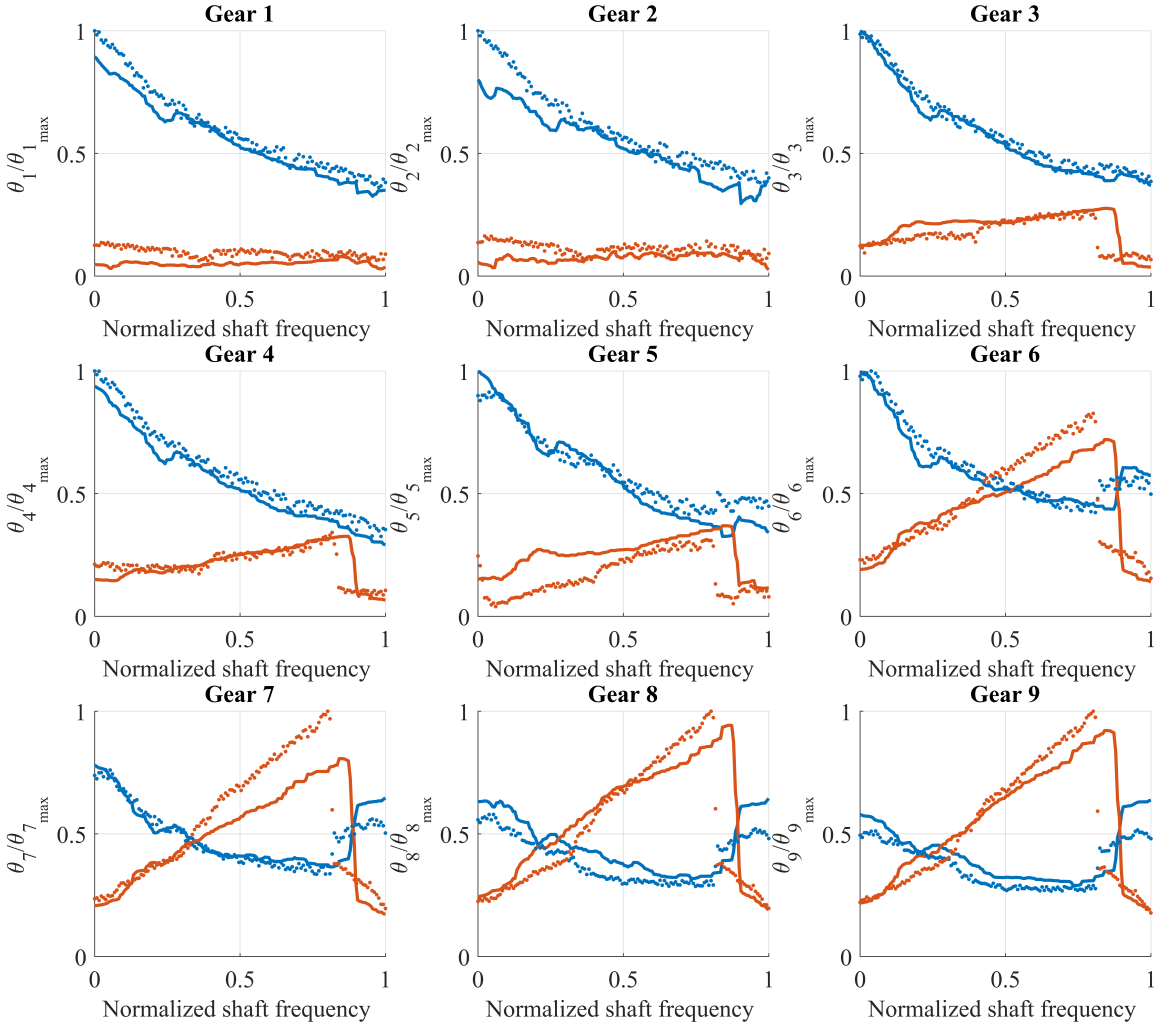

Figure 14: Generic engine order N (blue lines) and its multiple 2N (orange lines). Experimental results are represented by solid lines while numerical outcomes are depicted by dotted lines.

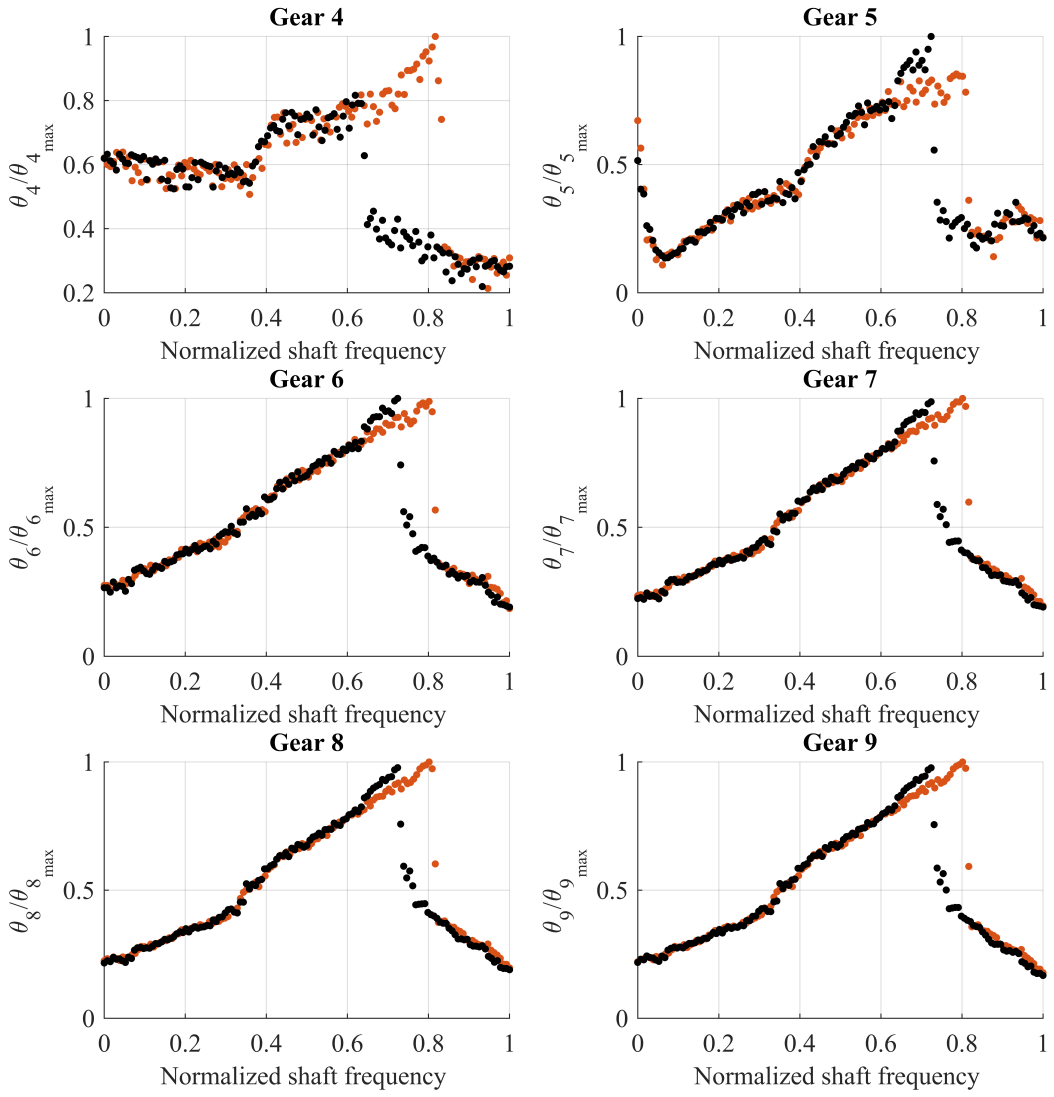

Figure 15: 2N engine order trend. The orange dotted line depicts the run up simulation, while the run down is represented by black dotted line.

3

A TAYLOR SERIES-BASED CONTINUATION METHOD FOR SOLUTION OF NON LINEAR DYNAMICS OF SPUR GEARS

The Chapter proposes the Asymptotic Numerical Method (ANM) combined to the Harmonic Balance Method (HBM) as a valuable approach to solve the nonlinear dynamics of gear pairs. The ANM is a continuation method based on high-order Taylor series expansion of the computed solution branch. The HBM is a periodic solution representation method based on high-order Fourier series. Thanks to a quadratic recast of the equation of motion, the Taylor and Fourier series can be computed in a very efficient way and each step produces a continuous representation of the solution branch making the continuation very robust. By employing this method, the periodic solutions may be easily expressed with respect to both the shaft rotation frequency and the gear mesh frequency as the adoption of a high number of harmonics has negligible effects on the computational burden. Effectiveness and reliability of the method are proved by comparing the numerical results with that obtained from the Runge-Kutta time integration scheme. Afterwards, a comparison in terms of computational efficiency is performed. Finally, some considerations are drawn in order to highlights the main differences between the two methods within gear dynamics computation.

3.1 INTRODUCTION

The mathematical model describing the geared rotor-bearing system dynamics is constituted by a system of ordinary differential equations characterized by a non smooth nonlinearity. In fact, the backlash-induced torsional vibrations may lead to vibro-impacts, generating unstable regions and bifurcations in the dynamic system response. For this reason, many authors focused on gear modeling in order to conduct stability analysis and bifurcations tracking. In the

work presented by Kahraman et al. [6], gear pair dynamics was computed by using two solution methods in order to highlight the main differences between them. The first one is a numerical method, consisting in time integration techniques based on Runge-Kutta scheme. On the other hand, an analytical approximate solution by using the Harmonic Balance Method is proposed. The authors gave evidence that results obtained from time integration techniques in multi-valued region are strongly related to system initial condition. Besides this aspect, the analytical approximate solution constructed with the Harmonic Balance Method is capable to find all stable solution branches. Parker et al. [63] proposed a nonlinear model of a spur gear pair providing comparison between numerical and experimental results. The authors used a combined surface integral/finite element solution method detailed in [64]. Later, Eritenel and Parker [65] realized a three dimensional nonlinear model of a gear pair. They examine the dynamic response of the system taking into account the partial contact loss and three dimensional dynamic displacements. They proved the effectiveness of the model by comparing the numerical results obtained from numerical integration with experimental outcomes. Very recently Wang and Parker [66] gather an analytical solution for resonances and parametric instabilities of a planetary gear set with a general phase. By starting from the resonance suppression rules [67] and modal proprieties [68] they obtained a closed-form amplitude-frequency relation. Theodossiades and Natsiavas [69] introduced a new analytical method to compute periodic motion of a gearpair system and their stability. This methodology combines features of piecewise linear systems involving constant coefficients [70] with perturbation methods considering time-varying coefficients [71].

Different authors investigate the stable and unstable regions of a geared system dynamic response by using continuation methods. Carbonelli et al. [72] combined the finite difference scheme in time domain with an arc-length continuation method to compute the periodic steady state response. Shin and Palazzolo [73] proposed a novel approach to model and analyze the non linear dynamic behavior of geared rotor system supported by journal bearing. Their method allows to compute coexisting, steady-state, autonomous and non-autonomous responses utilizing multiple shooting method and continuation algorithms. Wei et al. [74] used the interval harmonic balance method to solve the nonlinear dynamic problem of gears considering parametric uncertainty. The method was combined with pseudo-arc length continuation with the

Chebyshev inclusion function. Al-shyyab and Kahraman [75], [76] studied the nonlinear dynamic response of a multi-mesh gear system using a multi-term harmonic balance method coupled with discrete Fourier Transforms and a Parametric Continuation scheme. Hilali et al. [77] proposed an implicit high order algorithm based on the coupling of the Asymptotic Numerical Methods (Cochelin et al. [78]) and the implicit Newmark scheme. Mélot et al. [79] examined the effect of gear topology discontinuities on the nonlinear dynamic response of a gear pair. The equation of motion was solved by using the Harmonic Balance Method coupled with alternating frequency-time methods and an arc-length continuation procedure. Besides gear dynamics, similar methods have been applied in literature for the representation of periodic solution of different kind of dynamic systems. They can be time domain methods as shooting [80, 81] and piecewise polynomial orthogonal collocation [82], alternating frequency-time method [83, 84], mixed time and frequency methods [85] and purely frequency domain method with the full harmonic balance [86, 87].

The proposed literature survey demonstrates the wide interest on the solution of the gear dynamics by using continuation methods, as they allow to compute the nonlinear normal modes of geared systems. Usually, all of these methods are based on a predictor corrector procedure where the solution points of the analyzed branch are predicted from a previous solution step. Afterwards a corrector is applied to verify that the corrected solution actually pertains to the solution branch. This is a key common aspect since it makes the continuation of periodic solutions very onerous from a computational point of view. This critical issue does not allow the user to consider an high number of harmonics to approximate the behavior of the dynamic system. This aspect becomes particularly relevant in geared system dynamics as the carrying frequency of the external excitation is usually given by the first orders of the driving shaft rotation frequency. On the other hand, the internal excitation provided by the mesh stiffness and the static transmission error produce harmonics given by the driving shaft rotation frequency times the tooth number and its integer multiples. As a consequence, only high-order methods may be capable to solve the gear dynamics including both internal and external excitation.

In this Chapter the author proposes the solution of the gear pair dynamics by using the Asymptotic Numerical Method combined with the Harmonic

Balance Method. According to his best knowledge, this is the first time that these methods are combined together to solve the complex problem of gear dynamics. The HBM is a frequency domain method which allows to obtain an algebraic system by starting from ordinary differential system of equations. The classical HBM is very simple in its principle, on the other hand when the nonlinearities are strong and a large number of harmonics is required, it can be cumbersome or even impracticable [88]. Cochelin and Vergez [89], give proof that thanks to a quadratic recast of the initial system of equation the HBM can be applied with high efficiency accounting for an high number of harmonics. Once the system of algebraic equations is retrieved, the ANM continuation method is applied. The ANM was firstly described by Cochelin et al [90, 91] and it is based on high-order Taylor series expansion of the computed solution branch. Differently from the other continuation methods, most of the time this procedure does not require a correction step as it can be seen as an high-order predictor. Each step produces a continuous representation of the solution branch making the continuation very robust. This aspect allows the user to consider a very high number of harmonics to represent the behavior of the dynamic system. The continuation of periodic solution can be easily expressed with respect to both the shaft rotation frequency and the gear mesh frequency. As a matter of fact, this method provides the chance to study the effect of high frequency internal excitation in combination with a low frequency external torque. In order to compute the high-order Taylor and Fourier series coefficients of the solution branch in an efficient way, the key point is to adopt a quadratic formalism recasting the system of equations of motion. In fact, as depicted in [92] and [93], the quadratic recast is a part of the method itself for its generality and its performance. By recasting the dynamic system in a quadratic form, the computation of Taylor and Fourier series can be automatized. As a matter of fact, the variety of dynamic systems that may be studied within this procedure are limited only by the necessity of a quadratic expression of the equations. Within this framework, a continuation software was realized [94], able to implement the Asymptotic Numerical Method method by starting from a system of equations where all the nonlinearities are expressed in a quadratic form.

The Chapter is structured as follows. In the following section the elements of the theory on Asymptotic Numerical Method and Harmonic Balance Method are briefly recalled. In Section 3 the nonlinear lumped parameter model of a

spur gear pair with time-varying meshing stiffness and backlash is presented. The system of ordinary differential equation governing the gear dynamics is recast in a quadratic form. The procedure is firstly carry out on a purely torsional model. Afterwards, the same operations are executed on the classical 4 DOFs system, taking into account bearing and shaft compliance. Section 4 is devoted to numerical assessment. Firstly, by using the continuation software Manlab, the periodic solution of the geared system dynamic response are computed. Then, results are compared with that obtained from a well-known time integration technique, i.e. Runge-Kutta scheme. The comparison is performed for the purely torsional model and 4 DOFs model both. In addition, a comparisons in term of computational efficiency have been performed between the Asymptotic Numerical Method and the Runge-Kutta time integration scheme. Afterwards some considerations are drawn to highlights the main differences between the two methods within gear dynamics computation. Eventually, last section is devoted to concluding remarks.

3.2 THE ASYMPTOTIC NUMERICAL METHOD AND THE QUADRATIC FORMALISM

In this section a brief recall of the Asymptotic Numerical Method is presented. The key approach is the quadratic formalism. In fact, by recasting the system of equation in a quadratic form, it is possible to apply in an efficient and general way the Asymptotic Numerical Method. The main idea behind the quadratic recast consists in the introduction of auxiliary variables. The quadratic recast leads to a system of equation where all the nonlinearities are expressed by means of only quadratic terms. Suppose that the original system is in the form :

$$r(x) = 0 \tag{8}$$

where vector x contains all the main variables of the system.

In order to achieve the quadratic reformulation, it is needed to introduce a new system of equations, where the definition of auxiliary variables x_a appears:

$$r_a(x, x_a) = 0 \tag{9}$$

The system which results from eq. 8 and 9 is called the full system of equations:

$$r_f(x_f) = \begin{bmatrix} r_m(x_f) \\ r_a(x_f) \end{bmatrix} \quad with \quad x_f = \begin{bmatrix} x \\ x_a \end{bmatrix} \tag{10}$$

where $r_m(x_f)$ represents the main system in eq. 8 recast quadratically by using auxiliary variables x_a. Once the system has been recast in a quadratic form, it can be written by using a constant operator c, a linear operator l and a bilinear operator q:

$$r_f(x_f) = c + l(x_f) + q(x_f, x_f) \tag{11}$$

It is worth to underline that for the purpose on the current work, the system of equations 8 only involves sum, product and roots operators. By dealing with systems where transcendental functions appear, the quadratic recast is still achievable as explained in [92].

3.2.1 *Taylor series based continuation method*

Once the quadratic formalism has been recalled the main idea behind continuation methods is briefly defined. Consider the algebraic system of equation:

$$r(x, \lambda) = 0 \tag{12}$$

where $x \in \mathbb{R}^n$ is the vector of unknown, $\lambda \in \mathbb{R}$ is a parameter of interest and $r : \mathbb{R}^n \times \mathbb{R} \to \mathbb{R}^n$ is an analytical function of x and λ. Let $U = (x, \lambda)$ be the vector of all the unknows to simplify the notation. The main goal of continuation consists in the computation of solution branches in the space (x, λ) where the system of equations 12 is satisfied. By starting from a known solution point $U_0 = (x_0, \lambda_0)$ the solution branch is continued by searching for other solution from the starting point. The concept of continuation is theoretically justified by a well known mathematical theorem, i.e. the implicit function theorem. It states that, if the Jacobian matrix of r at the point U_0 is invertible, the solution branch in the neighborhood of the starting point U_0 exists and it is unique and regular. Consider U_1 as a tangent vector at U_0, the

solution branch around $U = U_0$ is computed by using a Taylor series with respect to the pseudo arc-length parameter, $a = U_1^t(U_0 - U)$:

$$U(a) = U_0 + aU_1 + a^2U_2 + a^3U_3 + ... + a^NU_N \tag{13}$$

This Taylor series expansion is the base of Asymptotic Numerical Method. Once the eq.12 is recast quadratically, it is written in the form of eq. 10. Then the variable x_f are developed in Taylor series and introduced in the quadratic equations. Afterwards the terms of the same order with respect to a are collected and equated to zero, leading to the following system of equations:

$$\begin{gathered} Order\ 0 : c + l(x_0) + q(x_0, x_0) = 0 \\ Order\ 1 : l(x_1) + q(x_0, x_1) + q(x_1, x_0) = 0 \\ Order\ 2 : l(x_2) + q(x_0, x_2) + q(x_2, x_0) + q(x_1, x_1) = 0 \\ ... \\ Order\ p : l(x_p) + q(x_0, x_p) + q(x_p, x_0) + \sum_{k=1}^{p-1} \left(q(x_k, x_{p-k})\right) = 0 \end{gathered} \tag{14}$$

More detail about the computation of the series are given in [92]. It is worth noticing that thanks to the quadratic recast the computation of Taylor series 13 can be automatized as shown by the system of equations 14. The quadratic recast is part of the method itself as it allows the resolution of a large class of nonlinear dynamic systems.

3.2.2 *The Harmonic Balance Method for ODE*

In this Chapter the Asymptotic Numerical Method is used to compute the periodic solution of ordinary differential equations (ODE). The procedure described in the last subsection can be applied to an algebraic system of equations. By starting from a classical ODE system, the key point is to obtain an algebraic system by applying the well known Harmonic Balance Method. Given an ODE system:

$$\dot{y} = f(t, y, \lambda) \tag{15}$$

where y is an unknown function of the time, λ is a parameter of interest and f is an analytic function, the variable y can be expressed as a truncated Fourier series:

$$y(t) = y_0 + \sum_{k=1}^{H} \left(y_{c_k} \cos(k\omega t) + y_{s_k} \sin(k\omega t)\right) \tag{16}$$

where y_0 is the variable mean value, while y_{c_k} and y_{s_k} are the amplitude related to the $k-th$ harmonic of the cosine and sine respectively. The Harmonic Balance Method working principle is to introduce eq. 16 in eq. 15 and balancing the $2H+1$ harmonic terms. This procedure leads to an algebraic system of $2H+1$ equation where the unknowns are y_0, y_{c_k} and y_{s_k}. It is worth to underline that if eq. 15 has been recast in a quadratic form, the algebraic system obtained after the application of Harmonic Balance Method is already quadratic. It means that its periodic solutions can be continued with the Asymptotic Numerical Method as explained in 3.2.1

3.3 NONLINEAR DYNAMIC MODEL

In this section the nonlinear lumped parameter model of a single gear pair is recalled. The equation governing the motion of the system is rewritten in a dimensionless form. After the non-dimensionalization procedure the equation is recast in a quadratic form in order to be solved with the Asymptotic Numerical Method as explained in the previous section. The procedure is firstly executed on a purely torsional model. Afterwards, the same operations are carried out on the classical 4 DOFs system, taking into account bearing and shaft compliance. For the sake of clearness, differently from the model introduced in the previous Chapter, the load varying mesh and bearing stiffness as well as the squeeze force are not considered here. In addition, in order to simplify the quadratic recast a constant damping coefficient is adopted.

3.3.1 *Gear pair purely torsional model*

In this subsection the nonlinear lumped parameter model of a single degree of freedom gear pair is recalled. Figure 16 shows the schematic representation of the dynamic system. Gears are mounted on rigid shafts and bearings. One degree of freedom is assigned to each gear, namely θ_i. The gear mesh is described by a backlash clearance x_b, a time-varying mesh stiffness $k_m = k_m(t)$ and a viscous damping c_m.

Before analyzing the nonlinear system dynamics, a focus on linearized equations is needed. In fact the two degrees of freedom may be combined to obtain a single degree of freedom system, as a rigid motion occurs when $\theta_2 = \frac{R_1}{R_2}\theta_1$.

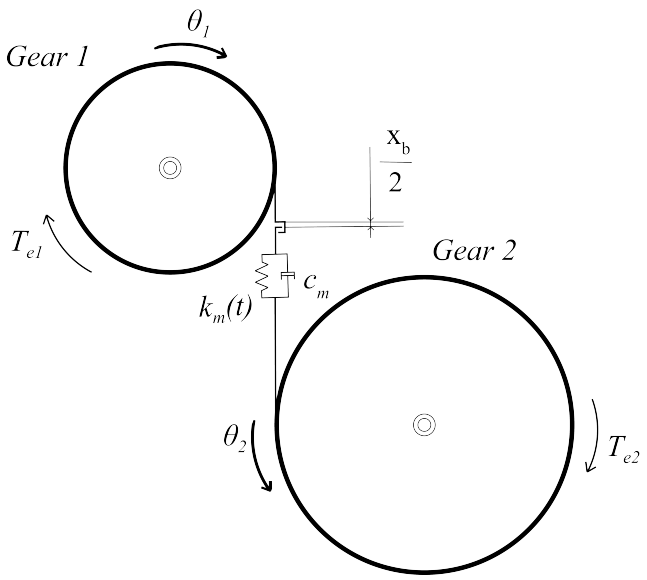

Figure 16: Torsional lumped parameter model of a gear pair

The motion of the system is described by the system of equations:

$$\begin{cases} J_1\ddot{\theta_1} + c_m R_1(R_1\dot{\theta_1} - R_2\dot{\theta_2}) + k_{m0}R_1(R_1\theta_1 - R_2\theta_2) = T_e 1 \\ J_2\ddot{\theta_2} - c_m R_2(R_1\dot{\theta_1} - R_2\dot{\theta_2}) - k_{m0}R_2(R_1\theta_1 - R_2\theta_2) = -T_{e2} \end{cases} \tag{17}$$

where k_{m0} is the mean value of meshing stiffness, J_i represents the inertia, R_i is the base radius and T_{ei} is the external torque applied to gear i, with $i = 1, 2$. In order to focus the attention on the internal excitation, external torques on each gear are set as constant terms. Eq. 1 and 2 of system 17 may be reduced to one single equation in terms of x_r, which is defined as dynamic transmission error [15].

$$x_r = R_1\theta_1 - R_2\theta_2 \tag{18}$$

By replacing eq. 18 into system 17 and combining the two equations together, one may obtain:

$$m_{eq}\ddot{x_r} + c_m\dot{x_r} + k_{m0}x_r = F_e \tag{19}$$

Where $m_{eq} = \frac{1}{R_1^2/J_1+R_2^2/J_2}$ represents the equivalent gear pair mass, and $F_e = \frac{T_{e1}R_1/J1+T_{e2}R_2/J2}{R_1^2/J_1+R_2^2/J_2}$ is the average force transmitted through the mating teeth. In order to represent the nonlinear features, time varying meshing stiffness and backlash clearance are inserted into the model. Gear teeth contact loss is modeled by a nonlinear non-analytic function $f_{nl}(t)$. It can be defined as a piecewise linear function:

$$f_{nl}(t) = \begin{cases} [(x_r - x_b/2)] & \text{if } x_r > x_b/2 \\ 0 & \text{if } |x_r| \leqslant x_b/2 \\ [(x_r + x_b/2)] & \text{if } x_r < -x_b/2 \end{cases} \tag{20}$$

The equation of motion is now reformulated as:

$$m_{eq}\ddot{x_r} + c_m\dot{x_r} + k_m(t)f_{nl}(t) = F_e \tag{21}$$

Once the contact function has been defined, a non-dimensionalization procedure is applied to eq. 21. The starting point is the introduction of the dimensionless time, i.e. $\tau = \omega_n t$ where ω_n is the eigenvalue of the eq. 19 and its value is $\omega_n = \sqrt{k_{m0}/m_{eq}}$.

$$m_{eq}\omega_n^2\ddot{x_r} + c_m\omega_n\dot{x_r} + k_m(\tau)f_{nl}(\tau) = F_e \tag{22}$$

At this point two more steps are necessaries for the fulfillment of the dimensionless procedure. First a new variable is introduced, $x = \frac{x_r}{x_b/2}$, then eq. 22 is divided by the mean value of meshing stiffness k_{m0}.

$$\ddot{x} + 2\zeta\dot{x} + \frac{k_m(\tau)}{k_{m0}}f'_{nl}(\tau) = F \tag{23}$$

Where $F = \frac{F_e}{k_{m0}xb/2}$ is the dimensionless average force between teeth, parameter $\zeta = \frac{c_m}{2m_{eq}\omega_n}$ represents the modal damping factor and $f'_{nl}(\tau)$ can be expressed as follows:

$$f'_{nl}(\tau) = \begin{cases} [(x-1)] & \text{if } x > 1 \\ 0 & \text{if } |x| \leqslant 1 \\ [(x+1)] & \text{if } x < -1 \end{cases} \tag{24}$$

In order to perform a full quadratic recast, a regularization technique is applied to the non-smooth nonlinearity to obtain an analytical function. Eq. 24 can be smoothed by the irrational equation:

$$f'_{nl}(\tau) \approx \left(x + \frac{1}{2}\left(\sqrt{(x-1)^2 + 4\eta^2} - \sqrt{(x+1)^2 + 4\eta^2} \right) \right) \tag{25}$$

The parameter η represents the smoothing factor. Figure 17 shows a comparison between the nonlinear contact function computed with eq. 24 and eq. 25 for different value of η.

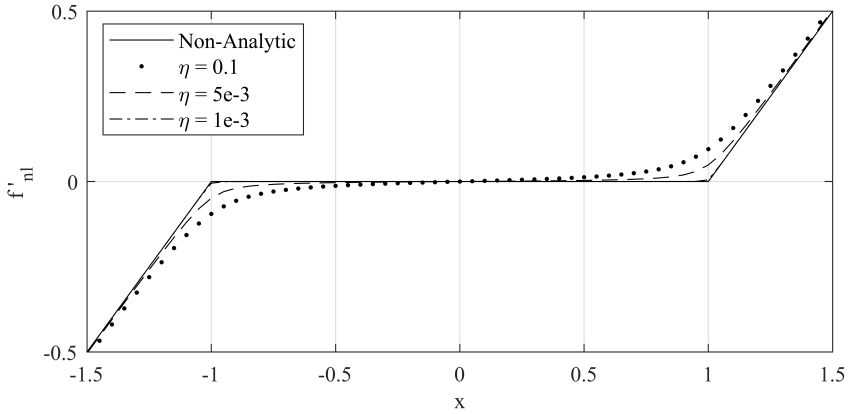

Figure 17: Nonlinear contact function. The curve related to $\eta = 1e-3$ is almost overlapped with the non analytical definition

Once the contact function has been smoothed the final form of the equation of motion yields to:

$$\ddot{x} + 2\zeta\dot{x} + \frac{k_m(\tau)}{k_{m0}}\left(x + \frac{1}{2}\left(\sqrt{(x-1)^2 + 4\eta^2} - \sqrt{(x+1)^2 + 4\eta^2} \right) \right) = F \tag{26}$$

which now has a suitable form for the quadratic recast of the system. Meshing stiffness is a periodic function whose angular pulsation is $\Omega_m = z\Omega_s$, where Ω_s is the shaft rotational velocity and z is the number of teeth of the considered gear. As a matter of fact, it may be expressed by means of a truncated Fourier series:

$$k_m(\tau) = k_{m0} + \sum_{k=1}^{H} k_{mc_k} \cos\left(k\frac{\Omega_m}{\omega_n}\tau\right) + k_{ms_k} \sin\left(k\frac{\Omega_m}{\omega_n}\tau\right) \tag{27}$$

k_{mc_k} and k_{ms_k} are the amplitude of the $k-th$ harmonic of meshing stiffness related to cosine and sine respectively.

In order to make the continuation for the computation of periodic solution by using the Asymptotic Numerical Method, the equation must be written in a quadratic form as depicted in section 3.2. The only expression which is not in a quadratic form is the smoothed function. Auxiliary variable are introduced:

$$r_a = \begin{cases} v_{a1}^2 = (x-1)^2 + 4\eta^2 \\ v_{a2}^2 = (x+1)^2 + 4\eta^2 \end{cases} \tag{28}$$

The time varying mesh stiffness represents the internal excitation of the system and it is considered as an external variable whose periodicity is assigned. Equation 28, together with Eqs. 26 and 27, leads to the equation system in its final form:

$$r_f = \begin{cases} y = \dot{x} \\ \dot{y} + 2\zeta y + v(x + \frac{1}{2}(v_1 - v_2)) = F \\ v = 1 + \sum_{k=1}^{H} \frac{k_{mc_k}}{k_{m0}} \cos\left(k\frac{\Omega_m}{\omega_n}\tau\right) + \frac{k_{ms_k}}{k_{m0}} \sin\left(k\frac{\Omega_m}{\omega_n}\tau\right) \\ v_1^2 = (x-1)^2 + 4\eta^2 \\ v_2^2 = (x+1)^2 + 4\eta^2 \end{cases} \tag{29}$$

3.3.2 *Gear pair complete lumped parameter model*

In this subsection the dynamic model of a gear pair with compliant bearings is established. Figure 18 shows a schematic representation of the system

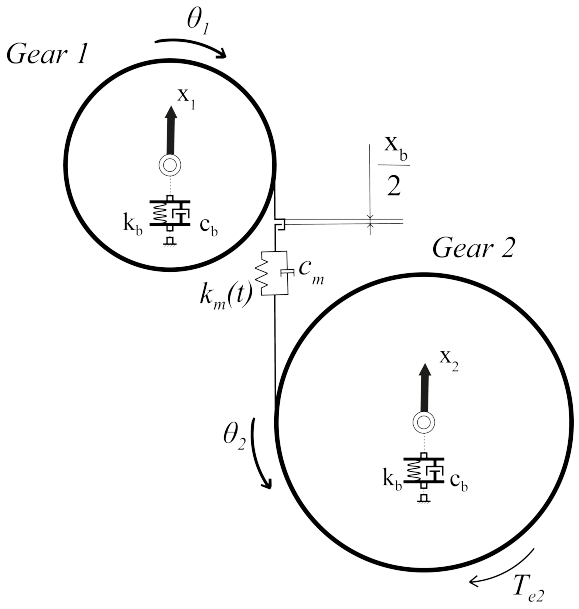

Figure 18: Lumped parameter model of a gear pair with compliant bearing

layout. Gears are mounted on compliant bearings whose stiffness yields k_b and damping coefficient c_b. Two degrees of freedom are assigned to each gear, namely θ_i and x_i. The gear mesh is described by a backlash clearance x_b, a time-varying mesh stiffness $k_m = k_m(t)$ and a viscous damping c_m. In order to analyze the effects of internal excitation on system dynamics, the prime mover is connected to the frame by means of a torsional spring, whose stiffness value is k_t and its damping coefficient is c_t. The equation of motion of the gear pair yields to:

$$\begin{cases} m_1\ddot{x_1} + c_b\dot{x_1} + k_b x_1 - c_m\dot{x_r} - k_m(t)f_{nl}(t) = 0 \\ J_1\ddot{\theta_1} + c_t\dot{\theta_1} + k_t\theta_1 + R_1 c_m\dot{x_r} + R_1 k_m(t)f_{nl}(t) = 0 \\ m_2\ddot{x_2} + c_b\dot{x_2} + k_b x_2 + c_m\dot{x_r} + k_m(t)f_{nl}(t) = 0 \\ J_2\ddot{\theta_2} - R_2 c_m\dot{x_r} - R_2 k_m(t)f_{nl}(t) = -T_{e2} \end{cases} \tag{30}$$

where $f_{nl}(t)$ has been defined in eq. 20 and x_r is the dynamic transmission error:

$$x_r = R_1\theta_1 - R_2\theta_2 + x_2 - x_1 \tag{31}$$

As the single-degree-of-freedom model, a non-dimensionalization procedure is applied to system of equation 30. This procedure is slightly different from that related to one DOF system. The system in figure posses four DOFs, i.e. four eigenvalues and eigenvectors are computed. After the modal analysis on linearized system the last eigenvalue, namely ω_{n4}, is used to obtain the dimensionless time. Afterwards the two variables are introduced: $\chi_i = \frac{x_i}{x_b/2}$ and $\vartheta_i = \frac{\theta_i}{x_b/2}$. The introduction of the latter allows the expression of a dimensionless transmission error, namely $\chi_r = R_1\vartheta_1 - R_2\vartheta_2 + \chi_2 - \chi_1$. At this point the nonlinear contact function can be reformulated as in eq. 24 providing the substitution of x with χ_r. The latter is then smoothed in the same manner adopting the irrational equation:

$$f'_{nl}(\tau) \approx \left(\chi_r + \frac{1}{2}\left(\sqrt{(\chi_r - 1)^2 + 4\eta^2} - \sqrt{(\chi_r + 1)^2 + 4\eta^2}\right)\right) \tag{32}$$

Now, by introducing the dimensionless time, replacing χ_i, ϑ_i and eq. 32 into system of equation 30 the final dimensionless form of the equation of motion is:

$$\begin{cases} \frac{m_1\omega_{n4}^2}{k_{m0}}\ddot{\chi_1} + \frac{c_b\omega_{n4}}{k_{m0}}\dot{\chi_1} + \frac{k_b}{k_{m0}}\chi_1 - \frac{c_m\omega_{n4}}{k_{m0}}\dot{\chi_r} - \frac{k_m(\tau)}{k_{m0}}f'_{nl}(\tau) = 0 \\ \frac{J_1\omega_{n4}^2}{R_1k_{m0}}\ddot{\vartheta_1} + \frac{c_t\omega_{n4}}{R_1k_{m0}}\dot{\vartheta_1} + \frac{k_t}{R_1k_{m0}}\vartheta_1 + \frac{c_m\omega_{n4}}{k_{m0}}\dot{\chi_r} + \frac{k_m(\tau)}{k_{m0}}f'_{nl}(\tau) = 0 \\ \frac{m_2\omega_{n4}^2}{k_{m0}}\ddot{\chi_2} + \frac{c_b\omega_{n4}}{k_{m0}}\dot{\chi_2} + \frac{k_b}{k_{m0}}\chi_2 + \frac{c_m\omega_{n4}}{k_{m0}}\dot{\chi_r} + \frac{k_m(\tau)}{k_{m0}}f'_{nl}(\tau) = 0 \\ \frac{J_2\omega_{n4}^2}{R_2k_{m0}}\ddot{\vartheta_2} - \frac{c_m\omega_{n4}}{k_{m0}}\dot{\chi_r} - \frac{k_m(\tau)}{k_{m0}}f'_{nl}(\tau) = -\frac{T_{e2}}{\frac{x_b}{2}k_{m0}R_2} \end{cases} \tag{33}$$

The system 33 can now be recast in a quadratic form by introducing the auxiliary variables defined in eq. 28 where the variable x is replaced by χ_r. The final system in quadratic form is :

$$
r_f = \left\{ \begin{array}{c}
\nu_{\chi_1} = \dot{\chi_1} \\
\frac{m_1\omega_{n4}^2}{k_{m0}}\dot{\nu_{\chi_1}} + \frac{c_b\omega_{n4}}{k_{m0}}\nu_{\chi_1} + \frac{k_b}{k_{m0}}\chi_1 - \frac{c_m\omega_{n4}}{k_{m0}}\dot{\chi_r} - \nu_k(\chi_r + \frac{1}{2}(\nu_{a1} - \nu_{a2})) = 0 \\
\nu_{\vartheta_1} = \dot{\vartheta_1} \\
\frac{J_1\omega_{n4}^2}{R_1k_{m0}}\dot{\nu_{\vartheta_1}} + \frac{c_t\omega_{n4}}{R_1k_{m0}}\nu_{\vartheta_1} + \frac{k_t}{R_1k_{m0}}\vartheta_1 + \frac{c_m\omega_{n4}}{k_{m0}}\dot{\chi_r} + \nu_k(\chi_r + \frac{1}{2}(\nu_{a1} - \nu_{a2})) = 0 \\
\nu_{\chi_2} = \dot{\chi_2} \\
\frac{m_2\omega_{n4}^2}{k_{m0}}\dot{\nu_{\chi_2}} + \frac{c_b\omega_{n4}}{k_{m0}}\nu_{\chi_2} + \frac{k_b}{k_{m0}}\chi_2 + \frac{c_m\omega_{n4}}{k_{m0}}\dot{\chi_r} + \nu_k(\chi_r + \frac{1}{2}(\nu_{a1} - \nu_{a2})) = 0 \\
\nu_{\vartheta_2} = \dot{\vartheta_2} \\
\frac{J_2\omega_{n4}^2}{R_2k_{m0}}\dot{\nu_{\vartheta_2}} - \frac{c_m\omega_{n4}}{k_{m0}}\dot{\chi_r} - \nu_k(\chi_r + \frac{1}{2}(\nu_{a1} - \nu_{a2})) = -\frac{T_{e2}}{\frac{x_b}{2}k_{m0}R_2} \\
\chi_r = R_1\vartheta_1 - R_2\vartheta_2 + \chi_2 - \chi_1 \\
\nu_k = 1 + \sum_{k=1}^{H} \frac{k_{mc_k}}{k_{m0}}\cos\left(k\frac{\Omega_m}{\omega_n}\tau\right) + \frac{k_{ms_k}}{k_{m0}}\sin\left(k\frac{\Omega_m}{\omega_n}\tau\right) \\
\nu_{a1}^2 = (\chi_r - 1)^2 + 4\eta^2 \\
\nu_{a1}^2 = (\chi_r + 1)^2 + 4\eta^2
\end{array} \right. \tag{34}
$$

3.4 NUMERICAL ASSESSMENT

In this section numerical experiments are performed. Firstly the nonlinear dynamics of the described models is computed with the Asymptotic Numerical Method by using Manlab software. The same lumped parameter models are established in AMESim environment by following the procedure described in Chapter 2 and their dynamics is computed with a fixed time step integrator based on a 4th order Runge-Kutta method. Finally, the results coming from the two solution methods are compared for the purely torsional model and the 4 DOFs model both. In addition, a comparisons in term of computational performance is conducted and some considerations are drawn on the use of the Asymptotic Numerical Method to represents the gear vibration in radial direction. The continuation is performed with respect to the dimensionless frequency $\frac{\Omega_m}{\omega_n}$, considering 400 harmonics, i.e. 8 harmonics of gear mesh frequency as the prime mover has 50 teeth. The lumped parameter model has

been constructed by employing the gear data used by Melot et al. in [79]. Gear characteristics are shown in Tab. 1. Gear mesh stiffness has been approximated by using 8 harmonics. Figure 19 shows a comparison between the meshing stiffness calculated by Melot et al. [79] and the approximation derived from an eight-term truncated Fourier series. By focusing the attention on the purely torsional model, Figure 20 depicts the root mean square value (RMS) of the transmission error at different shaft speed rotation, $\Omega_s = \Omega_m/z_1$.

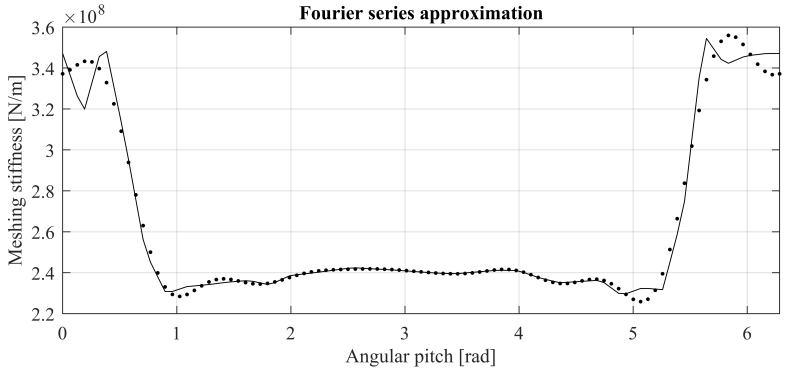

Figure 19: Meshing stiffness calculated by Melot et al. [79] (solid line) and its approximation derived from an eight-term truncated Fourier series (dotted line)

The results show a stable behavior when teeth are always in contact up to 4700 rpm, where the first bifurcation appears. In fact, by observing the results obtained with Runge-Kutta technique, the presence of a jump phenomenon is clearly recognized. On the other hand, the results obtained with Asymptotic Numerical Method shows the existence of an unstable branch. As a matter of fact in the speed range 4800-5800 rpm contact loss occurs. The stable regime of vibro-impact lasts up to 5800 rpm. Figure 21 shows the time domain evolution signal in different frequency range: under the resonance, along the stable vibro-impacts branch and over the resonance. It is worth noticing how the two solution methods are in agreement.

Once the method has been established and validated for the single degree-of-freedom system, the same procedure is executed for a gear pair with compliant shaft and bearings. Results related to the RMS of the 4 DOFs system transmission error are shown in figure 22. As for the single-degree-of-freedom system, one may recognize the presence of the jump phenomenon. Time integration techniques allow the computation of stable solution branches and bifurcations

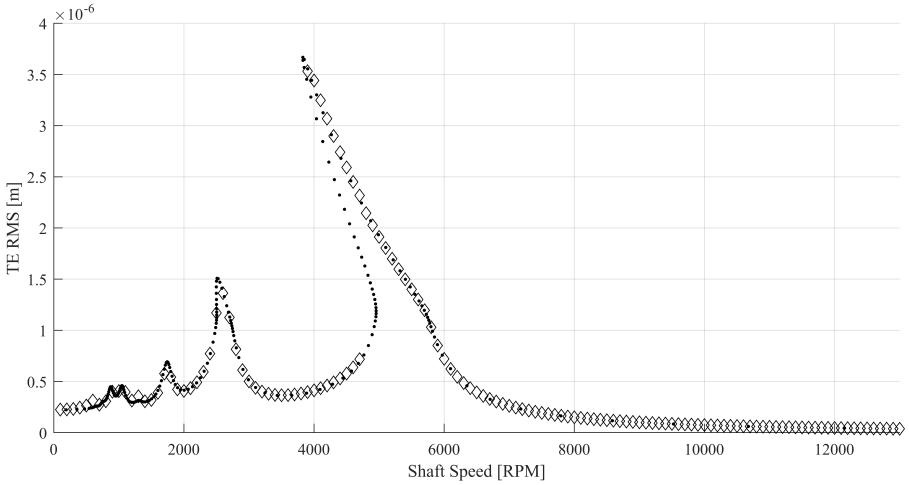

Figure 20: Root mean square of transmission error computed with the Runge-Kutta time integration scheme (diamond line) and Asymptotic Numerical Method (dotted line)

location. On the contrary, the Asymptotic Numerical Methods execute the computation of the unstable branch solution points, which are not captured by the Runge Kutta integration scheme. While time domain signals are compared in figure 23, 24, 25. In particular, figure 23 depicts the transmission error comparison at different rotational speed, while figure 24 and 25 show the radial displacement of gear 1 and 2 respectively. It is worth noticing how the results are in agreement at low speed as well as at high shaft rotational speed. As a matter of fact, the number of harmonics chosen for the representation of the dynamic model, allows to capture high frequency phenomena as depicted by the numerical signals. The computational time ratio, on a standard workstation, of Runge Kutta time integration scheme over Asymptotic Numerical Method is 95:1. In addition it may be underlined that the choice of an high number of harmonics to approximate the dynamics of the system, drastically affects the ANM computational performance. Nonetheless, it is 95 times faster than Runge Kutta time integration scheme, providing for excellent computational performance. Moreover, the ANM allows a continuous representation of the dynamic system response. By observing figures 20 and 22, each point obtained from the Runge Kutta method is chosen by the user, which perform the steady state simulation at a certain shaft speed. No information of dynamic system

Parameters	**Gear 1**	**Gear 2**
Mass [kg]	1.11	1.11
Mass moment of inertia [kgm^2]	0.0015	0.0015
Module [mm]	3	
Number of teeth	50	50
Pressure angle [deg]	20	
k_b bearing stiffness [N/m]	2e+8	2e+8
c_m meshing damping coefficient [kg/s]	950	
c_b bearing damping coefficient [kg/s]	300	
k_t torsional stiffness [Nm/rad]	1000	
c_t torsional damping coefficient [kg/s]	0.1	

Table 1: Design parameters

response can be gained between a solution point and another. On the other hand, the ANM provide for the extraction of the harmonic response in the whole frequency range. It must be underlined that the Asymptotic Numerical Method allows the user to obtain a better computational performance as the results are computed in frequency domain. Thanks to the quadratic recast, the Taylor series is computed in a very efficient way even if the number of harmonics chosen to represent the system dynamics is very high. On the other hand additional time is needed to rearrange the equation of motion by applying a dimensionless procedure and the quadratic recast. Beside this aspect, the power of the Asymptotic Numerical Method continuation method rely on the possibility to continue the periodic solution of a dynamic system with respect to an arbitrary parameter of interest as damping or stiffness. The simulations performed in the present work show a stable vibro-impact behavior when shaft speed is around 6000-8000 RPM. By observing figure 23, one may notice that only single-side impact occurs. In fact, when teeth are in contact on working flank the transmission error x_r is defined along the *Direct Line of Action*, as depicted in eq. 31. On the other hand, referring to eq. 20, when $x_r < -x_b/2$, the meshing force is transmitted along the *Back-side Line of Action*. As a matter of fact, the definition of the dynamic transmission error

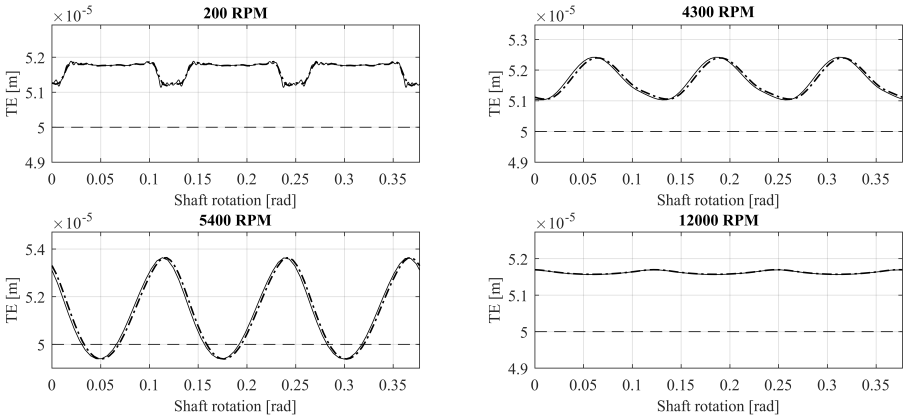

Figure 21: Transmission error computed with Runge Kutta time integration scheme (solid line) and transmission error computed with the Asymptotic Numerical Method (dash-dotted line). The dashed line represents half of the backlash value.

depends on which side of the tooth contact occurs. When gears are in contact on *Back-side Line of Action*, the expression of transmission error yields:

$$x_r = -R_1\theta_1 + R_2\theta_2 - x_1 \sin\varphi - y_1 \cos\varphi + x_2 \sin\varphi + y_2 \cos\varphi \tag{35}$$

where φ is the angle between y axis and the *Back-side Line of Action*. This aspect can be easily implemented with the Runge Kutta time integration scheme, where, by using a piece-wise linear non-analytic function, the definition of x_r can be changed at any time step. By working with the ANM coupled with the HBM, a definition of an analytical function in a quadratic form is needed. This aspect makes the modeling of radial dynamics a challenging task when double-sided impacts occurs. In fact, in case of bilateral impacts, more suitable numerical techniques may be employed. As an example the ANM may be combined with polynomial collocation techniques which allows the definition of the nonlinear contact function as a piece-wise linear non-analytic function. The employment of this technique will be investigated in the future and may represent the basis of further works. Beside this, the proposed methodology is an effective and reliable way to represent in a correct manner the complete dynamics of a gear pair when single sided impacts occurs. It is worth to underline that this phenomena only affect radial dynamics, any consideration about the torsional behavior of the system remains valid.

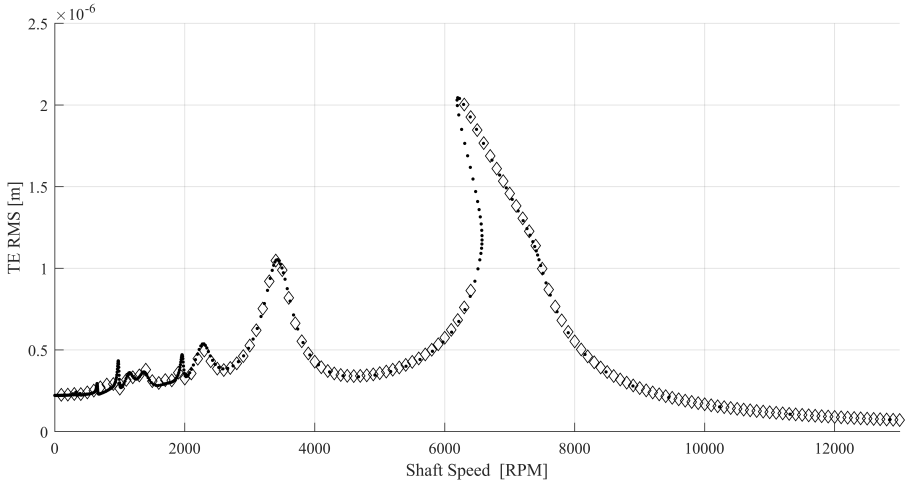

Figure 22: Root mean square of transmission error computed with the Runge Kutta time integration scheme (diamond line) and Asymptotic Numerical Method (dotted line)

3.5 CONCLUDING REMARKS

The Chapter is devoted to the application of the Asymptotic Numerical Method and the Harmonic Balance Method for the resolution of the nonlinear dynamics of a gearpair. In a first instance, the state of the art on the current methodologies is investigated. Among all the existing methods, it is characterized by an high efficiency in the computation of high-order Taylor and Fourier series. Usually, all the employed methods for the resolution of the nonlinear dynamics of a generic system, use a predictor corrector procedure for which the solution points are predicted from a previous solution step. Afterwards, a corrector is applied to verify that the corrected solution pertains to the solution branch. On the other hand, the Asymptotic Numerical Method can be seen as an high-order predictor, as most of the time, it does not require a correction step. In Section 3.2, a brief explanation of the method and its effectiveness is presented. Moreover it is shown how the adoption of a quadratic formalism to recast the equation of motion is useful for the computation of high-order Taylor series. This feature allows the user to consider an high number of harmonics to approximate the system response. Within geared system dynamics, this aspect

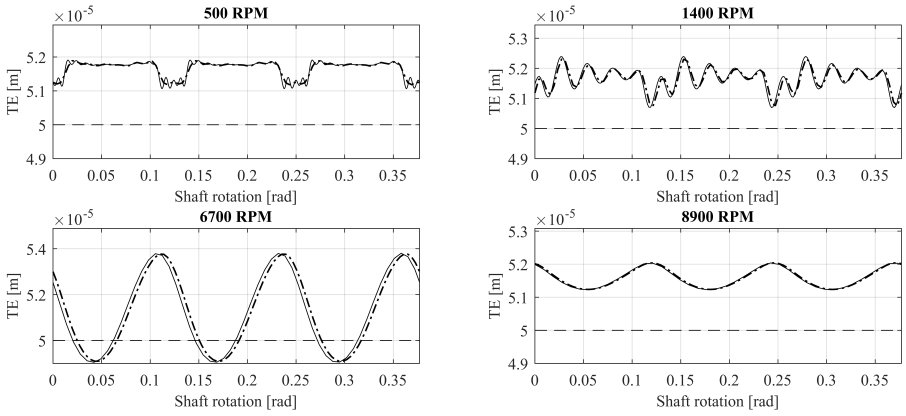

Figure 23: Transmission error computed with Runge Kutta time integration scheme (solid line) and with Asymptotic Numerical Method (dash-dotted line). The dashed line represents half of the backlash value.

become more relevant as it is possible to study the effect of internal excitation at high frequency and the effect due to low frequency external torque.

In Section 3.3, a nonlinear lumped parameter model of a spur gear pair with time-varying meshing stiffness and backlash is established. The system of equation is recast in a quadratic form in order to be solved with the Asymptotic Numerical Method. The quadratic recast is firstly conducted on a purely torsional system and successively on the classical 4 DOFs system where the bearing and shaft compliance are considered. In Section 3.4, the periodic solution of geared systems are computed by implementing the quadratic equations in Manlab continuation software. A comparison between the two solution methods in terms of computational performance is conducted. The Asymptotic Numerical Method is faster than Runge-Kutta time integration scheme, as the first one works in frequency domain. As proved by the numerical simulation, the adoption of an high number of harmonics does not represent a critical aspect. Thanks to the quadratic formalism, the high-order Taylor series can be computed in a very efficient way. On the contrary, additional time is needed to rearrange the equation of motion in a quadratic form, while this is not needed when employing the Runge-Kutta time integration scheme. Within geared system dynamics, the real limit of the Asymptotic Numerical Method coupled with the Harmonic Balance Method is represented by the necessity to express the nonlinear contact function as an analytical smoothed one. In fact,

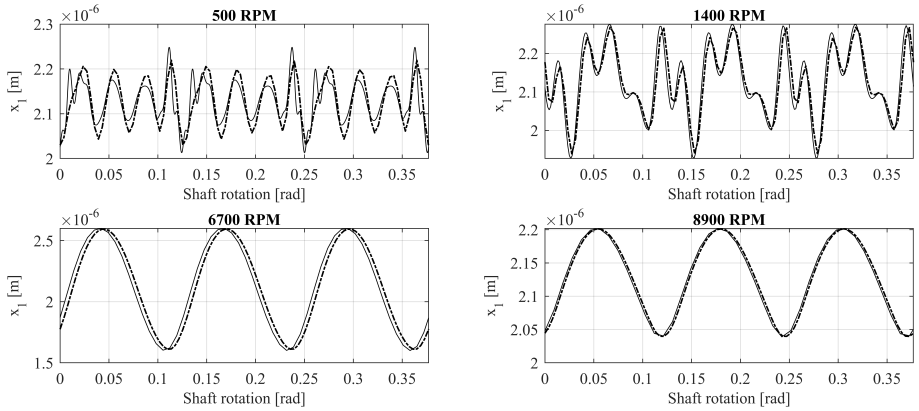

Figure 24: Radial displacement of gear 1, x_1, computed with Runge Kutta time integration scheme(solid line) and with Asymptotic Numerical Method (dash-dotted line)

when double-sided impacts occur, the transmission of forces takes place on the *Back-side Line of Action*. This aspect can lead to an erroneous estimation of bearing reaction forces as the definition of dynamic transmission error assumes a different expression. Despite the radial dynamics can not be correctly forecast when back side impact takes place, it must be underlined that the torsional dynamics is not affected by this aspect. In order to overcome this particular issue, different numerical techniques may be adopted. In particular the ANM may be coupled with the polynomial collocation method, which permits the definition of the nonlinear contact function as a piece-wise linear non-analytic function.

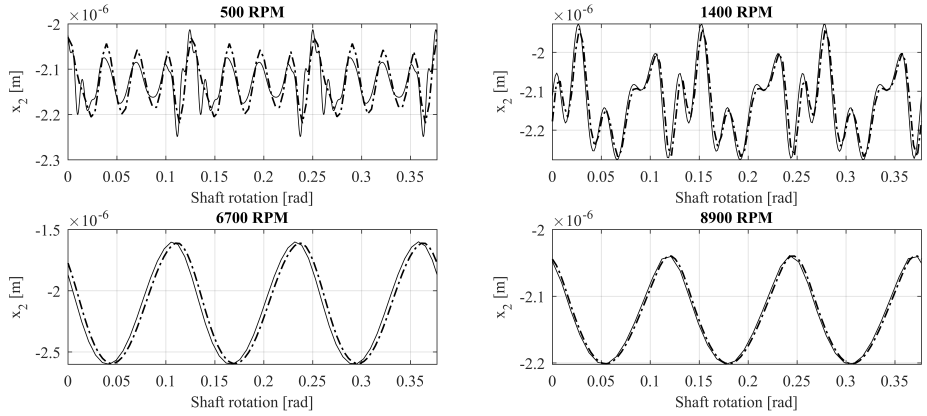

Figure 25: Radial displacement of gear 2, x_2, computed with Runge Kutta time integration scheme(solid line) and with Asymptotic Numerical Method (dash-dotted line)

4

A RATTLE INDEX FORMULATION FOR SINGLE AND MULTIPLE BRANCH GEARTRAINS

The Chapter proposes an analytical procedure for the generalization of the rattle index in any type of ordinary transmission layouts, single or multiple branch, both in idle and loaded conditions. Its definition is obtained by a recursive analytical formulation of the rotational dynamics of gears. Numerical analytical studies are exploited to examine the effectiveness and reliability of the introduced index. Several geartrain layouts are investigated and results show its capability to instantaneously describe the vibro-impact events related to any gear pair of the driveline. Moreover, the general definition is shown to be a proper indicator of the potential presence of mutual interactions between different gear pairs pertaining to the same driveline. The analysis of the results reveals an excellent agreement with the expected behavior of the outlined parameter.

4.1 INTRODUCTION

Rattle noise phenomenon has been the subject of numerous investigations due to its occurrence in idle gear dynamics. As an example, the oscillating torque generated by the irregularity of the internal combustion engine provokes impacts between the teeth of all the unloaded gears in manual transmission. More generally, any geartrain subjected to low mean value oscillating torque is willing to teeth detachment and consequent vibro-impacts. For this reason, many authors focused their attention to the development of non-linear models with the purpose to investigate rattle noise phenomenon and its relation with other mechanical components of the entire power transmission. Different solutions have been proposed to reduce or eliminate the emission of rattle noise in multispeed gearboxes. Bozca [95] studyed the influence of the geometric

parameters of the gearbox in particular, the module, number of teeth, axial clearance and backlash, in order to minimize rattle noise. Rigaud et al. [96] investigated rattle occurrence at various operating drag torques and mean rotational speeds. A certain amount of works have been conducted on the application of some devices as multi-stage clutches or dual mass flywheels that aim either to reduce the rattle noise emission or eliminate its occurrence. Shangguan et al. [97] realized a guideline to select clutch's stiffness and damping to limit rattle noise emission for a car at idle. Yoon and Kim [98] investigated rattle phenomena by developing a non-linear model for the multi-staged clutch damper. Brancati et al. [56] developed an analytical model that considers the effects of hysteretic friction in the clutch springs and the oil damping effect between the impacting teeth. The same authors [99] investigated the gear rattle reduction in an automotive driveline due to the adoption of a flywheel with an innovative torsional vibration damper. Miyasato et al. [100] have made a comparison between the effects of changing some clutch parameters with those given by modifying some properties of the system, such as the flywheel inertia, gear backlash, and damping parameters of the gearbox, in order to verify which approach guarantees results with a lower rattle noise level. Another possibility to reduce gear rattle noise is offered by the lubricant oil. Baumann et al. [101] conducted an experimental study on various lubricants, analyzing gear pair dynamics in different elastohydrodynamic conditions stating that rattle noise can be reducted using low traction lubricant. Theodossiades et al. [54, 55] proved that the presence of lubricant between the impacting teeth interface may act as a non-linear spring-damper system. Fernandez-del-Rincon et al. [53] investigated the calculation of hydrodynamics forces between teeth by following six different formulations under stationary conditions. Diez-Ibarbia et al. [102] analyzed the dynamic behavior of lightly loaded drivelines considering the fluid viscosity influence on hydrodynamic forces under non-stationary conditions. Fietkau et al. [103] examined the influence of different tribological and geometrical parameters on lubrication condition for a rattling and a loaded gear pair.

In geartrain design, the definition of a rattle index can be a powerful tool in order to identify the presence of rattle noise. R. Singh et al. [10] outlined the very first formulation of a parameter function of vibro-impacts occurrence. Considering the idler gear dynamics, an analytical rattle criterion has been given by comparing the dynamic transmission error with backlash. From a

physical point of view, the viscous drag torque generated at the interface idler gear-shaft must be sufficient to overcome the inertial torque to ensure rattle-free transmission . Rust et al. [104] adopted the same principles, by affirming that the gear rattle threshold can be formulated within critical angular acceleration value at which rattle appears. Padmanabhan et al. [105] affirm that the level of noise generated by this phenomenon is strictly related with the acceleration peak amplitude and the decay rate. Two indices are developed to evaluate the performance of any clutch in relation to noise control, one based on the ratio of mean-square values of the angular accelerations and one based on the ratio of the peak to peak values. More recently Slavkovsky et al [106] outlined the relationship between potential energy stored in meshing and rattle noise emission, showing that gears tend to detachment when mesh energy raises and the kinetic angular energy turns down.

Based on the proposed literature review, it is possible to notice that several studies have been focused on the identification of the rattle noise by using mathematical models. However, the investigation has been exclusively focused on idle gear pairs, since this is an unavoidable working condition in multi-speed gearboxes. Despite this may be considered as the most common scenario, the rattle noise phenomenon may also occur in other geartrain applications, such as engine timing systems. In this kind of drivelines, the camshaft motion induces a resistant oscillating torque with a low mean value that provokes vibro-impacts between teeth. The purpose of the current Chapter is to generalize the definition of the Rattle Index (RI) proposed by R. Singh et al. in [10] to any type of transmission, single or multiple branch. The proposed formulation also includes the definition for loaded geartrains. Several configurations of drivelines are investigated with the aim to present the effectiveness and reliability of outlined indices. In a first instance, the generalisation of the equation of motions for a generic geartrain is given. The dissertation is propaedeutic to the definition of a parameter related to rattle noise emission with general applicability. Moreover, simulation results for different geartrain layouts are shown in order to observe the accuracy of the outlined indices. The RI will remain under a certain threshold when gears are in contact on the drive side; as soon as teeth detachment takes place RI will respond with a peak, overcoming threshold value. The proposed study is intended to define a RI which instantaneously describes the vibro-impacts events related to any gear pair of the driveline. The resulting index will outline the tooth detachment of

considered gear pair. An important aspect that will be further discussed, is the comparison between indices related to consecutive meshings. The defined index, highlights that the rotary motion of considered gear pair is affected by vibro-impacts of all driveline.

The Chapter is structured as follows: in the next section the state of the art about the rattle index definition is introduced. Afterwards, the definition of rattle index is formulated for a generic geartrain, single or multiple branch, generalizing the statement for a driveline with an arbitrary number of gears. In section 4.3 rattle index properties are discussed by focusing on the results obtained from different driveline layouts. Eventually, last section is devoted to concluding remarks.

4.2 RATTLE INDICATOR

As described in [10], when gears are continuously in contact on drive side, no rattle emission could occur. Rattle will take place if gears are separated and free to move within the backlash, with a consequent single-sided or double-sided impact on tooth flanks. The double-sided impact involves the opposite flank of the tooth moving the transmission of forces along the *Back-side Line of Action*. In this study the phase shift effect for forward and backward contact is considered by using the same approach defined in [107]. Based on the definition given by R. Singh [10], rattle in a single gear pair will take place under the following condition:

$$x_r(t) : \begin{cases} \leqslant x_b/2 : \text{rattle} \\ > x_b/2 : \text{no rattle} \end{cases} \tag{36}$$

The same criterion can be reformulated in terms of angular acceleration of the driven gear. By considering the idle gear dynamics, $T_{e_2} = 0$ and focusing on the second equation of system in Eq. 1, it is possible to outline the gear mesh force term:

$$f_m = \frac{-J_2\ddot{\theta}_2}{R_2} - \hat{\alpha}\frac{J_2\dot{\theta}_2}{R_2} \tag{37}$$

It has to be noticed that the condition $x_r > x_b/2$ is equivalent to $-J_2\ddot{\theta}_2/R_2 - \hat{\alpha}J_2\dot{\theta}_2/R_2 > 0$ but $-J_2\ddot{\theta}_2/R_2 - \hat{\alpha}J_2\dot{\theta}_2/R_2 = 0$ is not equivalent to $x_r = x_b/2$. In

fact, condition $x_r = x_b/2$ expresses the limit condition in which teeth are in contact, while $-J_2\ddot{\theta}_2/R_2 - \hat{\alpha}J_2\dot{\theta}_2/R_2 = 0$ expresses the free flight motion of gear, i.e. teeth are not in contact. With this assumption the rattle criterion can be reformulated as follows:

$$-J_2\ddot{\theta}_2/R_2 - \hat{\alpha}J_2\dot{\theta}_2/R_2 : \begin{cases} \leqslant 0 : \text{rattle} \\ > 0 : \text{no rattle} \end{cases} \tag{38}$$

Previous works ([107], [56], [10], [108]) limited this consideration to only idle dynamics, where the driven gear is unloaded or lightly loaded by the viscous drag torque. The main purpose of this work is to introduce a rattle criterion suitable for any type of ordinary transmission layouts, single or multiple branch, both in idle and loaded conditions. By focusing on the torsional equation of motion of the driven gear and taking into account the considerations outlined in Eq. 38, it is possible to introduce the Rattle Index for loaded gears:

$$RI(t) = \left| \frac{J_2\ddot{\theta}_2}{\hat{\alpha}J_2\dot{\theta}_2 - T_{e_2}} \right| \tag{39}$$

$$RI(t) : \begin{cases} \geqslant 1 : \text{rattle} \\ < 1 : \text{no rattle} \end{cases} \tag{40}$$

The index defined above is valid for a single gear pair where the driven gear can be loaded or unloaded. It is worth noticing that if $T_{e_2} = 0$ the Eq.40 is equivalent to Eq.38. Furthermore, it should be noted that Eqs.38, 39 and 40 do not depend on gear velocity ratio τ and contact ratio ϵ.

It is worth to describe how the inequalities have been handled to determine the rattle index and the relative rattle criterion. By assigning a positive rotation of driver gear $\theta_1 > 0$, then gear 2 rotation will be negative, i.e. $\theta_2 < 0$. The meshing torque applied on gear 2 will have a negative sign as long as teeth are in contact on drive side tooth flank. The meshing torque sign will change, passing through zero, when $x_r \leqslant x_b/2$. Starting from inequation $-J_2\ddot{\theta}_2/R_2 - \hat{\alpha}J_2\dot{\theta}_2/R_2 \leqslant 0$, it is then possible to obtain the rattle criterion:

$$-J_2\ddot{\theta}_2 \leqslant \hat{\alpha}J_2\dot{\theta}_2 \tag{41}$$

by dividing both side of the inequation for $\hat{\alpha}J_2\dot{\theta_2}$ and considering $\hat{\alpha}J_2\dot{\theta_2} < 0$, one can obtain:

$$-\frac{J_2\ddot{\theta_2}}{\hat{\alpha}J_2\dot{\theta_2}} \geqslant 1 \tag{42}$$

$$\frac{J_2\ddot{\theta_2}}{\hat{\alpha}J_2\dot{\theta_2}} \leqslant -1 \tag{43}$$

which may lead to RI definition:

$$RI(t) = \left|\frac{J_2\ddot{\theta_2}}{\hat{\alpha}J_2\dot{\theta_2}}\right| \tag{44}$$

and relative rattle criterion statement:

$$RI(t) : \begin{cases} \geqslant 1 : rattle \\ < 1 : no\ \ rattle \end{cases} \tag{45}$$

It is worth noticing that rattle criterion does not depend on the rotation direction. In case of negative rotation of driver $\theta_1 < 0$, the gear 2 rotation will be positive, i.e. $\theta_2 > 0$. In this case the meshing torque applied on gear 2 will have a positive sign as long as teeth are in contact on drive side tooth flank:$-J_2\ddot{\theta_2}/R_2 - \hat{\alpha}J_2\dot{\theta_2}/R_2 \geqslant 0$. The rattle index definition and the relative criterion remain unaltered.

A novel proposal of the authors for RI definition in case of single or multiple branch geartrain is defined in the next subsections.

4.2.1 *Single Branch geartrain*

In this subsection the generalization of the gear rattle index for single branch loaded geartrains is outlined. By considering a driveline with an arbitrary number of gears (see Figure 26), its rotary motion is completely described by the equation system in Eq. 46. Despite the translational DOFs concur in the definition of the dynamic transmission error, equations defining the radial

balance are hereinafter omitted as only torsional dynamics is necessary for the proposed dissertation.

$$\begin{cases} \frac{J_1\ddot{\theta_1}}{R_1} + \hat{\alpha}\frac{J_1\dot{\theta_1}}{R_1} + f_{m_{12}} = \frac{T_{e_1}}{R_1} \\ \frac{J_2\ddot{\theta_2}}{R_2} + \hat{\alpha}\frac{J_2\dot{\theta_2}}{R_2} + f_{m_{12}} + f_{m_{23}} - \frac{T_{e_2}}{R_2} = 0 \\ \cdots \\ \frac{J_i\ddot{\theta_i}}{R_i} + \hat{\alpha}\frac{J_i\dot{\theta_i}}{R_i} + f_{m_{(i-1,i)}} + f_{m_{(i,i+1)}} - \frac{T_{e_i}}{R_i} = 0 \\ \cdots \\ \frac{J_n\ddot{\theta_n}}{R_n} + \hat{\alpha}\frac{J_n\dot{\theta_n}}{R_n} + f_{m_{(n-1,n)}} - \frac{T_{e_n}}{R_n} = 0 \end{cases} \tag{46}$$

The equation system is formed by "n" equations, were the generic equation related to gear "i" contains two meshing force terms, the first one related to the engagement between gear i and $i-1$ and the other term referring to the engagement between i and $i+1$. With the purpose to achieve the RI statement, the first step is to rewrite the equations of motion in such manner to obtain for each gear, an expression where meshing force $f_{m_{(i-1,i)}}$ is expressed as a function of external excitation torques, inertial torques and the viscous damping torques. By focusing on the equation system defined in Eq. 46, it is possible to notice that the equation related to the n-th gear already satisfies this requirement:

$$f_{m_{(n-1,n)}} = \frac{T_{e_n}}{R_n} - \frac{J_n\ddot{\theta_n}}{R_n} - \hat{\alpha}\frac{J_n\dot{\theta_n}}{R_n} \tag{47}$$

By combining the equation of motion relative to gear $n-1$ with Eq. 47 it is possible to isolate the term $f_{m(n-2,n-1)}$:

$$f_{m_{(n-2,n-1)}} = \frac{J_n\ddot{\theta_n}}{R_n} - \frac{J_{(n-1)}\ddot{\theta_{(n-1)}}}{R_{(n-1)}} + \hat{\alpha}\frac{J_n\dot{\theta_n}}{R_n} - \hat{\alpha}\frac{J_{(n-1)}\dot{\theta_{(n-1)}}}{R_{(n-1)}} + \frac{T_{e_{(n-1)}}}{R_{(n-1)}} - \frac{T_{e_n}}{R_n} \tag{48}$$

By adopting this iterative approach until the second gear, it is possible to write a generalized expression for the generic gear "i" :

$$(-1)^i f_{m_{(i-1,i)}} + \sum_{k=i}^{n} (-1)^k \left[\frac{J_k\ddot{\theta_k}}{R_k} + \hat{\alpha}\frac{J_k\dot{\theta_k}}{R_k} - \frac{T_{e_k}}{R_k}\right] = 0 \tag{49}$$

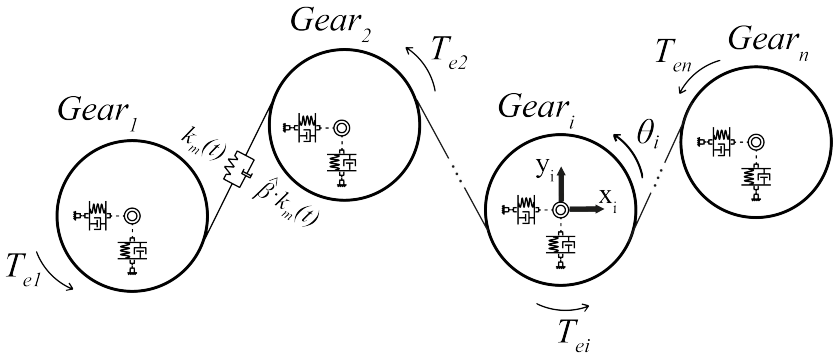

Figure 26: Lumped parameter model of a single branch driveline

Starting from Eq. 49 the definition given in Eq. 39 may now be extended by introducing the expression of the rattle index referred to the generic gear pair $(i-1, i)$ of the driveline:

$$RI_{(i-1),i} = \left| \frac{\sum_{k=i}^{n} (-1)^k \frac{J_k \ddot{\theta}_k}{R_k}}{\sum_{k=i}^{n} (-1)^k \left(\hat{\alpha} \frac{J_k \dot{\theta}_k}{R_k} - \frac{T_{e_k}}{R_k} \right)} \right| \tag{50}$$

The expression in Eq. 50 may be considered a general formulation for the rattle index since it may be applied to any gear pair of any single branch driveline. Reliability and limitations of the proposed index will be further discussed in section 4.3.

4.2.2 *Multiple Branch geartrain*

In this subsection the definition of the generalized gear rattle index is extended to multiple branch geartrains. By considering the generic driveline shown in Figure 27 it is possible to observe the presence of a single gear simultaneously in meshing with other three gears, namely the hub's gear. Based on this observation, it is possible to identify three different branches denoted with three different indices i, h, k. Branch i is formed by n gears identified by subscript l. The first gear of branch i is considered as the driving gear of the entire driveline. The branch k has m gears identified by subscript u while branch h has a total number of q gears denoted by subscript v. On the basis of the defined nomenclature, the hub's gear will be simultaneously considered as

the last one of branch i and the first gear of branch k as well as the first gear of branch h. Hence, the two driveline branches k and h can be considered as single geartrains where the hub's gear represents the driving one. With this assumption, it is now possible to apply the general formulation defined in Eq.49 to both k and h branches:

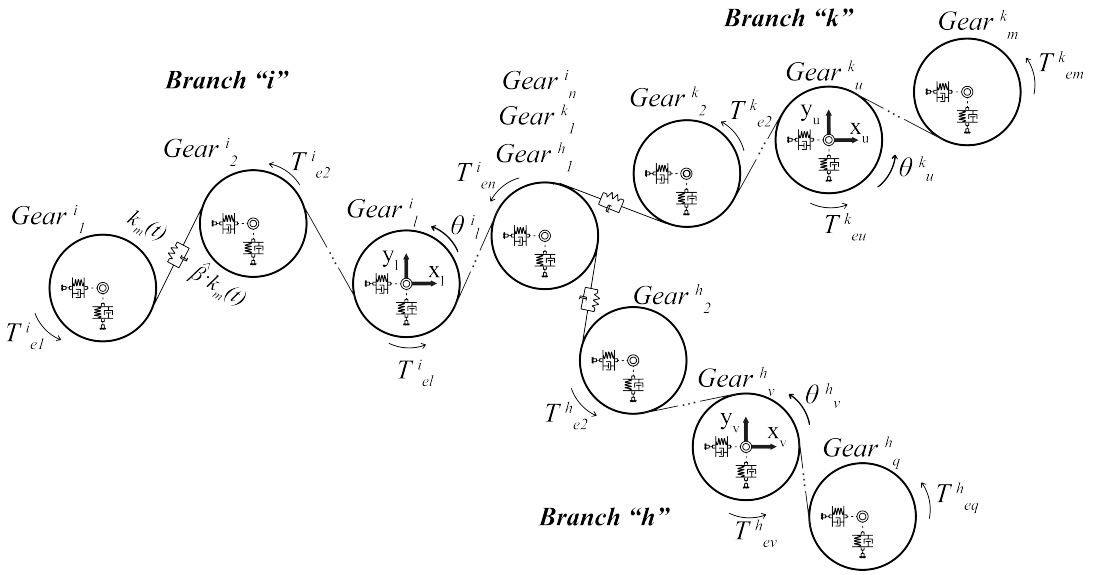

Figure 27: Lumped parameter model of a multiple branch geartrain

$$(-1)^{u} f^{k}_{m_{(u-1,u)}} + \sum_{j=u}^{m} (-1)^{j} \left[\frac{J^{k}_{j} \ddot{\theta}^{k}_{j}}{R^{k}_{j}} + \hat{\alpha} \frac{J^{k}_{j} \dot{\theta}^{k}_{j}}{R^{k}_{j}} - \frac{T^{k}_{e_j}}{R^{k}_{j}} \right] = 0 \tag{51}$$

$$(-1)^{v} f^{h}_{m_{(v-1,v)}} + \sum_{j=v}^{q} (-1)^{j} \left[\frac{J^{h}_{j} \ddot{\theta}^{h}_{j}}{R^{h}_{j}} + \hat{\alpha} \frac{J^{h}_{j} \dot{\theta}^{h}_{j}}{R^{h}_{j}} - \frac{T^{h}_{e_j}}{R^{h}_{j}} \right] = 0 \tag{52}$$

Where h and k superscripts denote the respective branch. Since branches h and k are characterized by the same formulation defined for the single branch geartrain, the rattle index of a generic gear pair pertaining to such branches may be directly obtained by applying Eq.50. As a consequence, by considering

the hub's gear as the n-th gear of branch i, the following equation completely describes its rotary motion:

$$\begin{aligned}&(-1)^n f^i_{m_{(n-1,n)}} + (-1)^n \left[\frac{J^i_n \ddot{\theta}^i_n}{R^i_n} + \hat{\alpha}\frac{J^i_n \dot{\theta}^i_n}{R^i_n} - \frac{T^i_{en}}{R^i_n}\right] + \\ &(-1)^{n+1}\left[\sum_{j=2}^{m}(-1)^j\left[\frac{J^k_j \ddot{\theta}^k_j}{R^k_j} + \hat{\alpha}\frac{J^k_j \dot{\theta}^k_j}{R^k_j} - \frac{T^k_{ej}}{R^k_j}\right] + \right. \\ &\left.\sum_{j=2}^{q}(-1)^j\left[\frac{J^h_j \ddot{\theta}^h_j}{R^h_j} + \hat{\alpha}\frac{J^h_j \dot{\theta}^h_j}{R^h_j} - \frac{T^h_{ej}}{R^h_j}\right]\right] = 0\end{aligned} \tag{53}$$

At this point, $F^i_{m(n-1,n)}$ is expressed as a function of external excitation torques, inertial torques and the viscous damping torques. By following the same recursive approach, the equation of motion for the rotational degree of freedom of the generic gear l of branch i is given by:

$$\begin{aligned}&(-1)^l f^i_{m_{(l-1,l)}} + \sum_{p=l}^{n}(-1)^p\left[\frac{J^i_p \ddot{\theta}^i_p}{R^i_p} + \hat{\alpha}\frac{J^i_p \dot{\theta}^i_p}{R^i_p} - \frac{T^i_{ep}}{R^i_p}\right] + \\ &(-1)^{n+1}\left[\sum_{j=2}^{m}(-1)^j\left[\frac{J^k_j \ddot{\theta}^k_j}{R^k_j} + \hat{\alpha}\frac{J^k_j \dot{\theta}^k_j}{R^k_j} - \frac{T^k_{ej}}{R^k_j}\right] + \right. \\ &\left.\sum_{j=2}^{q}(-1)^j\left[\frac{J^h_j \ddot{\theta}^h_j}{R^h_j} + \hat{\alpha}\frac{J^h_j \dot{\theta}^h_j}{R^h_j} - \frac{T^h_{ej}}{R^h_j}\right]\right] = 0\end{aligned} \tag{54}$$

As a result, Eqs. 51, 52 and 54, may be used to describe the mesh force of a generic gear pair pertaining to the generic branch of the driveline. Based on the defined formulation, it is straightforward to deduce the rattle index related to the engagement between gear l and $l-1$ of branch i:

$$RI_{l-1,l} = \left|\frac{N}{D}\right| \tag{55}$$

where N and D yelds to:

$$\begin{aligned}N = &\sum_{p=l}^{n}(-1)^p\left[\frac{J^i_p \ddot{\theta}^i_p}{R^i_p}\right] + (-1)^{n+1}\sum_{j=2}^{m}(-1)^j\left[\frac{J^k_j \ddot{\theta}^k_j}{R^k_j}\right] + \\ &(-1)^{n+1}\sum_{j=2}^{q}(-1)^j\left[\frac{J^h_j \ddot{\theta}^h_j}{R^h_j}\right]\end{aligned} \tag{56}$$

$$\begin{aligned}D = &\sum_{p=l}^{n}(-1)^p\left[\hat{\alpha}\frac{J^i_p \dot{\theta}^i_p}{R^i_p} - \frac{T^i_{ep}}{R^i_p}\right] + (-1)^{n+1}\sum_{j=2}^{m}(-1)^j\left[\hat{\alpha}\frac{J^k_j \dot{\theta}^k_j}{R^k_j} - \frac{T^k_{ej}}{R^k_j}\right] + \\ &(-1)^{n+1}\sum_{j=2}^{q}(-1)^j\left[\hat{\alpha}\frac{J^h_j \dot{\theta}^h_j}{R^h_j} - \frac{T^h_{ej}}{R^h_j}\right]\end{aligned} \tag{57}$$

It is worth noticing that the proposed methodology is not limited to geartrain layouts characterized by three branches but it may similarly be extended to drivelines with an arbitrary number of branches and hub's gears.

It is worth underlining that the purposes behind the definition of RI are not limited to the detection of teeth detachment, which may be directly evaluated through the gear mesh displacement time histories, found as part of the solution. The outlined index may be further processed in order to obtain an indication of rattle level severity related to a specific meshing pair of the geartrain. According to [10], the root mean square value of the rattle index expressed in a logarithmic scale may be adopted to represent the severity level associated to the observed rattle phenomena.

4.3 NUMERICAL ASSESSMENT

The task of the present section is to highlight the potentials of the given definition of RI. In order to fulfill this purpose, the index will be applied to various geartrain layouts. In a first instance the idle gear dynamics is investigated. Afterwards the RI for loaded geartrain is illustrated and some considerations are made on its validity and effectiveness. Finally results for multiple branch geartrain are shown.

The numerical analysis has been carried out by using the block diagram model developed by the author in Simcenter Amesim environment. Each gear pair is modeled by adopting the methodology explained in Chapter 2 and solved by using the fixed time step integrator based on Runge-Kutta method of order 4. The time step is set to 10^{-6} s throughout the entire numerical study. In order to simplify the analytical dissertation, the squeeze force due to lubricant is neglected. A comparison between experimental and numerical results could be an interesting feedback to assess the proposed analytical methodology. Despite this, it has to be clarified that the tool used for the numerical study is based on a well-known gear pair modeling strategy that rests its reliability and consistency on experimental comparisons reported in several previous works in the literature [109, 16]. Moreover, an application of the adopted tool including experimental validation is available in Chapter 2. Regarding the RI formulation, the proposed dissertation represents an extension of the index previously introduced by R.Singh in [10] to a large variety of geartrain layouts. Based on this characteristic, in analogy to the formulation given in

[10], the proposed RI generalization does not depend on empirical terms since its computation is executed by using the mathematical quantities estimated by the dynamic model. For this reason, it may be deduced that the reliability of the proposed index directly depends on the reliability of the numerical results.

4.3.1 *Unloaded single branch geartrain*

In this subsection the steady state idle gear dynamics of two different geartrain layouts is investigated. In this condition, the geartrain is characterized by an angular speed oscillating around a constant value and no external loads applied to the driven gears, except for the drag torque due to friction which is proportional to the velocity of the related gear. First of all, RI behavior related to idle gear pair is shown. This first analysis, despite recalling well known literature results, will help the comprehension of the further examples. Secondly a three gears single branch geartrain is used to highlight the effectiveness of the outlined index and demonstrate that the comparison between indices related to consecutive meshings allows to detect mutual interactions among gears. The gear mesh stiffness is obtained by using the analytical method proposed by Kuang and Yang in [23], while damping coefficients have been chosen with the purpose to obtain a damping factor ζ from to 2% to 10% within the frequency range of interest, which represent a realistic range of values for this kind of mechanical systems, based on the author's experience.

4.3.1.1 *Single gear pair scenario*

By focusing the attention on the single gear pair dynamics, numerical studies have been carried out at a mean rotating speed equal to 1000 rpm. Design parameters are shown in table 2. Simulations have been run for a total time of 1 second: during the first 0.3 s the rotating speed is constant, afterwards acceleration excitation $\ddot{\theta}_p$ is imposed on the driver gear, to simulate the speed fluctuation and induce tooth detachments:

$$\ddot{\theta}_p = \begin{cases} 0 & \text{if } t \leqslant 0.3s \\ \hat{A}\sin(2\pi f_a t) & \text{if } t > 0.3s \end{cases} \tag{58}$$

where $\hat{A}$ and f_a are the amplitude and the frequency of the angular acceleration excitation, respectively. Their value is shown in table 2. For the sake of clarity,

Parameters	**Gear 1**		**Gear 2**
Mass [kg]	0.12		0.181
Mass moment of inertia [kgm^2]	8.49e-5		1.6e-4
Module [mm]		3	
Number of teeth	25		32
Pressure angle [deg]		20	
Gear mesh stiffness [N/m]		40.8e + 6 (max) 26.91e+6 (min)	
k_b bearing stiffness [N/m]	2e+8		2e+8
$\hat{\alpha}$ damping coefficient [s^{-1}]		5	
$\hat{\beta}$ damping coefficient [s]		8e-5	
Backlash [μm]		115	
f_a [Hz], frequency of acceleration excitation $\ddot{\theta}_p$	30		
$\hat{A}$ [rad/s^2], amplitude of acceleration excitation $\ddot{\theta}_p$	1000		
f_t [Hz], frequency of external torque T_{e_2}	30		
$\hat{B}$ [Nm], amplitude of external torque T_{e_2}	25		

Table 2: Design parameters for single gear pair

the choice of a zero initial phase does not affect the general applicability of the proposed analysis. This statement remains valid hereinafter, throughout the entire numerical study. It is worth noticing that the defined modeling approach coincides with the standard methodology adopted in the literature to assess rattle (see refs. [107], [56], [10]) since it is the responsible of tooth detachment in idle pairs within gear transmissions. By observing the results related to the single gear pair, (see Figure 28), it is noticeable that as long as the acceleration excitation is zero, gears are in meshing on the front side of the tooth and no detachment events are recognized (Figure 28a). As expected, the RI values always remain below the rattle threshold (Figure 28c). On the other hand, Figure 28b shows that the occurrence of double-sided impacts comes out when the acceleration excitation induces an oscillating rotating speed. As discussed in section 4.2, RI produces a periodic peak overcoming the threshold value when vibro-impacts occur (see Figure 28d).

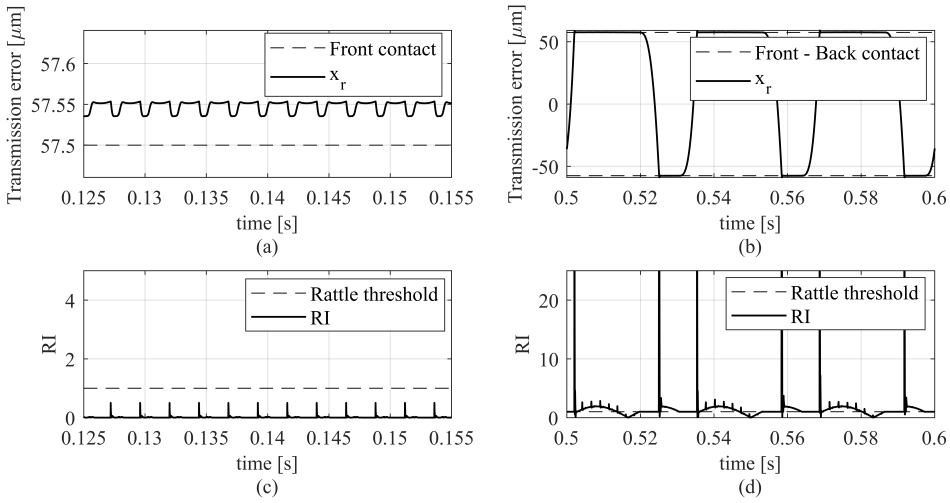

Figure 28: Transmission error and rattle index calculated for the unloaded single gear pair under full contact conditions (a and c, respectively) and under rattle conditions (b and d, respectively).

4.3.1.2 *Three gears geartrain scenario*

Once the RI behavior pertaining to a single gear pair has been recalled, attention is now focused on its application to a single branch geartrain constituted by three gears. Design parameters are depicted in table 3. For the sake of uniformity, the same working conditions adopted for the previous example are simulated, including also the excitation defined in Eq. 58. Results are reported in Figure 29. In particular, Figure 29a shows the transmission errors x_{r12} and x_{r23} in the time domain, while Figure 29b e 29c show the trend related to RI_{12} and RI_{23}, respectively. As it can be observed from Figure 29a, detachment occurs on both meshing phenomena, however, the analysis of RI_{12} and RI_{23} underlines the presence of a different behavior. In particular, RI_{12} trend, shows two peaks at each tooth engagement between gear 1 and gear 2, while RI_{23} produces only one periodic peak. In order to better understand the reason behind this scenario, attention may be focused on Figure 30 showing a detailed view of the instants when impacts occur on the *Direct Line of Action*. As it may be noticed, the first impact is recognized on x_{r12} due to the engagement between gear 1 and 2. Within this time instant, gear 2 and 3 are not in contact. For this reason, this event is detected by RI_{12} but it cannot be recognized on

Parameters	Gear 1	Gear 2	Gear 3
Mass [kg]	0.12	0.181	0.243
Mass moment of inertia [kgm^2]	8.49e-5	1.6e-4	1.07e-4
Module [mm]	3		
Number of teeth	25	32	17
Pressure angle [deg]	20	20	
Gear mesh stiffness [N/m]	40.8e + 6 (max) 26.91e+6 (min)	26.8e + 6 (max) 17.38e+6 (min)	
k_b bearing stiffness [N/m]	2e+8	2e+8	2e+8
$\hat{\alpha}$ damping coefficient [s^{-1}]	5		
$\hat{\beta}$ damping coefficient [s]	8e-5		
Backlash [μm]	115		
f_a [Hz], frequency of acceleration excitation $\ddot{\theta}_p$	30		
Â [rad/s^2], amplitude of acceleration excitation $\ddot{\theta}_p$	1000		
f_t [Hz], frequency of external torque T_{e_2}	30		
$\hat{B}$ [Nm], amplitude of external torque T_{e_2}	25		

Table 3: Design parameters for single branch geartrain composed of three gears

x_{r23} and therefore RI_{23} remains under the threshold value. On the other hand, the second impact occurs when gear 2 and 3 start enganging. However, within this timeframe gear 1 and 2 are engaged and therefore the impact force can transmit itself throughtout the entire geartrain. As a consequence, the event is concurrently recognized by RI_{23} and, by RI_{12} with a lower amplitude. The enlightened phenomena demonstrates that the general definition of the rattle index is effectively capable to detect the events occurring on each meshing and the potential presence of mutual interactions between them.

In addition, the analysis is repeated for three different values of the angular acceleration amplitude of driver gear $\ddot{\theta}_p$ in order to demonstrate that rattle index RI may lead to a quantitative estimation of the rattle severity by computing the root mean square value of RI, according to [10]. In order to underline this aspect, simulations have been repeated for three different values of amplitude Â: 1000 rad/s^2, 2500 rad/s^2 and 5000 rad/s^2. As it may be observed in Figure 31 showing the results related to RI_{12} and RI_{23}, as the acceleration amplitude increases, the impact between teeth become more severe leading the overall rattle level to rise. Table 4 illustrates the root mean square value for each case of study, demonstrating the increasing trend of RI magnitude.

Amplitude of $\ddot{\theta}_p$ [rad/s^2]	Root mean square value of RI_{12}	Root mean square value of RI_{23}
$\hat{A}1 = 1000$	12.70	15.51
$\hat{A}2 = 2500$	13.00	16.32
$\hat{A}3 = 5000$	15.09	18.46

Table 4: Value of $\ddot{\theta}_p$ amplitude and related RI_{12} and RI_{23} root mean square values

4.3.2 *Loaded geartrain*

In this subsection the loaded gear dynamics of a single gear pair is investigated. In a first place RI trend is shown, afterwards, some considerations are made on its validity and application. Geometrical parameters are related to the same single gear pair layout defined in section 4.3.1 (see Table 2). In this particular study, teeth detachment is caused by an external torque applied on the driven gear. Numerical simulations are carried out at a mean rotating speed of 1000 rpm, while an oscillating torque (Te_2 in Eq. 59) on the driven gear is applied in order to induce rattle:

$$T_{e_2} = \begin{cases} 0 & \text{if } t \leqslant 0.3s \\ \hat{B}\sin(2\pi f_t t) & \text{if } t > 0.3s \end{cases} \tag{59}$$

where $\hat{B}$ and f_t are the amplitude and the frequency of the external torque and their value is shown in table 2. A dedicated driving torque T_{e_1} in Eq. 60 behaves as a proportional integrator (PI) controller that is capable to keep the mean velocity of gear 1 at the desired value without neglecting its dynamic behavior:

$$T_{e_1} = k_c\,(\theta_{1kin} - \theta_1) + c_c(\dot{\theta_{1m}} - \dot{\theta_1}) \tag{60}$$

where θ_{1kin} and $\dot{\theta_{1m}}$ are respectively the angular kinematic displacement and mean angular velocity of gear 1. k_c and c_c denote the proportionality and integral gain of controller. Results of the proposed analysis are shown in Figure 32. In particular, Figure 32a shows the transmission error x_r in time domain, while Figure 32b shows RI trend, that exhibits a periodic peak overcoming the threshold value when vibro-impacts occur. From a qualitative perspective, the detected behavior is similar to the one observed regarding the idle gear pair in Figure 28. However, for the sake of clarity, it is worth noticing that the results depicted in Figure 32 cannot be directly obtained by applying the exact

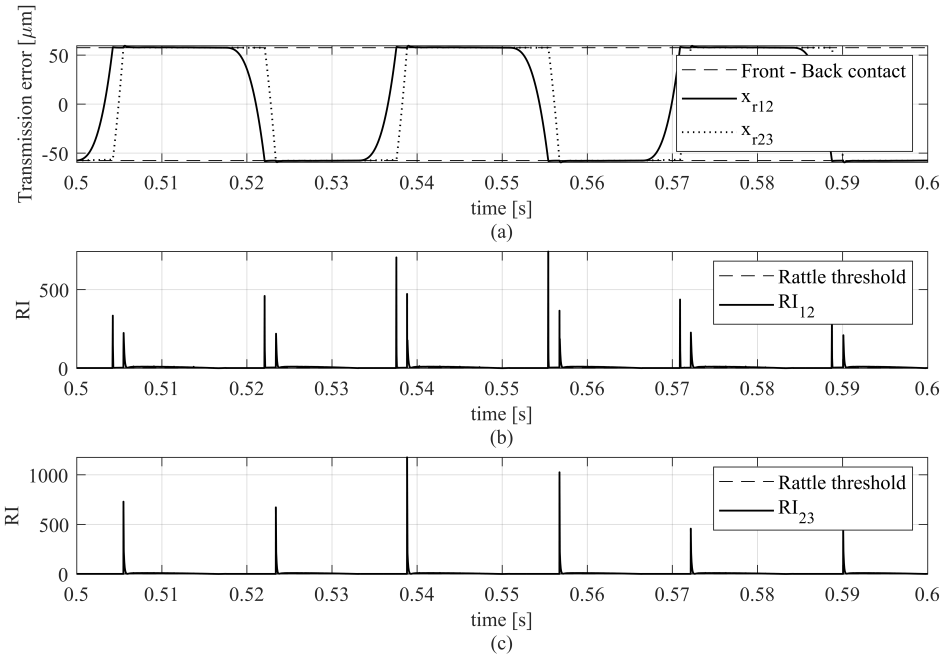

Figure 29: Transmission errors of all gear pairs of a three gears single branch geartrain with no external loads applied (a) and rattle index calculated for each gear pair (b and c) under rattle conditions.

definition of RI. According to Eq.50, the outlined index tends toward infinity as the denominator tends to zero. As a result, the condition $Te_2 \approx \hat{\alpha} J_2 \dot{\theta}_2$ implies an instant growth in RI trend that overcomes the rattle threshold producing an erroneous indication of rattle occurrence. It is therefore necessary to provide some conditions on its validity. By defining the denominator of Eq. 50 as:

$$\hat{\delta} = \left| \sum_{k=i}^{n} (-1)^k \left(\hat{\alpha} \frac{J_k \dot{\theta_k}}{R_k} - \frac{T_{e_k}}{R_k} \right) \right| \tag{61}$$

it may be defined a threshold for RI authenticity, by excluding the results when $\hat{\delta}$ is close to zero:

$$RI_{(i-1),i} = \begin{cases} 0 & \text{if } \hat{\delta} \leqslant \text{threshold} \\ \left| \frac{\sum_{k=i}^{n} (-1)^k \frac{J_k \ddot{\theta_k}}{R_k}}{\delta} \right| & \text{if } \hat{\delta} > \text{threshold} \end{cases} \tag{62}$$

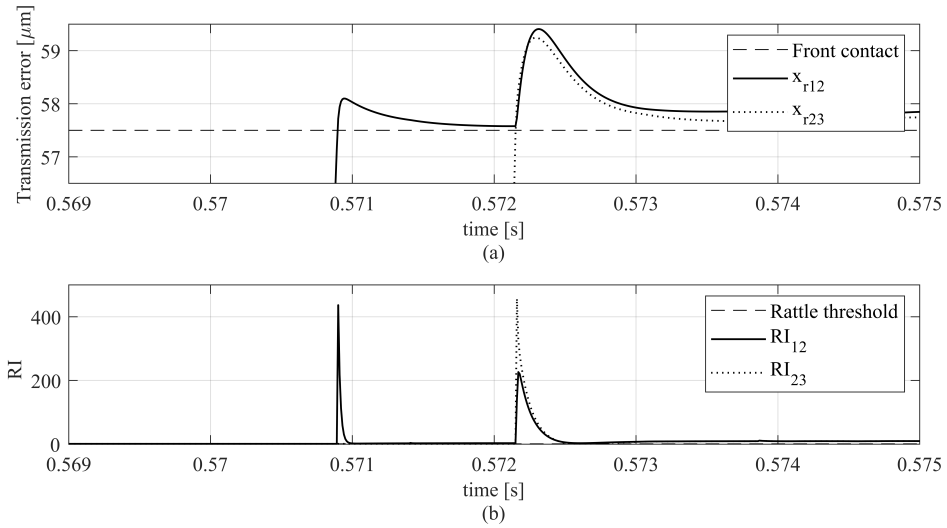

Figure 30: Transmission errors related to meshing $1-2$ and $2-3$ of a three gears single branch geartrain (a) and rattle index detail (b) with no external loads applied.

where $i = 2$ and $n = 2$ in this specific example. By using the definition of Eq. 62, results shown in Figure 32 are obtained. A detailed view of the impact phenomena and related RI peak is given in Figure 33.

Based on the purpose to further explain this scenario, Figure 34b shows external torque Te_2 and viscous drag torque $\hat{\alpha}J_2\dot{\theta}_2$ in the time domain, Figure 34c shows the RI trend obtained by applying directly the Eq. 50, while Figure 34d shows the $\hat{\delta}$ behavior. The presence of a peak in the neighborhood where the external torque is equal to the viscous drag one may be clearly recognized. By introducing a threshold value to guarantee the reliability of RI and adopting the consideration delighted in Eq. 62, it is evident that a part of information related to the signal representing RI is lost in the neighborhood where $Te_2 \approx \hat{\alpha}J_2\dot{\theta}_2$. Thus, the choice of the threshold value has to be made to limit as much as possible signal losses but also excluding RI results related to erroneous indication of rattle occurrence. To fulfill the purpose of making an adequate choice for the mentioned threshold, numerical studies have been conducted on single branch geartrain constituted by 4 gears. The presented geartrain layout is simulated by considering the same working conditions defined for the loaded gear pair, where the external torque is applied on the last gear

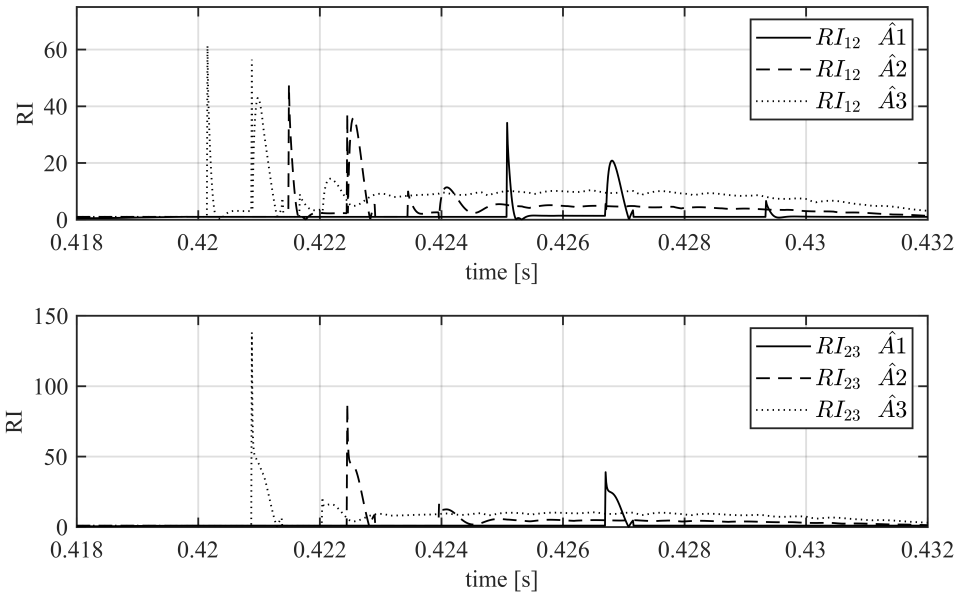

Figure 31: RI_{12} (a) and RI_{23} (b) trend, calculated for each case of study

of the driveline. Geometrical parameters are reported in Table 5. Numerical investigations have demonstrated that the choice of threshold value is based on the magnitude of $\hat{\delta}$. Figure 35 a,b and c show RI trend related to all meshing gears of the driveline, while Figure 35d,e and f show the $\hat{\delta}$ magnitude and its relative threshold. Even if it is not possible to define an absolute value for the threshold rate, it has been observed that its magnitude has to be around the 5% of the maximum value assumed by $\hat{\delta}$. It is worth noticing that Figure 35 a,b and c shows the deletion of the erroneous peak in RI trend, given from Eq. 50.

4.3.3 *Multiple branch geartrain*

In this subsection the calculation of RI for multiple branch geartrain is investigated. The geartrain layout considered in this study is constituted by a total number of three branches and ten gears. The geartrain layout is shown in figure 36. Design parameters are shown in Table 6 and 7. The numerical

Parameters	$Gear_1$	$Gear_2$	$Gear_3$
Mass [kg]	0.12	0.181	0.243
Mass moment of inertia [kgm^2]	8.49e-5	1.6e-4	1.07e-4
Module [mm]	3		
Number of teeth	25	32	17
Pressure angle [deg]	20	20	
Gear mesh stiffness [N/m]	40.8e+6 (max) 26.91e+6 (min)	26.8e+6 (max) 17.38e+6 (min)	
k_b bearing stiffness [N/m]	2.0e+8	2.0e+8	2.0e+8
$\hat{\alpha}$ damping coefficient [s^{-1}]	5		
$\hat{\beta}$ damping coefficient [s]	8e-5		
Backlash [μm]	115		

Parameters	$Gear_3$	$Gear_4$
Mass [kg]	0.243	0.45
Mass moment of inertia [kgm^2]	1.07e-4	8.02e-4
Number of teeth	17	36
Pressure angle [deg]	20	
Gear mesh stiffness [N/m]	77.3e+6 (max) 52.4e+6 (min)	
k_b bearing stiffness [N/m]	2.0e+8	2.0e+8

Table 5: Design parameters for single branch geartrain composed of four gears

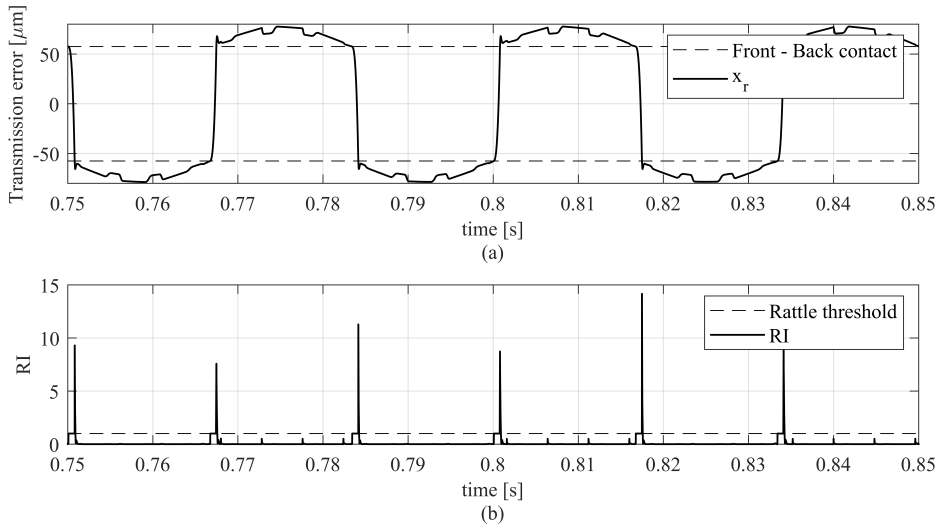

Figure 32: Transmission error and rattle index calculated for the loaded single gear pair, under rattle conditions (a and b, respectively)

analysis is performed at a mean rotating speed equal to 1000 rpm, while an oscillating torque is applied on gear 7 and 10:

$$T_{e_7} = T_{e_{10}} = \begin{cases} 0 & \text{if } t \leqslant 0.1s \\ C\sin(2\pi f_t t) & \text{if } t > 0.1s \end{cases} \tag{63}$$

where C and f_t are the amplitude and the frequency of the external torques. Their value is reported in table 7. Results are shown for gear 8 (Figure 37), for the gear 4 (Figure 38) and for gear 2 (Figure 39). It is worth noticing that the presence of external loads implies the same considerations highlighted in section 4.3.2. In order to avoid erroneous indication of rattle, the denominator of each RI expression is compared to a threshold value according to Eq. 62. Due to the presence of a multitude of gears, their mutual interaction cannot be straightforwardly deduced. The peaks that overcome the threshold value are not only related to vibro-impacts caused by the considered meshing gears but they are affected by the dynamics of the entire driveline. Figure 37b provides an example of this scenario: the first peak on RI_{48} is clearly due the tooth engagement between gear 4 and 8, while the second peak cannot be directly related to this event. In the timeframe where the second peak takes place, gear 4 and 8 are in contact on front side and no impact phenomena are detected. By

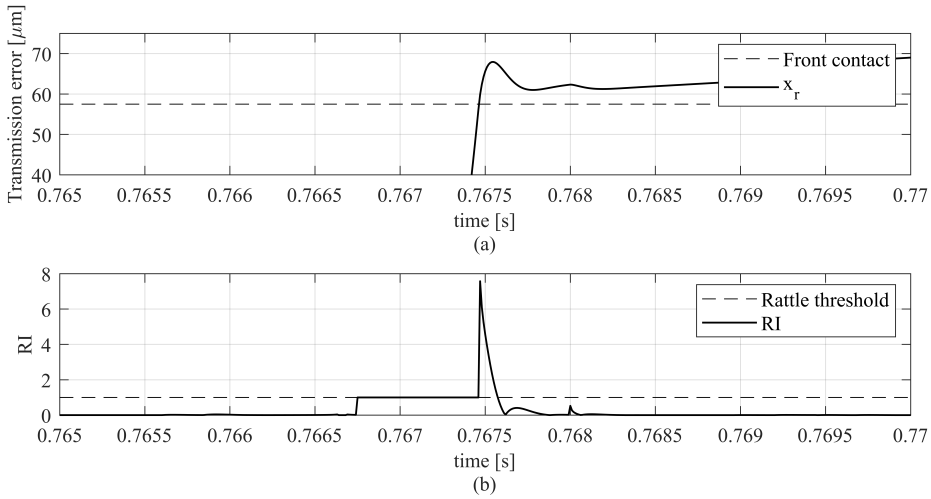

Figure 33: Transmission error and rattle index calculated for the loaded single gear pair under rattle conditions detail (a and b)

observing Figure 37a, it is noticeable that the transmission error $4-8$, namely x_{r48}, is affected by the engagement between gears 1 and 2, which produces the second peak. Similar considerations arise from Figure 38, representing the trends related to RI_{34} and the involved transmission errors. In the time interval where gear 3 and 4 are approaching, the impact caused by engagement of gears 4 and 8 affects gear pair $3-4$ dynamics. While gear 3 and 4 are in free flight motion, the impact between gears 4 and 8 is spread to the $3-4$ engagement, causing an evident slope modification in transmission error x_{r34} trend (see Figure 38a). As a consequence, the sharp peak in RI_{34} reaching the highest amplitude is slightly anticipated with respect to the actual collision between meshing gears 3 and 4 (see Figure 38b). By focusing on the second peak in RI_{34} trend, the same consideration made for RI_{48} may apply. In the time interval where the second peak occurs, gears 3 and 4 are engaging and no detachment events are recognized. Hence, impact provoked by meshing gears 1 and 2 is transmitted throughout the driveline. Finally, by considering results shown in Figure 39b, RI_{23} behavior presents just one peak related to vibro-impacts occurrence between gears 2 and 3. As it can be observed from Figure 39a the double-sided impacts described by x_{r12} affects gear pair $2-3$ dynamics, but in this case the impacts between gear pair $1-2$ and gear pair $2-3$ occur almost at the same time, generating only one peak in RI_{23} trend.

The illustrated results demonstrates the reliability of the general definition of the rattle index that can be a powerful tool to detect rattle occurrence in systems formed by multiple branch geartrain as geared timing system.

4.4 CONCLUDING REMARKS

The current study has defined a generalization of the Rattle Index proposed by R. Singh et al. in [10] to any type of ordinary transmission layouts, single or multiple branch, both in idle and loaded conditions. In particular, starting from the classical 6-DOFs equation system defining the nonlinear dynamics of a gear pair, a recursive analytical formulation of the rotational dynamics of gears is proposed. This mathematical expedient is adopted to deduce the generalization of the rattle index definition. In order to assess the theoretical dissertation, several driveline layouts have been investigated. First of all, RI for single branch unloaded geartrain is introduced. The general definition of the rattle index is shown to be a proper indicator of the vibro-impacts related to each gear pair of the driveline and the potential presence of mutual interactions between them. Then RI for single branch loaded geartrain is investigated. In this case considerations on RI validity are made and a threshold value for $\hat{\delta}$ is introduced, fulfilling the purpose to avoid numerical problems and erroneous indication of rattle occurrence. Moreover, observations on the appropriate choice of threshold value are made, in order to gain a compromise between the deletion of incorrect indications of rattle occurrence and the loss of signal informations. Finally, the definition of the generalized gear rattle index is extended to multiple branch geartrains, demonstrating the same accuracy and capabilities. The proposed index is able to instantaneously describe the vibro-impact events related to any gear pair of the driveline. Moreover, it allows to takes into account the mutual interactions among gears pertaining the geartrain. For all the described geartrain layouts, numerical analysis have been conducted and relative results have confirmed the effectiveness and reliability of outlined indices. Based on the detailed analysis, the proposed rattle index may represent a powerful tool to identify the presence of rattle in a wide range of geartrain layouts.

Parameters	$Gear_1$		$Gear_2$		$Gear_3$
Mass [kg]	0.12		0.181		0.243
Mass moment of inertia [kgm^2]	8.49e-5		1.6e-4		1.07e-4
Module [mm]		3			
Number of teeth	25		32		17
Pressure angle [deg]		20		20	
Gear mesh stiffness [N/m]		40.8e+6 (max) 26.91e+6 (min)		26.8e+6 (max) 17.38e+6 (min)	
k_b bearing stiffness [N/m]	2.0e+8		2.0e+8		2.0e+8
$\hat{\alpha}$ damping coefficient [s^-1]		5			
$\hat{\beta}$ damping coefficient [s]		8e-5			
Backlash [μm]		115			

Parameters	$Gear_3$		$Gear_4$		$Gear_5$
Mass [kg]	0.243		0.45		0.46
Mass moment of inertia [kgm^2]	1.07e-4		8.02e-4		2.5e-4
Number of teeth	17		36		22
Pressure angle [deg]		20		20	
Gear mesh stiffness [N/m]		77.3e+6 (max) 52.4e+6 (min)		26.8e+6 (max) 17.38e+6 (min)	
k_b bearing stiffness [N/m]	2.0e+8		2.0e+8		2.0e+8

Parameters	$Gear_5$		$Gear_6$		$Gear_7$
Mass [kg]	0.46		0.27		0.212
Mass moment of inertia [kgm^2]	2.5e-4		1.8e-4		1.75e-4
Number of teeth	22		26		20
Pressure angle [deg]		20		20	
Gear mesh stiffness [N/m]		140.7e+6 (max) 108.9e+6 (min)		102.75e+6 (max) 71.20e+6 (min)	
k_b bearing stiffness [N/m]	2.0e+8		2.0e+8		2.0e+8

Table 6: Design parameters for multiple branch geartrain.

Parameters	$Gear_4$	$Gear_8$	$Gear_9$
Mass [kg]	0.45	0.283	0.37
Mass moment of inertia [kgm^2]	8.02e-4	5.2e-4	2.3e-4
Number of teeth	36	34	25
Pressure angle [deg]	20	20	
Gear mesh stiffness [N/m]	72.33e+6 (max) 52.44e+6 (min)	69.78e+6 (max) 51.80e+6 (min)	
k_b bearing stiffness [N/m]	2.0e+8	2.0e+8	2.0e+8

Parameters	$Gear_9$	$Gear_{10}$
Mass [kg]	0.37	0.099
Mass moment of inertia [kgm^2]	2.3e-4	5.1e-5
Number of teeth	25	21
Pressure angle [deg]	20	
Gear mesh stiffness [N/m]	74.06e+6 (max) 46.05e+6 (min)	
k_b bearing stiffness [N/m]	2.0e+8	2.0e+8
f_t [Hz], frequency of external torques $T_{e_{10}}$, T_{e_7}	30	
C [Nm], amplitude of external torques $T_{e_{10}}$, T_{e_7}	10	

Table 7: Design parameters for multiple branch geartrain.

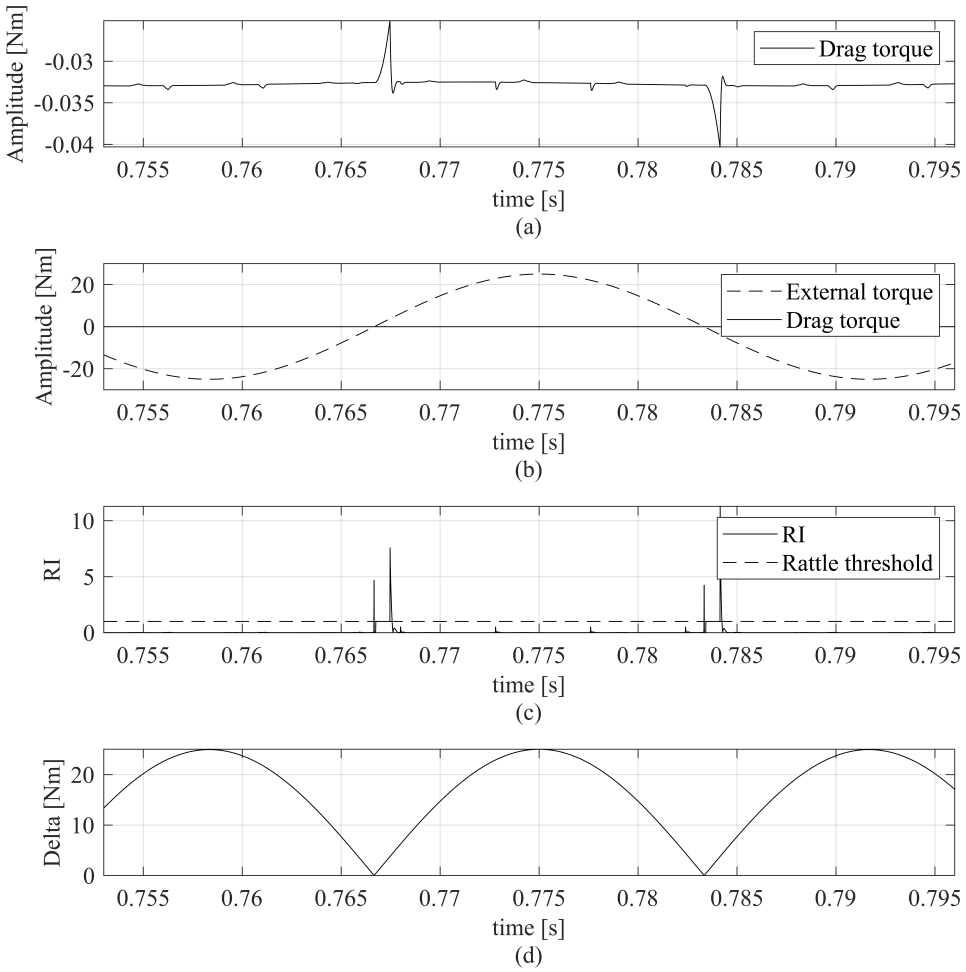

Figure 34: Viscous drag torque $\hat{\alpha}J_2\dot{\theta_2}$ (a), external torque Te_2 and viscous drag torque $\hat{\alpha}J_2\dot{\theta_2}$ (b), RI (c) and denominator $\hat{\delta}$ of Eq. 39 (d). Results are related to the single gear pair in loaded condition.

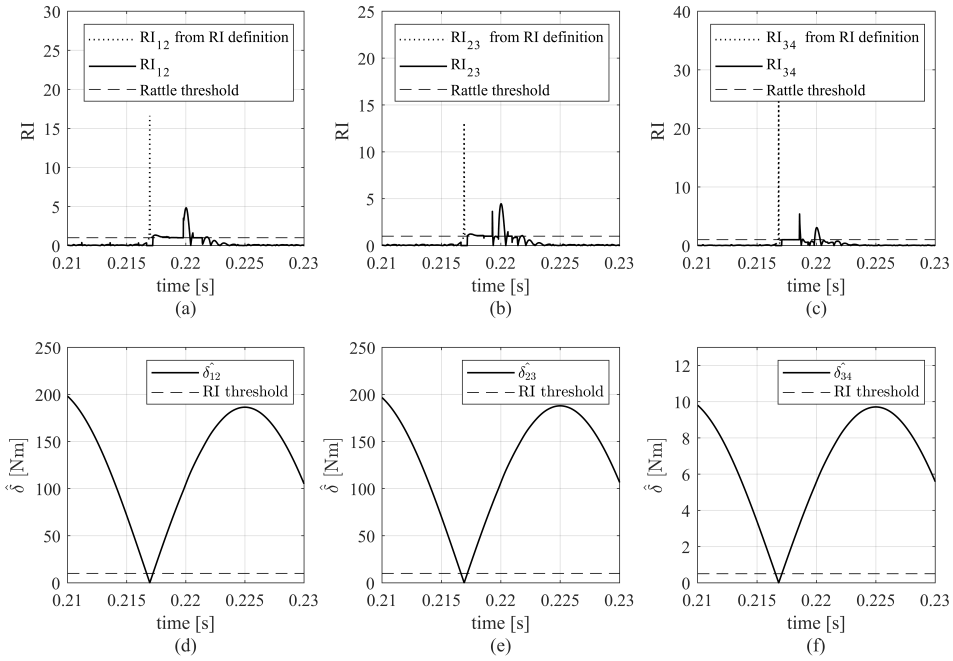

Figure 35: Rattle index related to consecutive meshings (a, b and c) and trend of denominator $\hat{\delta}$ of Eq. 50 for each meshing gear (e, f and g). For each engaging pair, RI definition is reported considering the formulation given in Eq. 50 and the modification due to comparison with RI threshold authenticity.

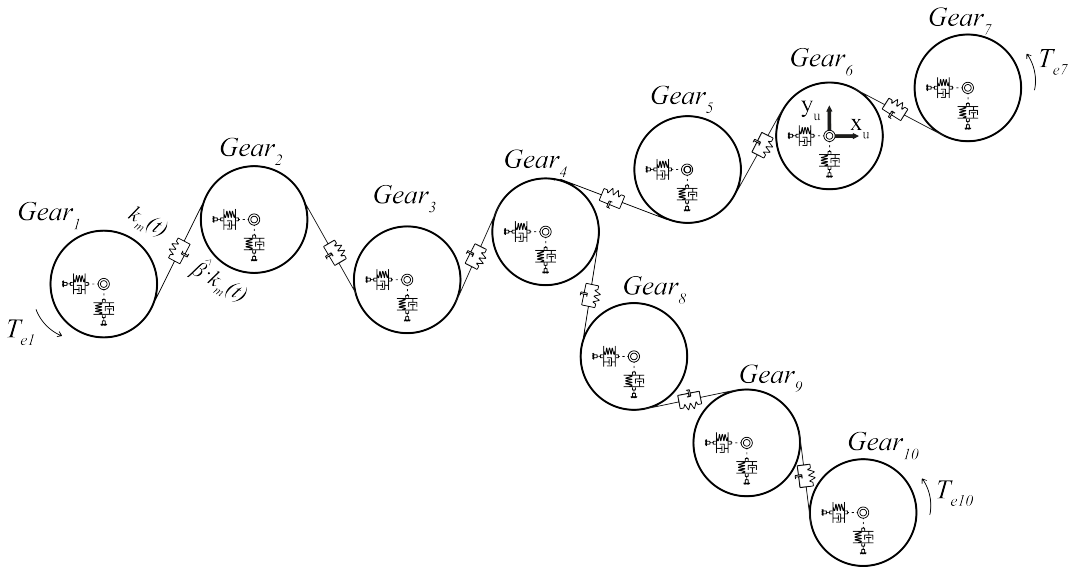

Figure 36: Multiple branch geartrain LP model

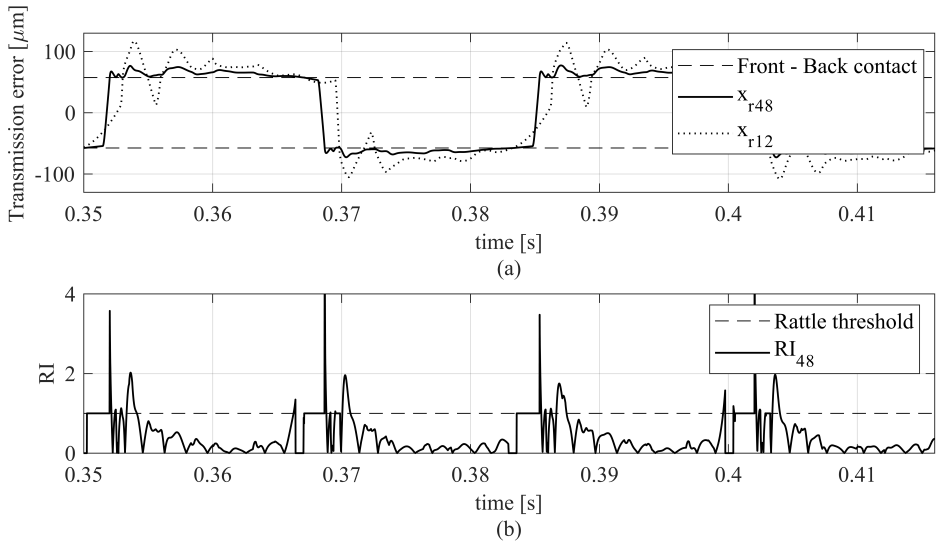

Figure 37: Transmission errors x_{r48} and x_{r12} (a) and rattle index RI_{48} (b).

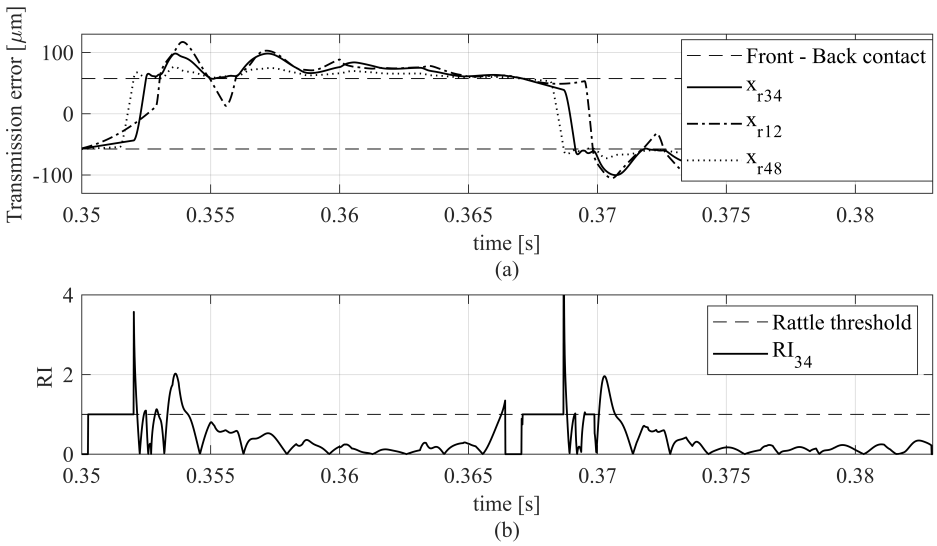

Figure 38: Transmission errors x_{r34}, x_{r12} and x_{r48} (a) and rattle index RI_{34} (b).

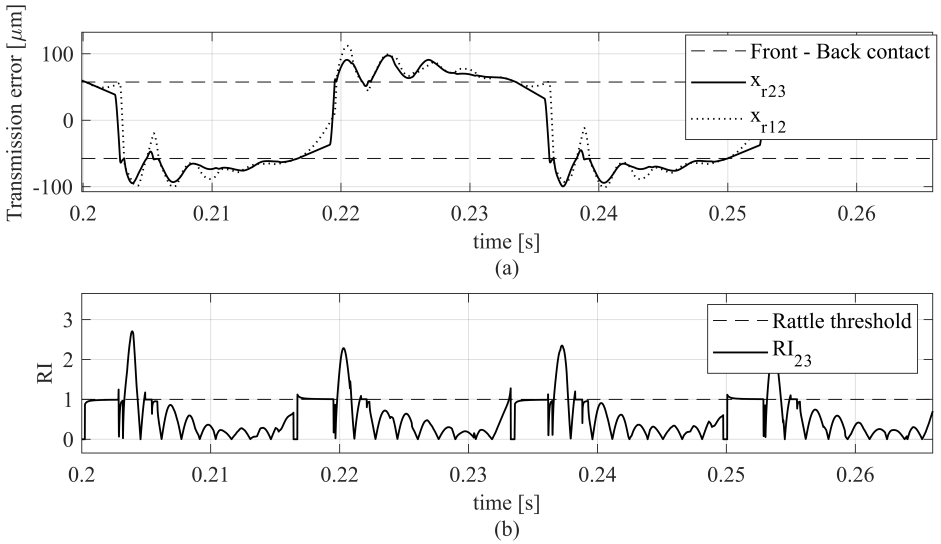

Figure 39: Transmission errors x_{r23} and x_{r12} (a) and rattle index RI_{23} (b).

5

THE ROLE OF GEAR LAYOUT AND MESHING PHASE FOR WHINE NOISE REDUCTION IN ORDINARY GEARTRAINS

Whine noise is one of major concern within geared system dynamics. The time-varying bearing forces are transmitted to the gearbox case, which coupled with the whole system assembly provokes an undesired noise emission. The Chapter proposes an analytical formulation able to forecast the main overall direction and magnitude of bearing reaction forces on idler gear when the geartrain works under quasi-static condition. Moreover, a parametric study is conducted by evaluating the influence of geartrain layout, the meshing phase shift and the amplitudes of meshing forces. Finally, numerical experiments are performed in order to evaluate discrepancies and similarities when the inertial effects become relevant.

5.1 INTRODUCTION

Gear whine noise is mainly caused by transmission errors variation [7], [8], [9]. In fact, this phenomenon is related to gear manufacturing errors, misalignment and time-varying meshing stiffness. Several studies have been conducted in order to analyze and reduce mesh stiffness and transmission error fluctuations. Gear tooth modification are used to obtain a smooth load transfer and reduce whine noise emission. The very first theory was proposed by Walker in 1930 [110]. He discovered that an optimization of micro-geometries could led to quieter transmission. Some years later Harris [111] observed that by setting the tip relief to a certain amount is possible to obtain a constant transmission error for the design load. Later, Litvin and Fuentes detailed the generation of micro-geometry in [112] considering spur gears, helical gears, spiral bevel gears, hypoid gears and planetary gear set. Chen and Shao [113], presented an

analytical formulation of the mesh stiffness and analyzed the effect of tip relief. Ma et al. [114], developed a mesh stiffness model suitable for profile shifted gears with addendum modification. Many authors investigate the possibilities to reduce transmission errors by micro-geometries optimization. Unless this, the best configuration can be found only for the design load even though, generally, gear transmission works under multiple load conditions.

Besides the internal excitation, gears are subjected to frictional excitation forces which may become relevant when the transmission error is low [115]. In fact, gear teeth in meshing area go through pure rolling only at pitch point. The approaching and recessing motions can generate friction forces which are in opposite direction. This rapid direction reversal can have a substantial impact on dynamic meshing forces [116]. Within this framework, Velex et al. [117] demonstrate that in heavy loaded geartrain, friction forces have a substantial role in noise generation. Houser et al. [118] conducted several experiments and revealed that friction force is a principal excitation for gear whine noise in higher harmonics of the mesh frequency. Vaishya and R. Singh [119] , [120] confirmed Houser et al. intuition, providing an analytical demonstration.

In planetary gear sets, a significant reduction of the vibration level can be achieved by properly setting planet meshing phase. One of the first demonstration of this principle was proposed by Schlegel and Mard in [121]. They experimentally measured a significant reduction of noise emission by properly setting planet meshing phase. By following Schlegel and Mard intuition, Seager in [122] proposed some geometrical conditions for the neutralization of the vibration amplitude at certain frequency. Parker in [123] conducted a deep study to investigate the meshing force pulsations on the sun-planets and planets-ring meshes in relation to the meshing phase shift. He affirmed that, by properly setting the planet phasing, one may be able to obtain a vibration level reduction. Later, Parker and Lin in [124] developed a complete analytical description of the phase difference relation between sun-planets meshes and planets-ring meshes. Canchi and Parker gave evidence that parametric instabilities of planetary gear system may be suppressed by adopting certain mesh phasing and contact ratio [125]. By considering the relevance of the matter, Guo and Parker proposed a study devoted to the analytical determination of mesh phase relations in general compound planetary gears in [126]. More recently, Espiga et al. in [127] studied the influence of meshing phase and planet spacing in planetary gears. The system geometry affects the transmis-

sion error dynamics. Furthermore, they investigates the influence of errors in planetary transmissions load sharing under different mesh phasing [128, 129]. Based on the current state of the art, many studies and experiments have been conducted on the planet phasing within planetary gear sets. As a matter of fact phase relationships between sun, planets and ring has now become an established concept in planetary gear set design. Besides this, meshing phase may have similar effects on vibration reduction of multi-mesh geartrain. Kartik and Houser in [130] affirmed that meshing phase may be a significant factor in the transmission error dynamics of multiple gear system. Liu and Parker in [131] conducted a study on the non-linear dynamics of idler gear systems. They gave evidence that meshing phase is an important aspect which affects the dynamic response of the geared system. As stated in ref. [132], in idler gear systems there is an additional opportunity to reduce whine noise emission, as the meshing gear phase affects the transmission error fluctuations. In [132] White et al. studied the meshing forces transmission in multimesh geartrain. They state that in quasi-static condition, the alternating component of bearing forces on idler gear describes an elliptical trajectory as the prime mover rotates along a pitch angle. The ellipse orientation and the values of semi-axis depend on the meshing phase. The phase is mainly related to three factors: gear number of teeth, tooth thickness and gear spatial position. When the internal excitation of the system is in a frequency range below the resonance, the overall mesh force may be considered as equal to the bearing reaction force, since the dynamic inertial effects can be neglected. The size of the ellipse and the direction of semi-axis are strongly related to gear whine noise emission. Despite White et al. [132] have got insight about quantities governing ellipse size and its orientation, a rigorous analytical formulation is still missing.

With the purpose to overcome this limitation, the author attempts to obtain an analytical formulation of the ellipse, establishing the mathematical quantities governing the ellipse shape and dimension. Furthermore, he investigates how this aspect is suitable in dynamic conditions, i.e. when the frequency of the internal excitation is close to the system resonance or above it. In order to achieve this goal, a numerical study has been carried out on a geartrain formed by three gears. In a first instance, the linearized eigenvalues and eigenvectors are calculated, then the system response is computed at various rotational speeds. The main objective is to observe the ellipse shape modification with respect to the excitation frequency and the different modal shapes. The re-

sults demonstrate that when excitation frequency approaches one eigenvalue, inertial effects become relevant and no information can be gained about the trajectory drawn by bearing forces amplitude. On the other hand they proved that the proposed dissertation is a reliable tool to get insight the main overall direction of bearing forces oscillating component when the system works under quasi-static condition. The Chapter is structured as follows: in the next section, the mathematical formulation of the elliptical trajectory of the bearing load is obtained. Its definition starts from an analytical expression of gear meshing forces. The result obtained is an analytical formulation to describe bearing forces transmission on idler gear in quasi-static condition. The parameters governing ellipse shape and dimensions are the gears spatial position, the meshing phase, and the amplitude of the meshing forces. In section 5.3 a parametric study is conducted in order to evaluate the influence of system parameters on ellipse size and orientation. Section 5.3.1 is dedicated to numerical experiments. By means of time domain simulations, the author evaluates the inertial forces contribution on bearing forces at different rotational velocities. The goal is to study ellipse shape and orientation in relation to the internal excitation frequency. Eventually, last section is devoted to concluding remarks.

5.2 MATHEMATICAL FORMULATION OF THE ELLIPTICAL TRAJECTORY

In this section the mathematical dissertation leading to the analytical formulation of the elliptical trajectory of the force on idler gear bearing is presented. Since gears may be characterized by strong nonlinear phenomena, the proposed methodology applies only 115 under specific hypotheses: quasi-static behavior of the system, continuous teeth contact and stationary working condition. These three hypotheses are usually satisfied when facing whine noise problems, where the gears are loaded by high mean torque values, and the system runs at low speed, i.e. when the carrier frequency of the main excitation is well below the main resonances of the system. On one hand, the presence of high torque 120 values avoids the chance of tooth detachment and make the system weakly nonlinear. On the other hand, the low speed requirement makes the inertia effects almost negligible. The geartrain layout is shown in Fig. 40. Gears are mounted on rolling bearings and teeth contact is guaranteed by the external torques T_{e1} and T_{e3}. According with this assumption, no teeth detachment is considered and two degrees of freedom are associated to each

gear: the rotation around z-axis, namely θ_i, and the translation along the direction parallel to the line of action, namely x_i, with $i = 1, 3$. This choice allows to minimize the number of degrees of freedom required to describe all the gear motions. Gear 2 has three degrees of freedom, namely θ_2, x_2 and y_2. The reference frame of the idler gear is chosen in such a manner that the x-axis acts as a bisector for the angle 2α, i.e. the angle between the two lines of action. By focusing on the radial motion of gear 2, its dynamics is described by:

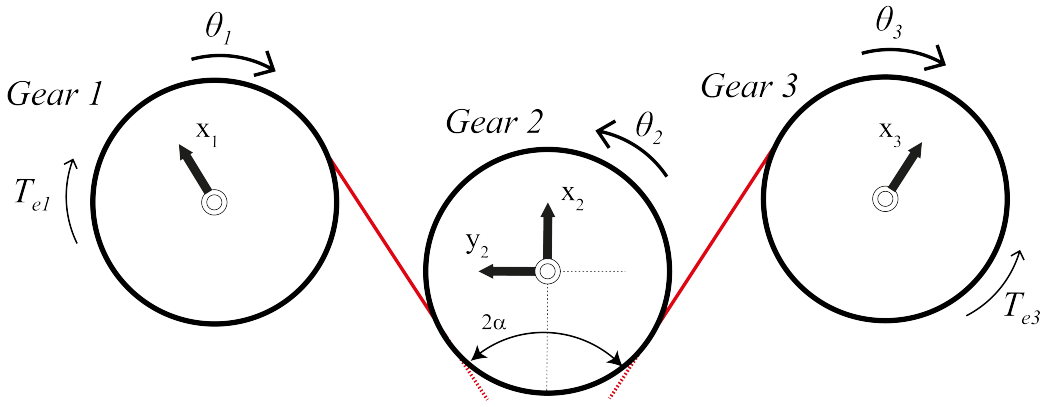

Figure 40: Schematic representation of the geartrain

$$\begin{cases} m_2 \ddot{x_2} + f_m^{x_2} + f_b^{x_2} = 0 \\ m_2 \ddot{y_2} + f_m^{y_2} + f_b^{y_2} = 0 \end{cases} \tag{64}$$

where m_2 denotes the mass, $f_b^{x_2}$ and $f_b^{y_2}$ are the bearing reaction forces in x_2 and y_2 directions. Terms $f_m^{x_2}$ and $f_m^{y_2}$ represent the meshing forces on gear 2 along x_2 and y_2. Both f_m and f_b account for elastic and damping contributions. By evaluating the dynamic behaviour of the system in a frequency range below the resonance, the elastic forces are predominant over the inertial ones. On the basis of this assumption, which is also at the basis of the dissertation in [132], Eq. 64 may be reduced to:

$$\begin{cases} f_m^{x_2} + f_b^{x_2} \approx 0 \\ f_m^{y_2} + f_b^{y_2} \approx 0 \end{cases} \tag{65}$$

It is worth noticing that $f_m^{x_2}$ and $f_m^{y_2}$ can be obtained by properly summing the force due to meshing with gear 1 and 3 in x_2 and y_2 direction.

Meshing forces are periodic and they may be expressed by means of Fourier series. By denoting with $f_{m_{12}}$ the alternating component of the meshing force along the line of action between gear 1 and 2 and with $f_{m_{23}}$ the alternating component of the meshing force along the line of action between gear 2 and 3, the generic $n-th$ harmonic can be expressed as follows:

$$f_{m12} = A_n \cos(n\Omega t + \phi_n) \tag{66}$$

$$f_{m23} = B_n \cos(n\Omega t + \phi_n - \Gamma_n) \tag{67}$$

where A_n and B_n are the amplitudes of the $n-th$ harmonic, Ω is the excitation frequency and ϕ_n and Γ_n are the phase shift, respectively. In order to obtain the total amount of meshing force along x_2 and y_2, $f_{m_{12}}$ and $f_{m_{23}}$ are expressed in Ox_2y_2 frame:

$$\begin{cases} f_{m12}^{x_2} = A_n \cos(n\Omega t + \phi_n)\cos\alpha \\ f_{m12}^{y_2} = A_n \cos(n\Omega t + \phi_n)\sin\alpha \\ f_{m23}^{x_2} = B_n \cos(n\Omega t + \phi_n - \Gamma_n)\cos\alpha \\ f_{m23}^{y_2} = B_n \cos(n\Omega t + \phi_n - \Gamma_n)(-\sin\alpha) \end{cases} \tag{68}$$

The present dissertation is conducted under the hypothesis that the meshing force excitation is composed of a single harmonic. This assumption does not produce any loss of generality, since on the basis of the superposition principle, it may be straightforwardly extended to an arbitrary number of harmonics. Therefore, by setting $n = 1$, $\phi_n = 0$, $A_1 = A$, $B_1 = B$ and $\Gamma_1 = \Gamma$, the meshing force on the idler gear along the x_2 axis becomes:

$$f_m^{x_2} = [A\cos\alpha + B\cos\alpha\cos\Gamma]\cos\Omega t + [B\cos\alpha\sin\Gamma]\sin\Omega t \tag{69}$$

while along the y_2 axis is:

$$f_m^{y_2} = [A\sin\alpha - B\sin\alpha\cos\Gamma]\cos\Omega t - [B\sin\alpha\sin\Gamma]\sin\Omega t \tag{70}$$

By introducing the following parameters:

$$a = [A\cos\alpha + B\cos\alpha\cos\Gamma] \tag{71}$$

$$b = [B \cos\alpha \sin\Gamma] \tag{72}$$

$$c = [A \sin\alpha - B \sin\alpha \cos\Gamma] \tag{73}$$

$$d = [B \sin\alpha \sin\Gamma] \tag{74}$$

the meshing force components may be rearranged as follows:

$$\begin{cases} f_m^{x_2} = a\cos(\Omega t) + b\sin(\Omega t) \\ f_m^{y_2} = c\cos(\Omega t) - d\sin(\Omega t) \end{cases} \tag{75}$$

Starting from this canonical form, by defining the following additional parameters:

$$\begin{array}{lll} \varphi = \arctan(b/a) & \gamma = \arctan(-d/c) & K = \sqrt{a^2 + b^2} \\ J = \sqrt{c^2 + d^2} & \psi = \Omega t - \varphi & \delta = \varphi - \gamma \end{array} \tag{76}$$

it is possible to express the meshing force components by using cosine terms exclusively:

$$\begin{cases} f_m^{x_2} = K\cos(\psi) \\ f_m^{y_2} = J\cos(\psi + \delta) \end{cases} \tag{77}$$

By carrying out simple mathematical operations as raising to the square Eq. 77 and summing the two of them together, the following expression may be deduced:

$$\left(\frac{f_m^{x_2}}{K}\right)^2 - 2\left(\frac{f_m^{x_2}}{K}\frac{f_m^{y_2}}{J}\right)\cos(\delta) + \left(\frac{f_m^{y_2}}{J}\right)^2 = \sin^2(\delta) \tag{78}$$

Eq. 78 represents a non-canonical ellipse in Ox_2y_2 frame and it describes the trajectory of the overall meshing force applied to the idler gear.

5.2.1 *Canonical ellipse formulation*

In relation to the geartrain layout and how the bearings are connected to the housing, the direction of the ellipse semi-axis and their value may play a relevant role. Thus, it becomes necessary to get insights about ellipse orientation and the value of the two semi-axes. In order to compute these quantities, it is crucial to retrieve the expression of the canonical ellipse in its reference frame. By recalling the general form of a conic curve on a plane:

$$\hat{a}x^2 + \hat{b}xy + \hat{c}y^2 + \hat{d}x + \hat{e}y + \hat{f} = 0 \tag{79}$$

where $\hat{a}, \hat{b}, \hat{c}, \hat{d}, \hat{e}$ and $\hat{f}$ are real coefficients, the type of conic section is defined by the discriminant, i.e. the quantity $\hat{b}^2 - 4\hat{a}\hat{c}$. If $\hat{b}^2 - 4\hat{a}\hat{c} < 0$, then Eq. 79 represents an ellipse in Oxy frame.

For the sake of clarity, Eq. 78 is now rewritten as:

$$\left(\frac{1}{K}\right)^2 (f_m^{x_2})^2 - 2\left(\frac{\cos\delta}{KJ}\right) f_m^{x_2} f_m^{y_2} + \left(\frac{1}{J}\right)^2 (f_m^{y_2})^2 - \sin^2(\delta) = 0 \tag{80}$$

Eq. 80 describes an ellipse with semi-axes rotated of a certain amount from the reference frame axes. The computation of the rotation angle is essential for the correct prediction of pulsating forces spatial directions, in order to focus on their transmission on neighbour components and gearbox case. Moreover, knowledge of this angle is mandatory to retrieve the canonical form of the ellipse. It may be proved that the rotation angle of one of the ellipse semi-axes with respect to Ox_2y_2 frame is:

$$\theta = \frac{1}{2}\arctan\left(\frac{2KJ\cos(\delta)}{K^2 - J^2}\right) \tag{81}$$

It is well known that, in order to obtain the canonical ellipse, coefficient b must be equal to zero, i.e. no xy term in Eq. 79 may exist. As a consequence, a rotation of θ is applied on the Ox_2y_2 plane to Eq. 80 as represented in Fig. 41, leading to the following expression:

$$\begin{aligned}
&\left(J^2\cos^2(\theta) + K^2\sin^2(\theta) - 2KJ\cos(\delta)\sin(\theta)\cos(\theta)\right)\left(f_m^{x'}\right)^2 + \\
&+ \left(K^2\cos^2(\theta) + J^2\sin^2(\theta) + 2KJ\cos(\delta)\sin(\theta)\cos(\theta)\right)\left(f_m^{y'}\right)^2 + \\
&+ \left((K^2 - J^2)\sin(\theta)\cos(\theta) - KJ\cos^2(\theta)\cos(\delta) + KJ\cos(\delta)\sin^2(\theta)\right) 2 f_m^{x'} f_m^{y'} + \\
&- K^2J^2\sin^2(\delta) = 0
\end{aligned}$$

(82)

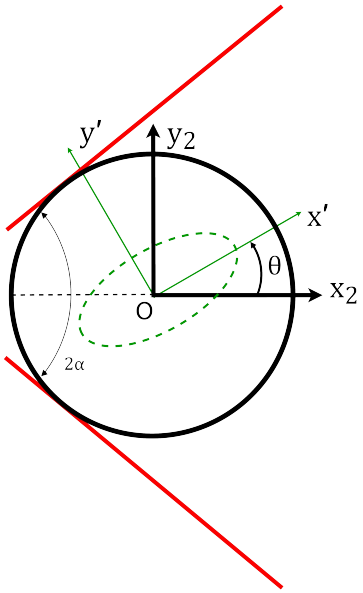

Figure 41: Elliptical trajectory drawn by the oscillating components of bearing forces (green dashed line). For the correct interpretation of this figure legend, color should be used in print.

By substituting Eq. 81 in Eq. 82, it may be observed that the coefficient multiplying term $f_m^{x'} f_m^{y'}$ is equal to zero, leading to the canonical form of the ellipse in the $Ox'y'$ frame:

$$\frac{f_m^{x'2}}{p^2} + \frac{f_m^{y'2}}{q^2} = 1 \tag{83}$$

where terms p and q denote the half value of the semi-axes of the ellipse, which are linked to the meshing force by the following expressions:

$$p^2 = \frac{K^2 J^2 \sin^2(\delta)}{\left(J^2 \cos^2(\theta) + K^2 \sin^2(\theta) - 2KJ \cos(\delta) \sin(\theta) \cos(\theta)\right)} \tag{84}$$

$$q^2 = \frac{K^2 J^2 \sin^2(\delta)}{\left(K^2 \cos^2(\theta) + J^2 \sin^2(\theta) + 2KJ \cos(\delta) \sin(\theta) \cos(\theta)\right)} \tag{85}$$

The ellipse is fully defined when parameters p and q are known. As it may be appreciated, parameters K, J and δ govern the shape and the size of the elliptical trajectory. In this framework, a focus on the latter is fundamental to understand the physical quantities governing the phenomenon. By retrieving the Eqs. from 71 to 74 and the defined parameters in Eq. 76, it is possible to observe that parameters K, J and δ depend on: the mounting angle α, the meshing phase Γ and the amplitude A and B of the considered harmonic of the meshing forces. The highlighted link makes the proposed dissertation a powerful tool to describe bearing forces transmission on idler gear in quasi-static condition. In fact, by properly setting the mounting angle α, the meshing phase Γ and the amplitude of the meshing forces, one may be able to control the direction of the transmitted forces in order to minimize the coupling with the whole structure. The proposed 205 method can be applied to any ordinary transmission layout with at least three gears. In addition, it is worth noticing that the analytical dissertation may be employed also if the idler gear is loaded by an external torque, since the methodology is retrieved by starting from radial dynamics.

5.3 PARAMETRIC STUDY

In this section, by starting from the analytical formulation proposed in Eq. 83, a parametric study is conducted on the ellipse shape and orientation. Parameters α, Γ, A and B are taken as control parameters to analyze ellipse shape and dimension modifications, i.e. to evaluate how the overall meshing force applied to the idler gear changes its behavior. The study is performed by varying each parameter without affecting the others, with the purpose to clearly detail the trends without masking them with further design hypotheses. The system parameters are set to the following values: $\alpha = 30°$, $\Gamma = 45°$, $A = 10N$ and $B = 7N$ and the influence of each of them is investigated while the other remains a constant.

Figure 42 represents ellipse orientation angle θ and the magnitude of each semi-axis as α varies from $0°$ to $180°$. According to design specifications and constraints, the charts demonstrate the possibility to control the direction of the overall force transmitted to the bearing of the idler gear. By observing the trend of the semi-axis magnitudes in Fig. 42, it may be noticed that their behavior is symmetric with respect to $\alpha = 90°$, while inclination axis θ is anti-symmetric.

When angle α is equal to 90°, 0° or 180°, the line of action of two meshings are parallel. As angle α approaches the value of 0° or 180° the magnitude of the minor semi-axis decreases, but the major semi-axis assumes its maximum value. The ellipse degenerates into a line parallel to x_2 axis, whose magnitude is the value of major semi-axis. A similar behavior is observed when the mounting angle α is close to 90°. In this configuration, the minor semi-axis is zero and the major one assumes its minimum value. This layout would assure the minimum value of major semi-axis and a transmission of forces along y_2 direction. The optimal configuration parameters depend on designer needs and geartrain configuration.

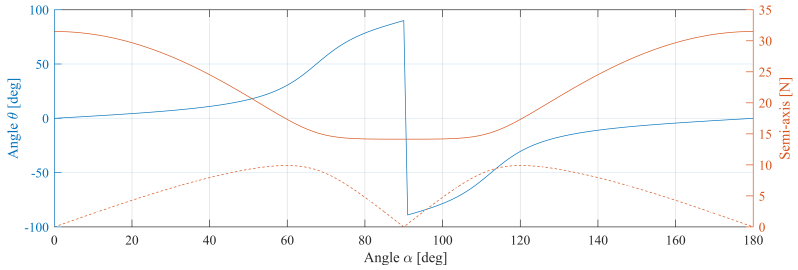

Figure 42: Influence of α on ellipse major and minor semi-axis (orange solid line and orange dashed line respectively) and semi-axis inclination angle θ (blue line). For the correct interpretation of this figure legend, color should be used in print.

In Fig. 43 the influence of the meshing phase Γ is evaluated. As Γ is varied from $-180°$ to 180°, the trend of semi-axis magnitude and inclination angle θ is symmetric with respect to $\Gamma = 0°$. When the oscillating components of meshing force 1-2 has no phase shift with respect to meshing 2-3 the major semi-axis trend presents its maximum, while the minor semi-axis value is equal to zero. The ellipse degenerates into a line rotated of a certain angle θ with respect to Ox_2y_2 frame. It may be concluded that, by applying a phase shift between the two gear meshings, a counterclockwise rotation of the ellipse would be generated, with the consequence to increase the value of minor semi-axis and decrease the magnitude of the major one.

Figures 44 and 45 represent the semi-axis magnitude and inclination angle θ variation in relation to the meshing force amplitude. This quantity is strongly related to meshing stiffness fluctuations. In fact, by adopting micro-geometry modifications, one may be able to modify meshing force harmonics without

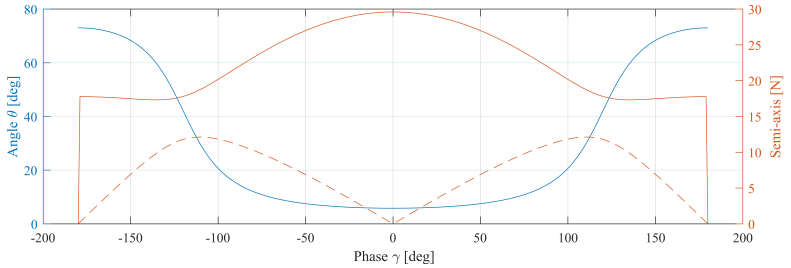

Figure 43: Influence of Γ on ellipse major and minor semi-axis (orange solid line and orange dashed line respectively) and semi-axis inclination angle θ (blue line). For the correct interpretation of this figure legend, color should be used in print.

consistently altering the gear macro-geometry. Results shown in Fig. 44 represent the semi-axis magnitude and inclination angle θ as the amplitude A varies from 1N to 13N. On the other hand, Fig. 45 shows the same parameters variation when the amplitude B is varied from 1N to 13N. By paying attention to both Fig. 44 and Fig. 45, it is possible to observe that, as both A and B increase, the value of semi-axis show an increasing trend, which is reasonable as the excitation magnitude raises. As a matter of fact, they act as gauge factors of the overall meshing force. The rotation angle θ presents a different behavior: as the amplitude A increases, the ellipse is rotated in counterclockwise direction (Fig. 44), conversely the rotation direction is reversed when amplitude B increases.

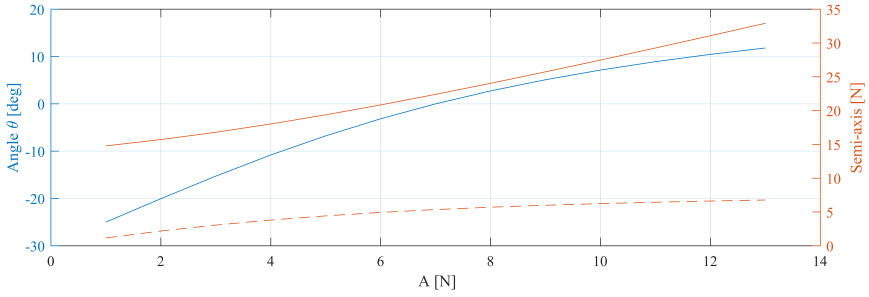

Figure 44: Influence of amplitude A on ellipse major and minor semi-axis (orange solid line and orange dashed line respectively) and semi-axis inclination angle θ (blue line). For the correct interpretation of this figure legend, color should be used in print.

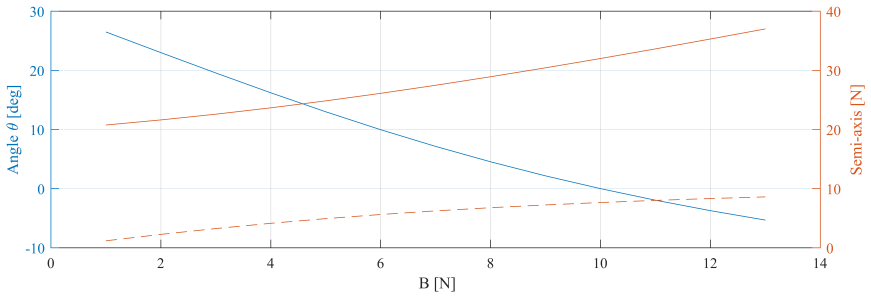

Figure 45: Influence of amplitude B on ellipse major and minor semi-axis (orange solid line and orange dashed line respectively) and semi-axes inclination angle θ (blue line). For the correct interpretation of this figure legend, color should be used in print.

Despite the obtained results are very useful during the driveline concept and design process, they remain valid only in quasi-static conditions, i.e. when the internal excitation is in a lower frequency range with respect to the system resonance. In order to provide further insights on the validity of the proposed approach in a real environment, the remaining part of the study is devoted to assess it in relation to the dynamics of the system. Within this framework, a dynamic model of the geartrain is realized and numerical simulations are performed, allowing to evaluate discrepancies and similarities when the system is close to its main resonance.

5.3.1 *Assessment under dynamic conditions*

In this subsection the effect of the internal excitation on the bearing force trajectory is investigated in dynamic conditions. In order to fulfill this purpose, a lumped parameter model is set and numerical analyses are conducted at various shaft rotational speeds. Figure 46 shows the lumped parameter model which has been realized by considering the geartrain layout described in section 5.2. Angle α has been set to 50° and a meshing stiffness phase shift of 50° is assigned on meshing 2-3.

Gear parameters are shown in Tab. 8. The prime mover is connected to an ideal motor by means of a compliant shaft, whose stiffness value is indicated in Tab. 8 as k_t. The numerical analyses are conducted in Simcenter AMESim environment by following the approach presented in Chapter 2. Geartrain

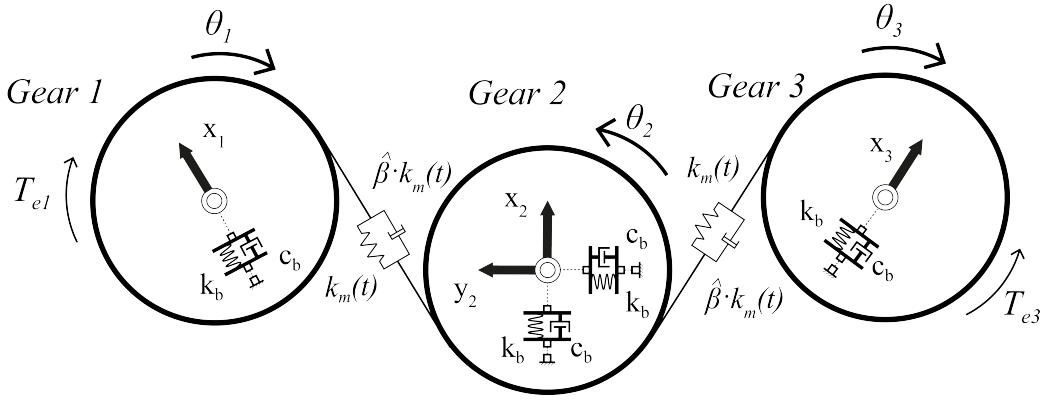

Figure 46: Lumped parameter model of the geartrain, k_b and c_b represent the bearing stiffness and damping, respectively.

dynamics is solved with a fixed time step integrator based on a 4^{th} order Runge-Kutta method. Gear time-varying mesh stiffness is set as a mono-harmonic function, this simplification is adopted in order to obtain a mono-harmonic meshing force when the excitation frequency is far from the system resonance, as assumed within the calculations shown in section 5.3. The mono-harmonic function has been determined in the following manner: first of all, the gear mesh stiffness has been estimated by following the analytic method described in [22], afterwards, only the first harmonic of the computed curve is considered. The viscous effects are modeled by adopting a Rayleigh's damping model, i.e. a proportional damping respect to mass and stiffness $C = \hat{\alpha}M + \hat{\beta}K$. With reference to Eq. 64, damping effects are included in $f_m^{x_2}$ $f_m^{y_2}$, $f_b^{x_2}$, $f_b^{y_2}$ definitions. Several simulations at different rotating speed values are performed and the elliptical trajectory drawn by the meshing force amplitude values is compared with the one generated by the amplitude of the bearing force. The main goal is to analyze the potential trajectory gap and shape modification when the inertial effects become relevant.

The starting point is the modal analysis of the gear set. First of all, the system is linearized by considering the mean value of meshing stiffness, then eigenvectors and eigenvalues are computed. Figure 47 represents the eigenvectors of the system with their respective eigenvalues. The last eigenvector is not represented as it does not participate at the whole system dynamics. Its eigenvalue is at 28040 Hz and the modal shape mainly involves the rotation of gear 1. Such a natural mode is due to the torsional stiffness which links the

Parameters	Gear 1	Gear 2	Gear 3
Mass [kg]	0.12	0.181	0.243
Mass moment of inertia [kgm^2]	8.49e-5	1.6e-4	1.07e-4
Module [mm]	3		
Number of teeth	25	32	17
Pressure angle [deg]	20	20	
Gear mesh stiffness [N/m]	2.1e+7 (max) 1.9e+7 (min)	2.1e+7 (max) 1.9e+7 (min)	
k_b bearing stiffness [N/m]	1e+7	1e+7	1e+7
$\hat{\alpha}$ damping coefficient [s^{-1}]	100		
$\hat{\beta}$ damping coefficient [s]	1e-5		
k_t torsional stiffness [Nm/rad]	2.61e+6		

Table 8: Design parameters

prime mover to the frame. Eigenvectors are represented as normalized vectors, where rotational degrees of freedom are multiplied for their respective base radii, in order to obtain comparable quantities. Once the modal shapes and their frequencies are known, it is possible to observe how they affect the elliptical trajectory. In fact different behaviors can be observed when the excitation frequency approaches one eigenvalue. Depending on the mode shape, meshing forces may play a predominant role over the bearing forces or vice-versa.

Figure 50 shows the ellipse described by bearing force and meshing force amplitudes as the frequency of the internal excitation raises. The ellipse is obtained by plotting the numerical results. When the shaft rotation speed is low, the two trajectories perfectly match, in agreement with the main hypothesis adopted for the analytical dissertation, i.e. inertia effects are negligible. On the other hands, a certain gap may be observed as the excitation frequency approaches the first vibration mode around 470 Hz. The inertia effects make the amplitude of bearing forces greater than the meshing ones. This phenomenon may be observed up to 1700 Hz, which corresponds to a shaft speed rotation of 4000 RPM. Around this frequency value, a substantial overlapping of the two curves is observed. By running the prime mover shaft at 5000 RPM, the excitation frequency gets close to the fifth eigenvalue, which modal shape involves simultaneously the meshing 1-2 and 2-3. As a consequence, in the frequency range 2000 - 5000 Hz the amplitude of meshing forces overcome the

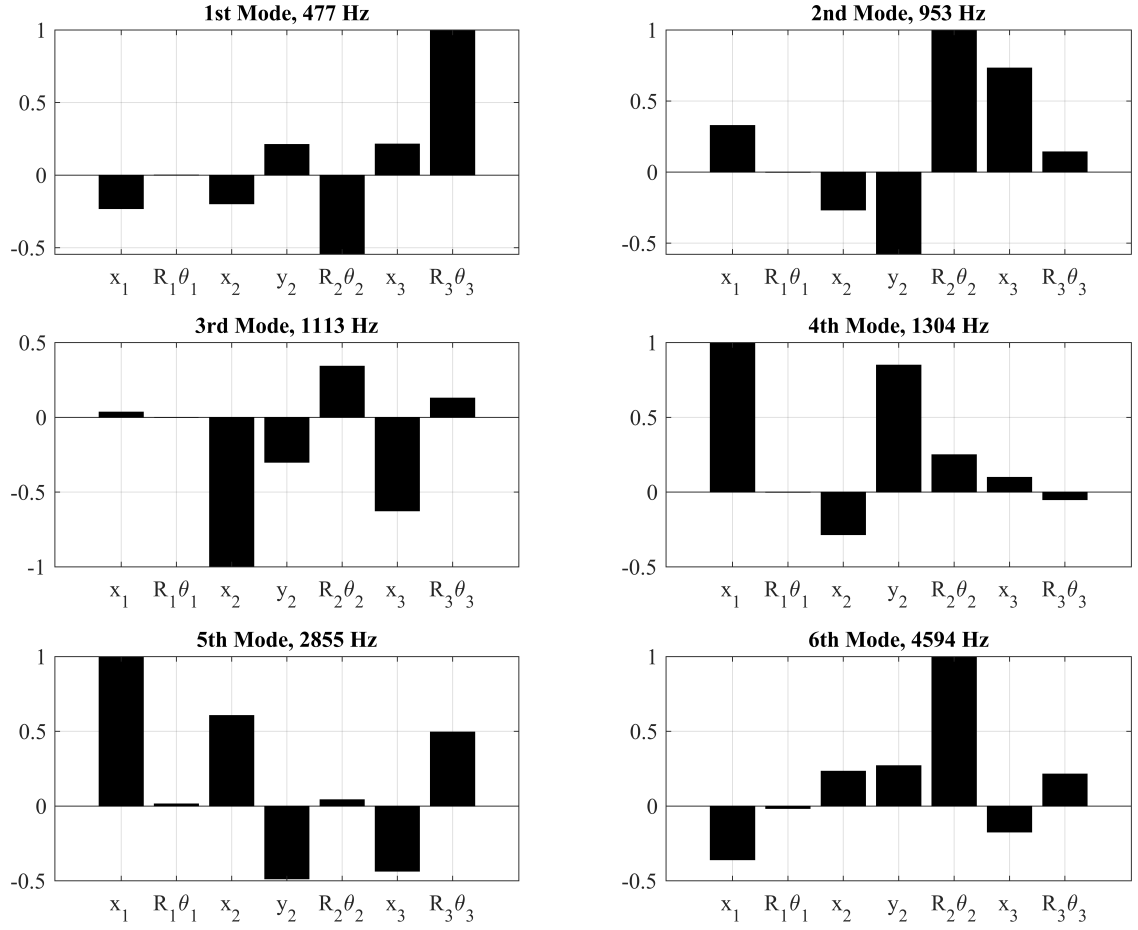

Figure 47: Normalized eigenvectors of the system with their respective eigenvalues

bearing one. In order to understand the reason behind this scenario a focus on Eq. 64 is needed. Bearing forces on idler gear are the result of the sum between inertia and meshing contribution. Figure 48 shows the time evolution signal of $m_2\ddot{y}_2$ and $f_m^{y_2}$ for each simulated speed. For the sake of clearness only results related to y direction are reported, as the same considerations may be applied to x direction. For low rotational speed values, inertia forces are close to zero, but as the system approaches the first mode shape, their value becomes to increase. Depending on phase relationship between $m_2\ddot{y}_2$ and $f_m^{y_2}$, bearing forces oscillating component magnitudes can results lower or higher with respect to the meshing forces. By paying attention to Fig. 49, it is possible

to observe the phase relationship evolution at different rotational speeds. Up to 3000 RPM, almost no phase shift occurs between the two signals. On the other hand, for higher values of the shaft speed rotation the phase shift approaches the value of $|\pi|$. When the two signals are in opposite phase, their combination leads to a bearing forces oscillating components whose magnitude is lower with respect to the meshing force.

Numerical experiments may be extremely useful to understand the ellipse modification when the excitation frequency sweeps out all eigenvalues of the dynamic system. The obtained results confirm that under the hypothesis of quasi-static motion the analytical dissertation provided in section 5.2 represents an effective and reliable tool to forecast the main overall direction of pulsating bearing forces. Unless this, not all the parameters governing the ellipse can be known a-priori. As an example, even if the mounting angle α and the phase shift between two consecutive meshings Γ can be chosen during the gear design concept phase, estimating amplitude of meshing forces is not a straightforward task. As stated in section 5.3, meshing forces oscillating components may be piloted by controlling meshing stiffness fluctuations acting on tooth micro geometry, but they cannot be unequivocally determined in geartrain design process. Gear meshing forces oscillating components are originated by an internal dynamic excitation linked to meshing stiffness and dynamic transmission error. When dynamic effects become relevant it is not possible to give an estimation of meshing forces amplitude. Based on these observations, it may be concluded that the proposed theory is a reliable tool to understand phenomena linked to bearing forces transmission direction. However, it cannot be used to correctly forecast the exact direction of bearing forces transmission due to the uncertainty of the meshing forces amplitude values.

The analytical dissertation proposed in section 5.2 is developed by considering only a single generic harmonic of the meshing force. In this section, the authors adopted the hypothesis of a single harmonic meshing stiffness in order to obtain almost a mono-harmonic response. As it is shown in Fig. 50, the path followed by the oscillating components of bearing and meshing forces not always represents an ellipse. This behavior appears when the system response is not mono-harmonic. In real systems, multi-harmonic excitation as well as mono-harmonic parametric resonances could generate multi-harmonic system responses. In these cases, the combination of the meshing forces oscillating

components could realize trajectories which may deviate from the elliptical one. Unless this, it may be demonstrated that the final trajectory is obtained as a sum of different ellipses generated by each harmonic of the response time history. By considering the final trajectories at 7000 RPM, Fig. 50, one may notice that meshing forces are not mono-harmonic. In fact at least two harmonics may be recognizable in time evolution signal, Fig. 48. This aspect is depicted in Fig. 51 where the ellipse drawn by each harmonic and the trajectory obtained by their sum are shown. It may be concluded that, when the excitation frequency is far from the system eigenvalues, the dissertation provided in section 5.2 represents a valid method which directly links the direction of the transmitted forces and their amplitude values with the geartrain layout, meshing phase and meshing stiffness fluctuations.

5.4 CONCLUDING REMARKS

The Chapter is devoted to obtain an analytical formulation of the trajectory drawn by the oscillating components of bearing forces on idler gear. By following the intuition of White et al. in [132], the authors established the physical quantities which govern the phenomenon. In detail, by starting from the definition of meshing forces as a mono-harmonic function the equation of a canonical ellipse is obtained, which constitutes a direct link between bearing forces transmission direction and the mounting angle α, the meshing phase Γ and the amplitude of the meshing forces. The latter constitutes the limit of analytical dissertation, in fact the amplitude of meshing forces can be controlled by adopting gear micro-geometry modification but it can not be determined unequivocally without solving the system of ordinary differential equation 64, as it is the result of internal excitation. The dissertation is conducted by considering a single harmonic of the meshing force. This assumption does not produce any loss of generality, since on the basis of the superposition principle, it may be extended to an arbitrary number of harmonics as confirmed by the numerical results. Successively a parametric study is conducted in order to evaluate the influence of different geometrical parameters on the ellipse shape and orientation. According to design specifications and constraints, the results demonstrate the possibility to control the direction of the overall force transmitted to the idler gear bearings. Finally numerical experiments are performed, in order to investigate how the internal excitation frequency affects the

elliptical trajectory. As a matter of fact, in quasi-static condition the elliptical trajectory depicted by the oscillating components of bearing forces perfectly match the meshing ones. On the other hand, when the internal excitation frequency approaches one eigenvalue of the system, the analytical dissertation can not be used to forecast the main overall direction and magnitude of bearing forces. It may be concluded that the developed theory is a reliable and effective instrument to understand phenomena linked to bearing forces transmission direction. However, it cannot be used to correctly forecast the exact direction of bearing forces transmission due to the uncertainty of the meshing forces amplitude values.

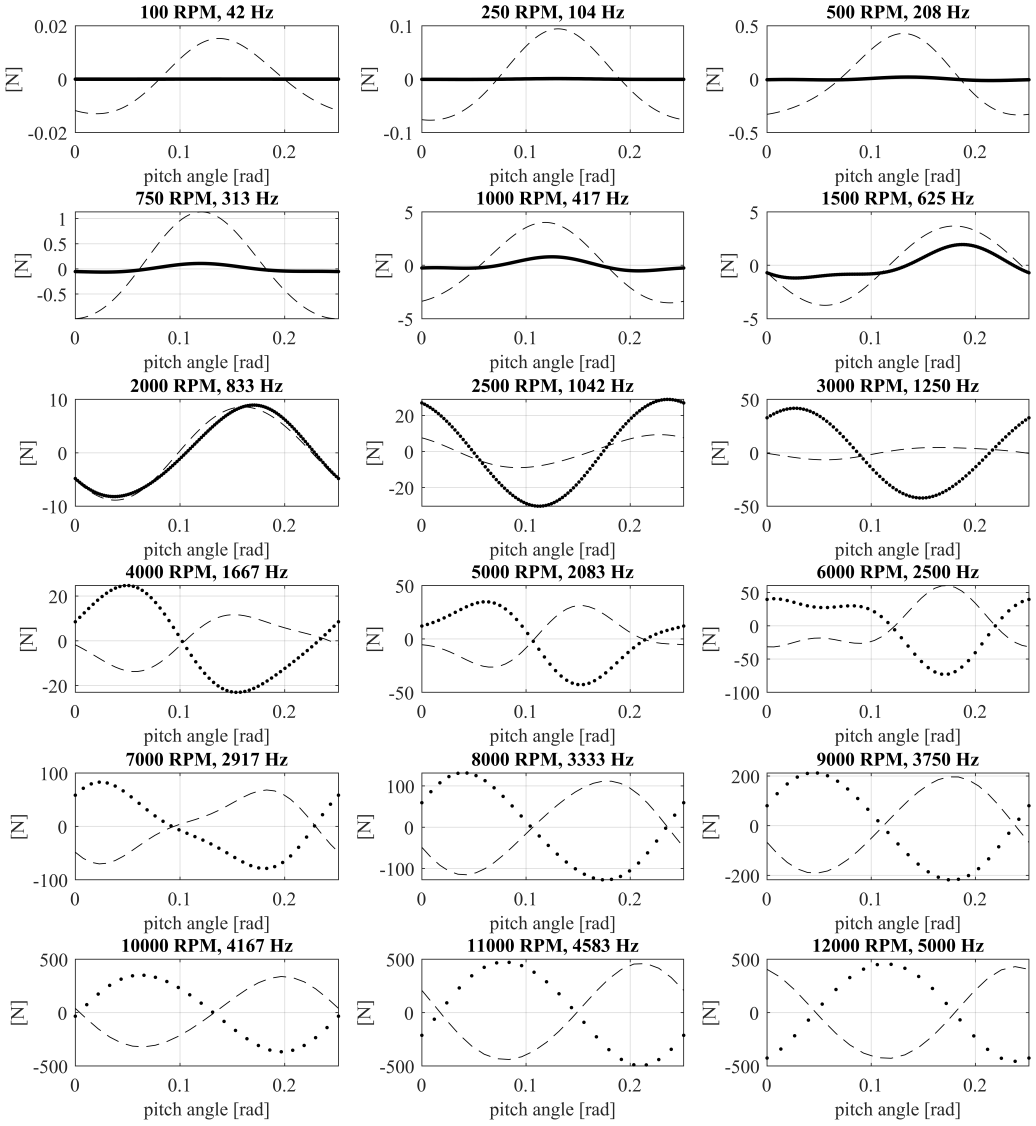

Figure 48: Time evolution signal of meshing (dashed line) and inertial forces (dotted line) oscillating components along y_2 direction

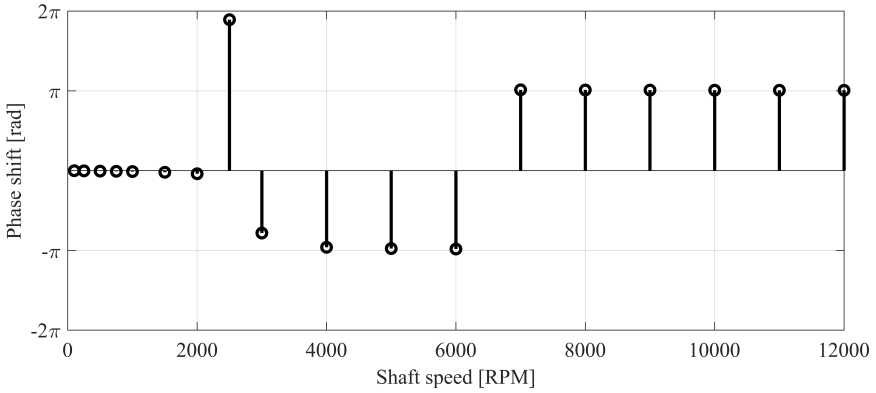

Figure 49: Phase shift between meshing and inertial forces. Phase shift is computed only on the first harmonic, where the higher energy content is stored

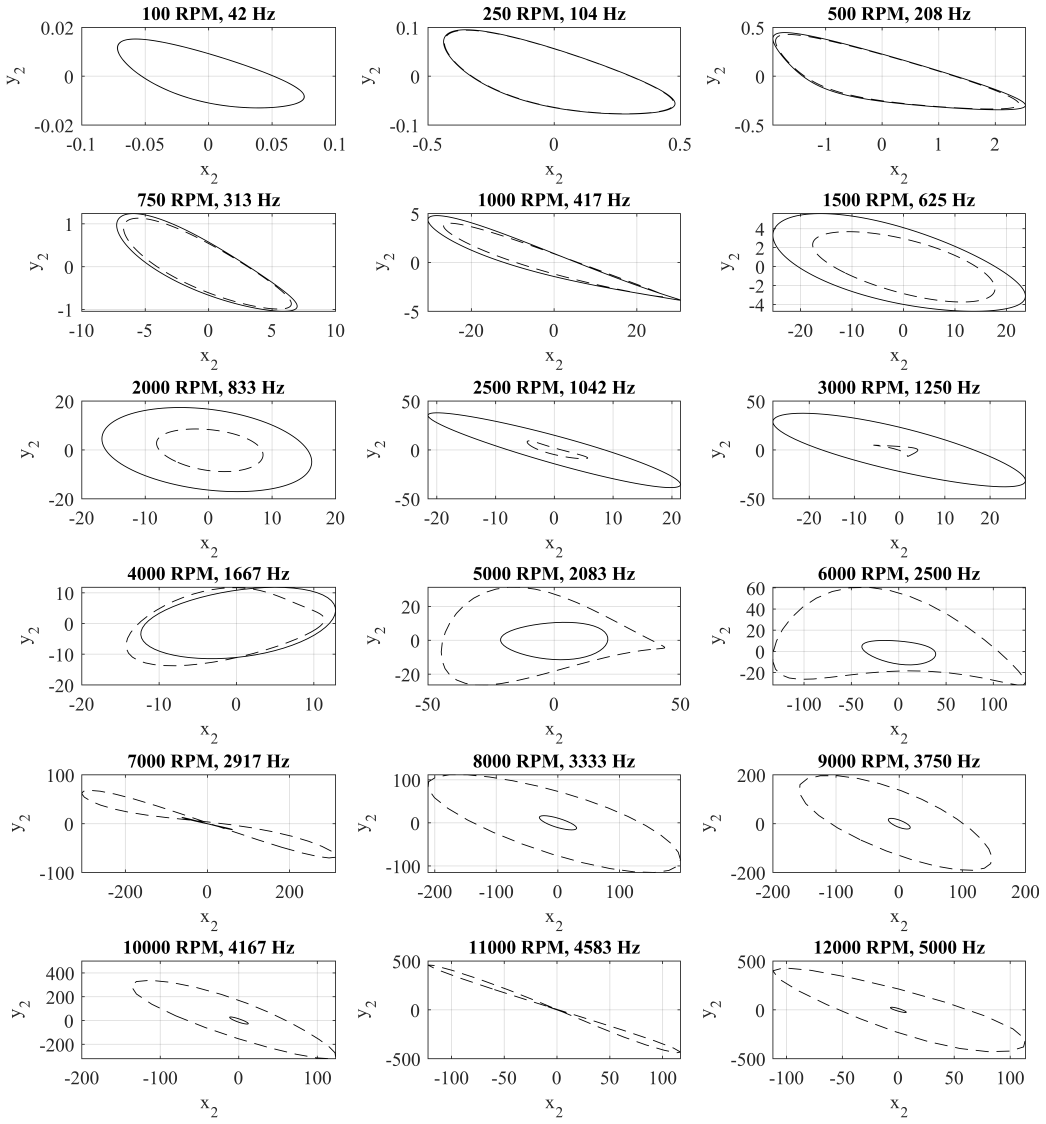

Figure 50: Elliptical trajectories drawn by meshing forces (dashed lines); Elliptical trajectories drawn by bearing forces(continue lines); x_2 and y_2 axis represent the amplitudes of forces [N] in that direction

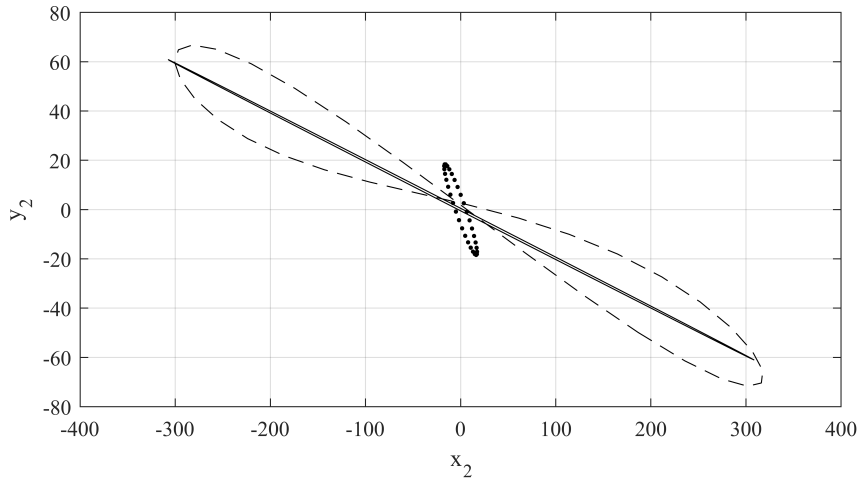

Figure 51: Elliptical trajectory drawn by 1st and 2nd harmonic of meshing force (continue line and dotted line respectively); final trajectory drawn by the total meshing force (dashed line). x_2 and y_2 axis represent the amplitudes of forces [N] in that direction

6

CONCLUDING REMARK

The thesis addresses analytical-numerical methodologies for studying the nonlinear dynamics of geared systems, by considering the critical aspects which are responsible for vibration and noise generation. The starting point is the investigation of the modeling approach and solution techniques used nowadays to represent the dynamic behavior of these mechanical systems. In particular, two modeling and solution strategies are analyzed in detail. The first one rely on Simcenter AMESim commercial software, while the second one is based on a Matlab interface continuation software. The difference between the two approach relies not only in the modeling strategy itself but also on the solution techniques adopted to compute the nonlinear system response. The first technique enhances the modeling approach as a user-friendly and effective tool in the realization of ordinary geared transmission models. Based on graphical software capabilities, the author propose detailed guidelines to build a complete geartrain model by connecting some pre-programmed devices between them. On the other hand, the second modeling strategy enhances the Asymptotic Numerical Method as resolution method for non linear dynamics of gears. After a peculiar recast of the equation of motion, the author underline benefit and drawbacks of the modeling strategy. After the investigation of the modeling possibilities, various aspect related to rattle and whine noise emission are deeply investigated. Regarding rattle noise, the research activity has lead to the introduction of a new analytic parameter able to detect teeth detachment in multi-mesh geartrains. In the same manner, the studies on whine noise have conducted to an analytical formulation able to forecast the main overall direction and magnitude of bearing reaction forces on idler gear when the geartrain works under quasistatic condition. The analytical formulations are supported by numerical assessment.

Chapter 1 represent an overview on geared system excitation mechanism and their modeling. Within this framework, the multiple factors giving rise to the vibration source are explained. In particular, the mechanism governing the internal excitation and the non-smooth non linearity due to the backlash clearance are introduced. The static transmission error and time-varying mesh stiffness are responsible for the internal excitation source and recognized as the main phenomena leading to whine noise emission. On the other hand, the backlash induced torsional vibrations leads to vibro-impacts between teeth generating the so called rattle noise. By starting from the introduced elements, it has been underlined the need of a detailed mathematical model capable to describe the complex nonlinear behavior of geared transmission system. The most effective modeling strategies lies on lumped parameter model. In addition, in pre-processing stage, different techniques may be adopted to compute bearing and meshing stiffness values as FEM analysis and analytical procedures. Besides the modeling strategy, the author underline the importance of the different solution techniques. Dealing with nonlinear systems, the choice of the numerical computation method may represent a key point to investigate the phenomena of interest. In fact, in Chapter 2 and Chapter 3 two modeling and solution strategies are analyzed in detail.

In Chapter 2, the nonlinear ordinary differential equations representing the motion of a single gear pair are established. The model accounts for all the phenomena playing a crucial role in gear dynamics. For instance, it encompasses the backlash non linearity, time-varying and load depended mesh stiffness, load depended bearing stiffness and lubricant squeeze force when teeth detachment occurs. Afterwards, a block diagram approach is proposed as an effective tool to realize geared transmission system models. The employed software is Simcenter AMESim, a commercial software which allows the simulation of physical multi-domain systems. In fact, by taking advantage from graphical user interface, a modular architecture is developed in order to construct any geartrain by connecting the pre-programmed element between them. Within this framework, a lumped parameter model of a driveline employed in automotive sector is developed. Numerical results are compared with experimental outcomes showing an excellent agreement. In particular, the dynamic phenomenon occurring during the experimental test represent an important element captured by the numerical model. In fact, bifurcations appear in the dynamic system response, which are perfectly represented by

the numerical outcomes. Once the author gave proof of the effectiveness and reliability of the model, he can affirm that the proposed modeling strategy may offer a great advantage in the model setup phase. In fact, the introduction of such tool in industrial environment may represent a key point to speed up the model setup phase. The limit of the proposed approach lies into the resolution techniques adopted to solve the ordinary differential equation system. In fact, Simcenter AMESim is limited to the already built-in time integration techniques which are not suited to perform unstable solution branch computation and bifurcation tracking. In order to get further insight on the issue, in Chapter 3 an additional modeling strategy is investigated.

Chapter 3 evaluates the Asymptotic Numerical Method as a valuable approach to compute the nonlinear dynamic response of a gear pair. This approach is a continuation method based on high-order Taylor series expansion. For instance, it is able to perform stable and unstable solution branch computation and it is suited to perform stability analysis and bifurcation tracking. After an investigation of the current state of the art, it was found that the method stands out from the others as it is a purely frequency domain method characterized by an high efficiency in the computation of high-order Taylor series. This aspect is achieved by recasting the system of equation in a quadratic form. In fact, once all the nonlinearities are expressed as a product of two variables, the computation of the series can be automatized and computed with high efficiency. The quadratic recast is a part of the method itself for its generality and performance. The Chapter provides a brief explanation of the method and its efficiency. Firstly, the lumped parameter model of a purely torsional gear pair model is recalled. The model accounts for time-varying mesh stiffness and backlash. For the sake of easiness, load depended bearing and mesh stiffness are not included in the model as well as squeeze force when teeth detachment occurs. Afterwards a 4 DOFs model of the gear pair is established. Results computed with Asymptotic Numerical Method are compared with that obtained from the Runge-Kutta time integration scheme, demonstrating an excellent agreement. The method provides for a full nonlinear dynamic response of the geared rotor bearing system, where the computation of unstable solution branches is performed in very a short simulation time. In addition, continuation may be performed with respect to any parameter of interest, as damping or stiffness. On the other hand, the proposed modeling approach relies on a quadratic recast of the system which may drastically increase the

model set-up phase. In addition, within geared system dynamics, the real limit of the Asymptotic Numerical Method is represented by the necessity to express the nonlinear contact function as an analytical smoothed one. In fact, when double-sided impacts occur, the transmission of forces takes place on the Back-side Line of Action. This aspect can lead to an erroneous estimation of bearing reaction forces as the definition of dynamic transmission error assumes a different expression. Beside this important aspect, any consideration related to torsional dynamics remains valid.

Chapter 4 is devoted to the generalization of the Rattle Index proposed by R. Singh et al. in [10] to any type of ordinary transmission layouts, single or multiple branch, both in idle and loaded conditions. In particular, by starting from the classical 6 DOFs equation system defining the nonlinear dynamics of a gear pair, a recursive analytical formulation of the rotational dynamics of gears is proposed. This methodology allows the generalization of the rattle index definition for any meshing pair pertaining to a multimesh driveline. The analytical definition is shown to be a proper indicator of the vibro-impacts related to each gear pair of the transmission. In addition, it is able to detect the potential presence of mutual interactions between them. In a first instance, the analytical procedure is carried out for a single branch unloaded geartrain. Afterwards, the definition is drawn out to single branch, loaded geartrain. Within this framework, consideration on rattle index validity are made. Some indications are given in order to avoid numerical problems and erroneous indication of teeth detachment occurrence. Finally, the dissertation is applied to multiple branch, loaded geartrain. After the definition of the rattle index is well established for the different geartrain layouts, numerical simulations are performed. Lumped parameter models of several driveline configuration are realized by following the modeling approach delighted in Chapter 2. The numerical outcomes, demonstrate the reliability and accuracy of the outlined parameter. The rattle index instantaneously describes the vibro-impacts events related to any gear pair of the driveline. In addition, it may lead to a quantitative estimation of vibro-impact severity. In fact, the numerical assessment proved that as long the oscillating torque amplitudes increases the the impact between teeth become more severe.

Chapter 5 proposes an analytical formulation able to forecast the main overall direction and magnitude of bearing reaction forces on idler gear when the geartrain works under quasi-static condition. By starting from the intuition

of White et al. in [132], the physical quantities governing the phenomenon are established. In detail, it has been proved that the alternating component of bearing forces on idler gear describes an elliptical trajectory as the prime mover rotates over a pitch angle. The ellipse orientation and the values of semi-axis depend on the meshing phase, gear spatial position and the amplitude of meshing forces. When the internal excitation is in a frequency range below the system resonance, the overall mesh force may be considered as equal to the bearing reaction force, since the dynamic inertial effects can be neglected. In this regard, the time-varying meshing forces are transferred to the bearing housing and the vibration is transmitted along the entire system assembly. The size of the ellipse and the direction of semi-axis are strongly related to gear whine noise emission. A parametric study is conducted in order to demonstrate that by properly setting the over-mentioned parameters one may be able to control the magnitude and direction of the overall idler bearing reaction forces. Finally, numerical experiments are performed to investigate if the proposed analytical methodology is suitable in dynamic conditions, when the inertial effect become relevant. The lumped parameter model is established by employing the Simcenter AMESim modeling strategy described in Chapter 2. The numerical outcomes confirmed that under quasi-static motion the analytical dissertation is an effective and reliable tool to forecast the main overall direction of pulsating bearing forces. On the other hand, when the excitation frequency approaches one system eigenvalue, it is not suitable as the inertial effect may be dominant. Nevertheless, the real limit of the analytical formulation lies in the uncertainty of some parameter governing the ellipse shape and dimension. The gears spatial position and the phase shift between two consecutive meshing can be chosen during the gear design concept phase, on the other hand, estimating the amplitude of meshing forces is not a direct matter as they are the result of internal excitation.

The methodologies introduced and discussed in the present thesis are characterized by different original aspects with practical implications in the development of advanced design and optimization procedures. In particular, the model described in Chapter 2 represents a very powerful instrument to be placed in industrial environment. In those context characterized by the need for rapid and effective calculation tools, the block diagram approach represent an effective way to speed up the model setup phase. On the other hand, the modeling strategy introduced in Chapter 3 outline a comprehensive tool able

to compute the complete response dynamic function of a nonlinear system. In this case the modeling set-up phase is drastically increased but the computational time is considerably reduced. Beside the modeling strategies and solution techniques, the analysis conducted in Chapter 4 on gear rattle noise constitutes a relevant novelty to the current state of the art. Finally, Chapter 5 provides a very powerful tool to control gear whine noise emission.

A

AXIAL PISTON PUMP, MODELING AND EXPERIMENTAL VALIDATION

The current study proposes a lumped parameter approach to represent axial piston pump of swashplate design pressure dynamics. By employing Simcenter AMESim commercial software, a model of the pump and experimental setup is realized. The test rig geometry and fluid resonance are modeled with high accuracy in order to catch the main pressure ripple amplification in a wide frequency range. Finally numerical results are compared with experimental outcomes with excellent agreement.

A.1 INTRODUCTION

Hydraulic displacement machines represent one of the main source of vibration and noise in hydraulic systems. Flow ripple at suction and delivery ports may cause large pressure magnitude variation. The pressure ripple is then responsible for the large dynamic forces inside the volumetric machine which can determine vibrations of the pump shell and consequently airborne noise. One of the first reference on the noise generated from an axial piston pump can be found on the PhD thesis by Helgestad [133]. Later Edge et al. published a work on the modelling of the flow ripple [134]. A detailed description of the internal forces and chamber evolution pressure is given by Invantysin in [135].

The purpose of the current study is to realize a lumped parameter model for an axial piston pump real test case. Numerical forecast of pressure ripple dynamics are compared with experimental results in order validate the reliability of the model. Firstly, the basic working principle of the volumetric machine is presented. By starting from the analytic model presented in [136], a lumped parameter model of axial piston pump pressure dynamics is realized.

Afterwards, numerical outcomes are compared with real test case experiments in a wide range of operating condition. The numerical-experimental correlation validates the consistence and effectiveness of the modeling strategy.

A.2 PRESSURE DYNAMICS MODELING

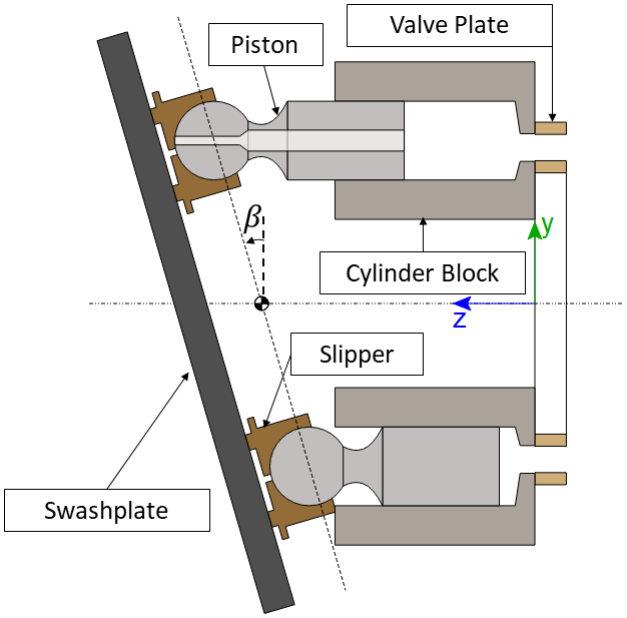

Figure 52: Axial Piston pump of swashplate design

The basic principle of an axial piston pump is depicted in figure 52. The cylinder block is provided of different cylinder bores. The pistons are arranged into cylinder bores and execute a linear movement as the cylinder block rotates around z axis. Piston heads are in contact with the swashplate by means of slippers, whose function is to reduce friction between piston heads and the swashplate. The latter is rotated of a generic angle β which modify the displacement of the pump, as depicted by figure 52. During a complete revolution, the piston execute a full stroke. The piston stroke is function of the angle β, in fact the flow direction can be reversed without changing the revolution direction of the shaft. The suction and delivery ports are connected to the cylinder blocks by means of a plane valve plate, see figure 53, which is provided by two kidney shaped openings corresponding to inlet/outlet ports.

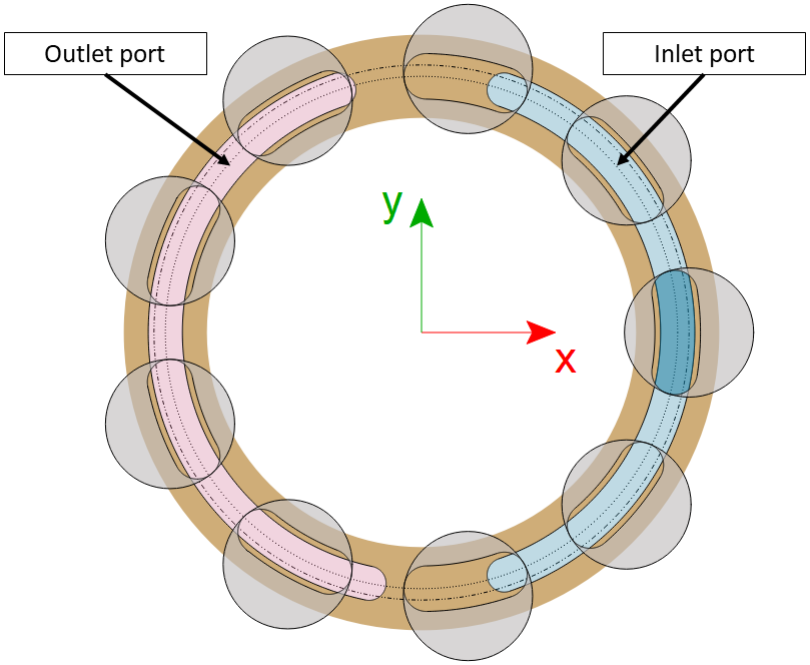

Figure 53: Valve plate

The delivery flow rate is the sum of the flow rate due to each cylinder bore. In this regard, the control volume is represented by the single piston chamber, see figure 54. The pressure evolution inside the control volume is governed by the following equation:

$$\frac{dp}{dt} = \frac{K}{V}(Q_r + Q_S - \frac{dV}{dt}) \tag{86}$$

where K represent the fluid bulk modulus, V is the fluid volume enclosed in cylinder chamber, $\frac{dV}{dt}$ is the change of the volume with respect to time. The fluid bulk modulus is a function of temperature and pressure and represent an essential characteristic, as it is a measure of the fluid resistance to compression. The flow rate Q_r represent the flow in and out of the piston bore through the valve plate opening, while the Q_S term is the total amount of external leakage. The volumetric losses Q_S, figure 54, are the sum of the flow rate through the

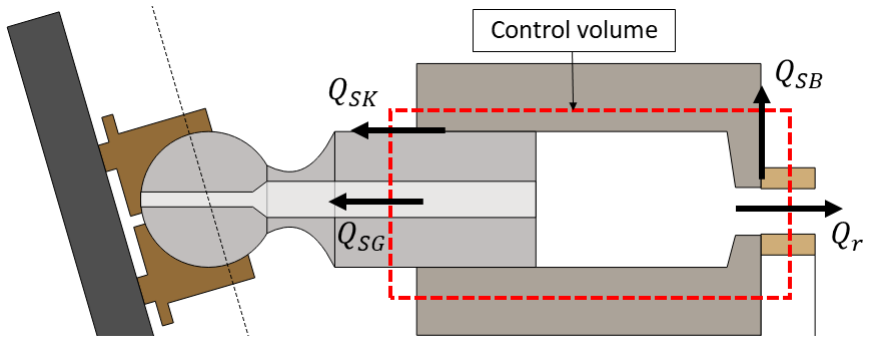

Figure 54: Control volume

valve plate opening Q_{SK}, the flow rate through the gap between cylinder block and valve plate Q_{SB} and the flow rate through the piston and slipper Q_{SG}:

$$Q_S = Q_{SK} + Q_{SB} + Q_{SG} \tag{87}$$

For each chamber the flow rate going through the suction/delivery ports can be expressed on the basis of the flow equation through orifices:

$$Q_r = \alpha_d A_r \sqrt{\frac{2}{\rho} \Delta P} \, sign(\Delta P) \tag{88}$$

where α_d is the orifice discharge coefficient, which is a function of the opening discharge area A_r and pressure. The area A_r is a function of the cylinder block rotation and depends on the design of the slots in the transition region on the valve plate. By denoting with Q_{r_i} the flow rate of a single piston chamber, the total amount of flow rate at delivery port is obtained by summing the contribution of each piston chamber: $Q_{tot} = \sum Q_{r_i}$, where N indicates the number of pistons. The volumetric losses are computed by employing the relations for laminar flow through a generic gap. Further insight on external leakage computation are given in [136].

In addition, the modeling of fluid wave effects within the pipe of the hydraulic circuit represents an essential aspect. The compressibility of the fluid and expansion of the pipe/hose wall with pressure are taken into account by using an effective bulk modulus. In case of flexible pipes, the stiffness of pipes wall play a crucial role in the calculation of the effective bulk modulus as depicted in [137].

A.3 NUMERICAL ASSESSMENT

The dynamic model introduced in the previous section has been implemented in Simcenter AMESim environment. Afterwards it is used to study the pressure dynamics on a real test case piston pump of swashplate design. The volumetric machine is composed by 9 pistons, developing a displacement of 100 cm^3/rev. The experimental setup is shown in figure 55. While a schematic representation

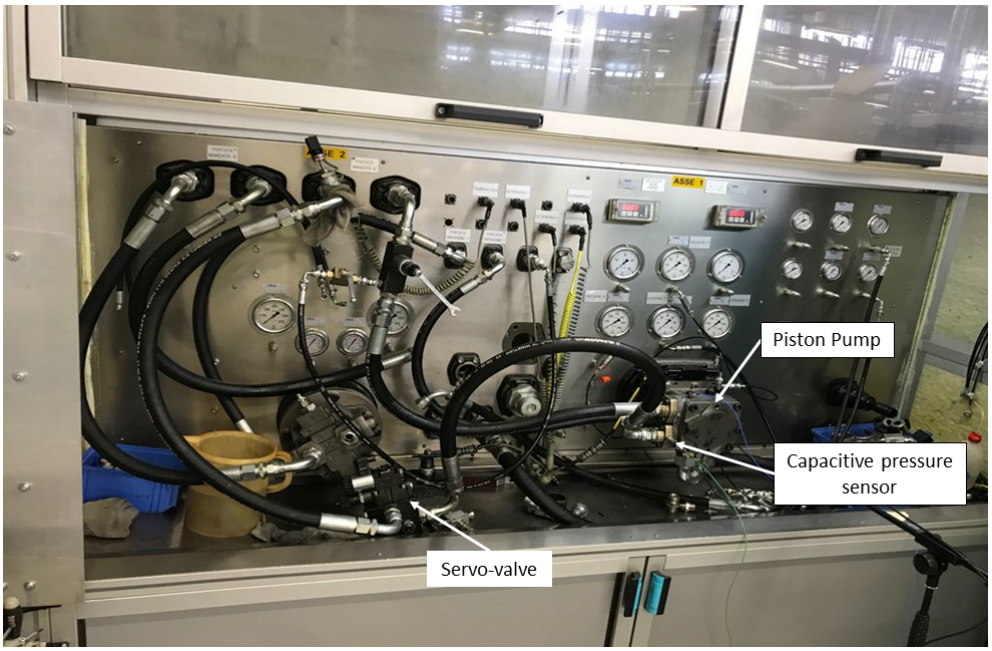

Figure 55: Experimental setup

of the hydraulic circuit is depicted in figure 56. Due to confidentiality reasons, pump parameters are not reported. The experimental test are performed over a wide range of working conditions. The cylinder block speed ranges from 1000 to 3000 RPM while the mean pressure at delivery ports varies from 100 to 350 bar. In a first instance the system is accelerated from 1000 to 3000 RPM in 60 seconds, at a mean delivery pressure of 100 bar. A servo-valve at delivery port modify the orifice dimension in order to keep the mean pressure as constant as possible. This run up experiment is done in order to evaluate the presence of fluid resonance in delivery pipe. Pressure dynamics is acquired by means of capacitive pressure sensor, whose position is depicted in fig. 55. The pressure

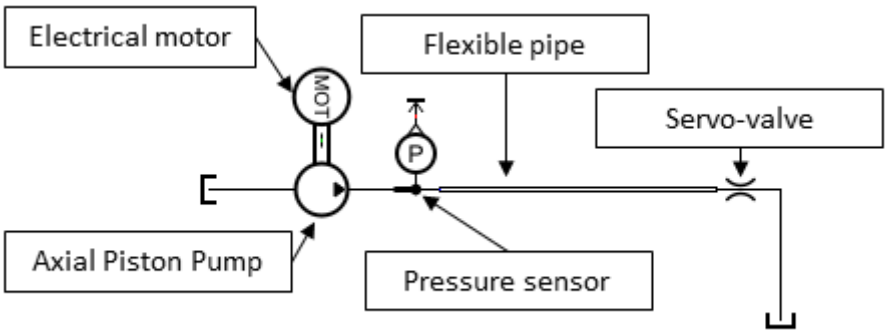

Figure 56: Hydraulic circuit scheme

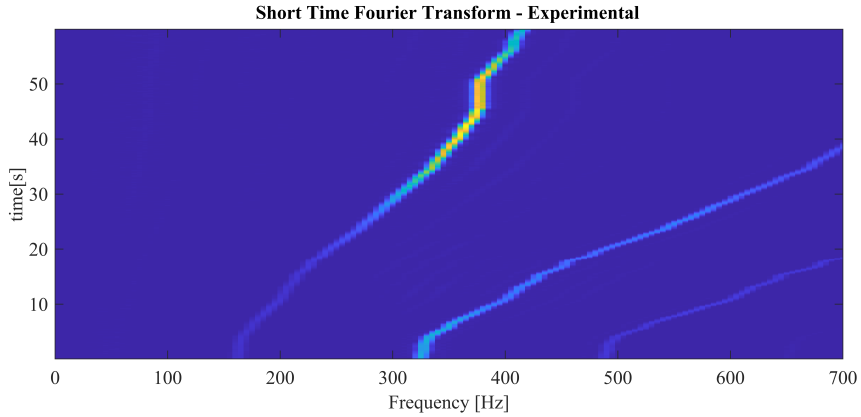

Figure 57: Experimental signal of pumping order trend

signal related to the run up test is post-processed and results are shown in terms of pumping orders, figure 57. As it can be observed from figure 57 a clear resonance zone governs the pressure dynamics in the frequency range 300-400 Hz. Fluid resonances are mainly related to dimensions and mechanical properties of the piping hydraulic circuit. Although pipe diameter and length are known, an estimation of their stiffness value is not a straightforward task. In fact the flexible pipes are characterized by a strong anisotropy which makes the calculation of their stiffness a challenging matter. Numerical run up simulation are performed and results in terms of order trend are shown in figure 58. The numerical model identify a resonance zone in the frequency range 250-420 Hz which is very close to the experimental resonance zone. Apart from the

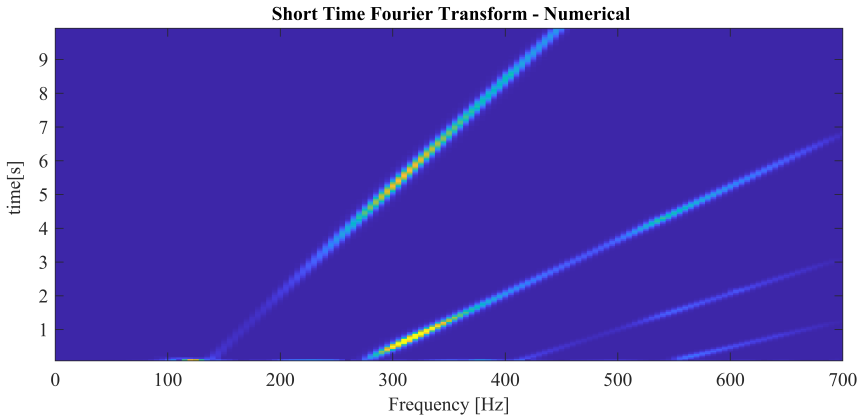

Figure 58: Numerical signal of pumping order trend

Delivery pressure [bar]	Shaft angular speed [RPM]		
100	1200	1600	2200
150	1200	1600	2200
200	1200	1600	2200
250	1200	1600	2200
300	1200	1600	
350	1200	1600	

Table 9: Working condition for the axial piston pump test case

run up test case, steady state experiments are conducted in order to compare the pressure ripple dynamics. The working condition tested within this study are depicted in table 9. The numerical-experimental correlation shown in the following diagrams depicts the pressure signals in angular domain and orders domain both. In addition, a comparison of mean delivery flow rate is depicted. It is worth to underline that the results are normalized in order to accomplish the confidentiality terms. By focusing the attention on figure 59, one may observe the excellent agreement between experiments and numerical results for low value of delivery pressure. As long as the pressure at outlet raises the numerical model tends to overestimate the pressure ripple amplitude. This aspect is not appreciable for different speed regime. In fact, by considering figure 60 and 61 the pressure ripple dynamics is captured by the numerical

model with high fidelity for all the mean pressure value. The reasons behind this scenario has to be found in the fluid resonance modeling. In fact, due to the incertitude on pipe stiffness, the experimental resonance range is not perfectly captured by the numerical model. At a mean rotating speed of 1200 RPM the first harmonic of the pumping frequency is at 180 Hz , while the second one is at 360 Hz. This frequency value falls into the resonance zone of the the system. In fact, by focusing on spectrum diagram in figure 59, it is worth noticing how the second harmonic of the pumping frequency overcome the first one. On the other hand, due to the shape of the frequency response function, the numerical model amplification overcome the real one. This aspect is more evident as long as the delivery pressure raises, as the magnitude of oscillating forces is more severe. In fact for low mean pressure at 1200 RPM a good correspondence is found. By observing figure 60, the numerical outcomes perfectly match the experimental results at each mean delivery pressure value. The frequency excitation at 1600 RPM falls outside the resonance zone, in fact the first and second harmonic can be found at 240 Hz and 480 Hz respectively. In figure 61, results related to 2200 RPM shaft speed are depicted. For this test, the two first harmonics of the excitation frequency are at 330 Hz and 680 Hz. In this case the first harmonic is in a frequency range for which the amplification due to the numeric resonance is consistent with that coming from experimental one.

The numeric results demonstrate the capability of the model to describe the real pressure dynamics of the tested piston pump. The reason why it is not possible to obtain a numerical-experimental matching at all speeds/pressures depends on the modeling of the hydraulic circuit and therefore of the fluid resonance. As stated previously, this task may not be a straightforward matter since the anisotropy which characterize the pipe stiffness represent a challenging aspect on the effective stiffness determination. Figure 62, 63 and 64 show the comparison between the normalized mean flow rate at outlet. For all the condition tested the numerical model provide for a good representation of the pump volumetric efficiency.

A.4 CONCLUDING REMARKS

The present study proposes a lumped parameter approach as a powerful modeling strategy to describe axial piston pump pressure dynamics. Firstly,

the basic working principle of an axial piston pump of swashplate design is explained. Afterwards, the dynamic model is briefly introduced. Finally a numerical-experimental comparison is shown in order to demonstrate the reliability of the numerical analysis. The limit of the modeling strategy is represented by the hydraulic circuit modeling. In fact, when flexible pipes are employed the estimation of their stiffness may lead to an erroneous identification of fluid resonance zone and its wideness. In this regard the harmonic components magnitude changes in relation to the rotational frequency. The components which are affected from major amplification are that whose frequency value is closer to the resonance frequency range. In fact, at 1200 RPM (figure 59) the second harmonic is significantly higher than the first one; on the other hand, at 1600 RPM(fig. 60) their are at most similar; while at 2200 RPM (figure 61) the first harmonic amplitude is clearly dominant over the second one. By testing a volumetric machine, the hydraulic circuit may be free from fluid resonance in the interested frequency range. If not, the resulting pressure dynamics trend may not be linked to the volumetric machine characteristics as it is governed by the resonance amplification.

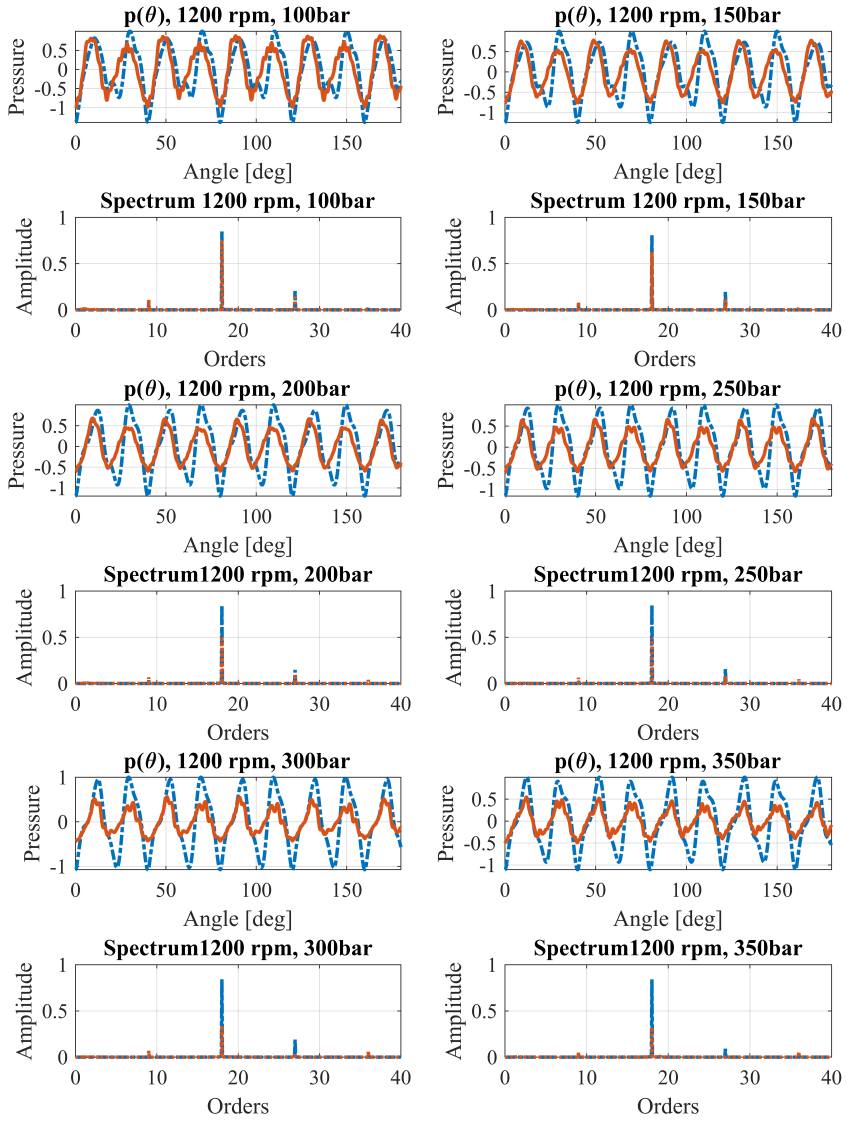

Figure 59: Pressure dynamics at delivery port over half cylinder block rotation. Orange line represents the experimental outcomes while blue dashed line depicts numerical results. The comparison is made for the dimensionless normalized pressure in angular and orders domain.

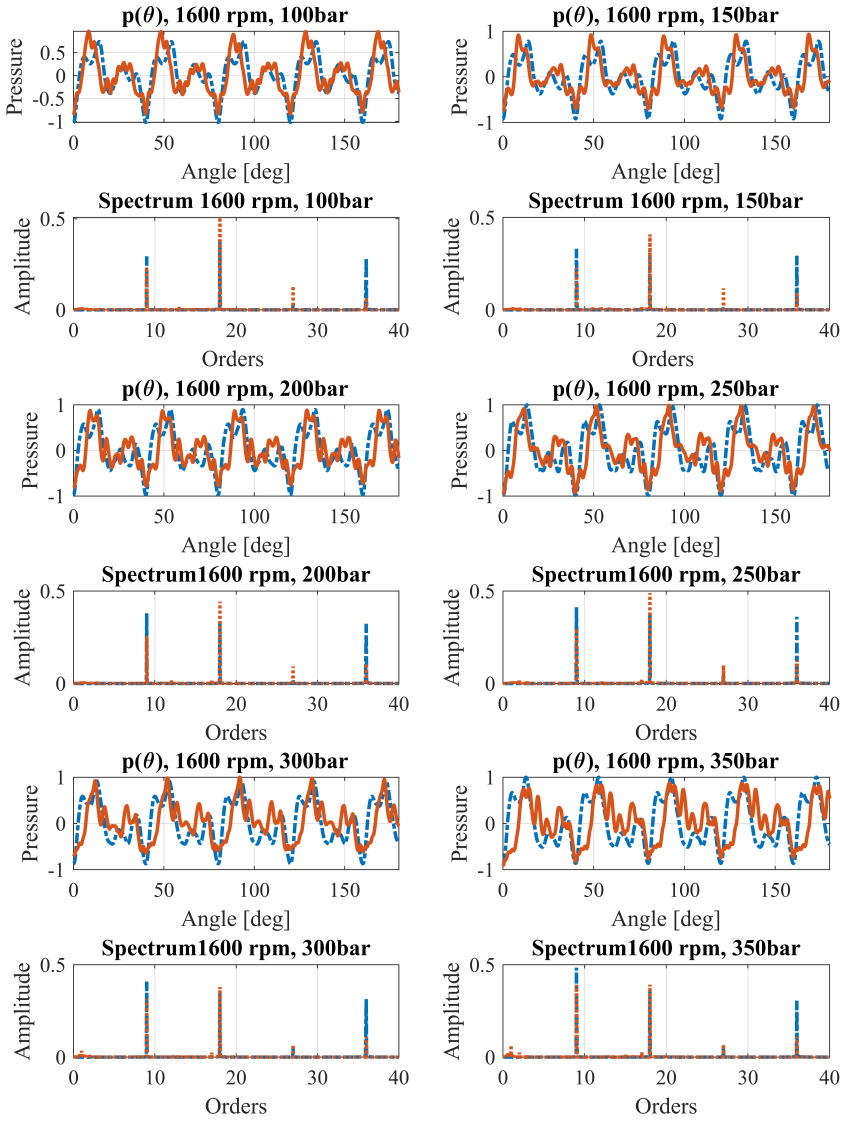

Figure 60: Pressure dynamics at delivery port over half cylinder block rotation. Orange line represents the experimental outcomes while blue dashed line depicts numerical results. The comparison is made for the dimensionless normalized pressure in angular and orders domain.

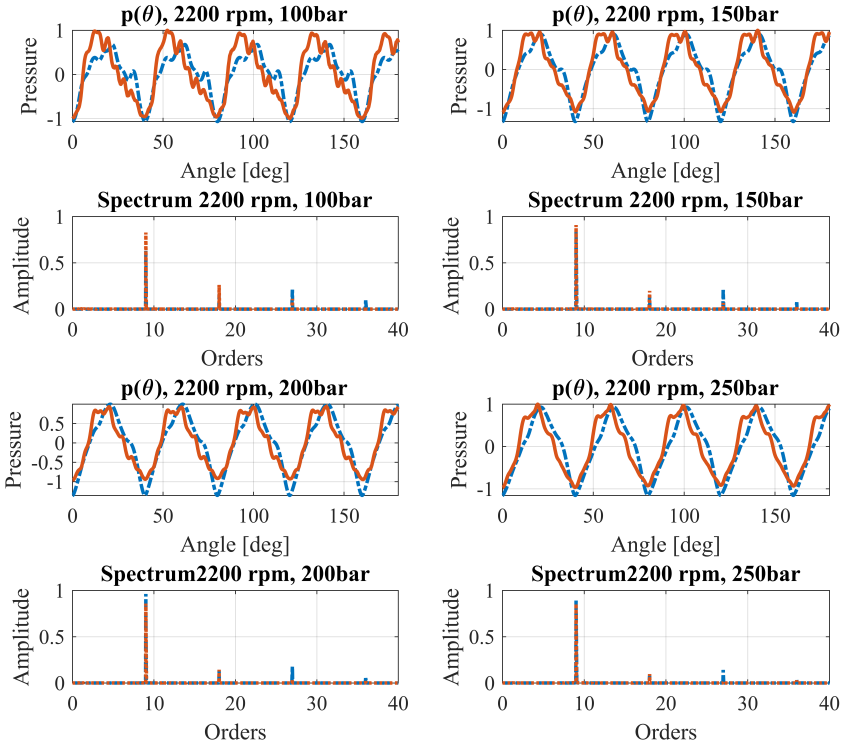

Figure 61: Pressure dynamics at delivery port over half cylinder block rotation. Orange line represents the experimental outcomes while blue dashed line depicts numerical results. The comparison is made for the dimensionless normalized pressure in angular and orders domain.

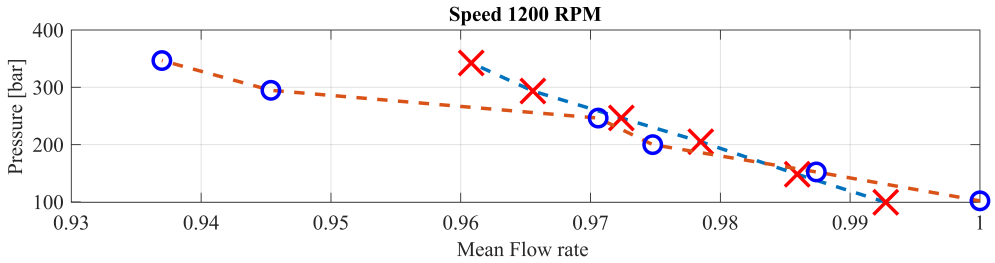

Figure 62: Mean delivery dimensionless normalized flow rate comparison. Orange dashed line represents the experimental outcomes while blue dashed line depicts numerical results.

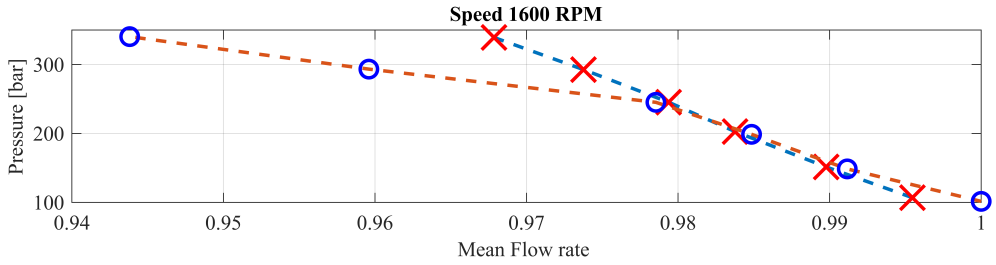

Figure 63: Mean delivery dimensionless normalized flow rate comparison. Orange dashed line represents the experimental outcomes while blue dashed line depicts numerical results.

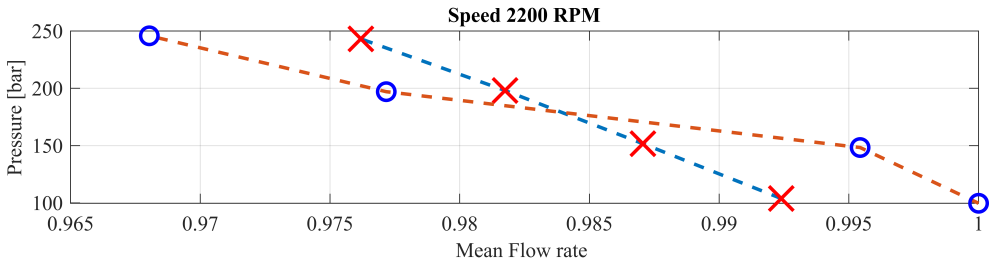

Figure 64: Mean delivery dimensionless normalized flow rate comparison. Orange dashed line represents the experimental outcomes while blue dashed line depicts numerical results.

BIBLIOGRAPHY

[1] A. Gabrielli, F. Pizzolante, E. Soave, M. Battarra, C. Mazzeo, M. Tarabra, E. Fava, and E. Mucchi. "A numerical model for NVH analysis of gearboxes employed on agricultural equipment." In: *Proceedings of ISMA 2020 - International Conference on Noise and Vibration Engineering*. 2020.

[2] Francesco Pizzolante, Mattia Battarra, Gianluca D'Elia, and Emiliano Mucchi. "A rattle index formulation for single and multiple branch geartrains." In: *Mechanism and Machine Theory* 158 (2021).

[3] Francesco Pizzolante, Mattia Battarra, and Emiliano Mucchi. "The role of gear layout and meshing phase for whine noise reduction in ordinary geartrains." In: *Mechanism and Machine Theory* (2022).

[4] Francesco Pizzolante, Mattia Battarra, Emiliano Mucchi, and Bruno Cochelin. "A Taylor series-based continuation method for solution of non linear dynamics of spur gears." In: *Submitted to Mechanical System and Signal Processing* (2022).

[5] J.D. Smith. *Gear Noise and Vibration*. Dekker Mechanical Engineering. Taylor and Francis, 2003. ISBN: 9780203912478. URL: https://books.google.it/books?id=0Y3TAjzoPI8C.

[6] A. Kahraman and R. Singh. "Interactions between time-varying mesh stiffness and clearance non-linearities in a geared system." In: *Journal of Sound and Vibration* 146.1 (1991), pp. 135–156.

[7] HK Kohler, A Pratt, and AM Thompson. "Paper 14: dynamics and noise of parallel-axis gearing." In: *Proceedings of the Institution of Mechanical Engineers, Conference Proceedings*. Vol. 184. 15. SAGE Publications Sage UK: London, England. 1969, pp. 111–121.

[8] Donald R Houser, Fred B Oswald, Mark J Valco, Raymond J Drago, and Joseph W Lenski. *Comparison of transmission error predictions with noise measurements for several spur and helical gears*. AIAA, 1994.

[9] D Palmer and RG Munro. "Measurements of transmission error, vibration and noise in spur gears." In: *British Gear Association Technical Congress*. Vol. 2. 1995.

[10] R. Singh, H. Xie, and R. J. Comparin. "Analysis of automotive neutral gear rattle." In: *Journal of Sound and Vibration* 2.131 (1989), pp. 177–196.

[11] H. Nevzat Özgüven and D. R. Houser. "Mathematical models used in gear dynamics—A review." In: *Journal of Sound and Vibration* 121.3 (1988), pp. 383 –411.

[12] A. Kubo, K. Yamada, T. AIDA, and S. Sato. "Research on ultra high speed gear devices (reports l-3)." In: *Transactions of the Japan Society of Mechanical Engineers* 38 (1972), pp. 2692 –2715.

[13] K. Umezawa, T. Sata, and J. Ishikawa. "Simulation of rotational vibration of spur gears." In: *Bulletin of the Japan Society of Mechanical Engineers* 38 (1984), pp. 102 –109.

[14] F. Kucukay. "Dynamic loads in gear teeth." In: *Proceedings of the Third Conference on Vibrations of Rotating Machinery, Institution of Mechanical Engineers,* 306 (1984), pp. 73–79.

[15] A. Kahraman and R. Singh. "Non-linear dynamics of a spur gear pair." In: *Journal of Sound and Vibration* 142.1 (1990), pp. 49–75.

[16] A. Kahraman and R. Singh. "Non-linear dynamics of a geared rotor-bearing system with multiple clearances." In: *Journal of Sound and Vibration* 144.3 (1991), pp. 469–506.

[17] GW Blankenship and A Kahraman. "Steady state forced response of a mechanical oscillator with combined parametric excitation and clearance type non-linearity." In: *Journal of Sound and Vibration* 185.5 (1995), pp. 743–765.

[18] Ahmet Kahraman and G Wesley Blankenship. "Interactions between commensurate parametric and forcing excitations in a system with clearance." In: *Journal of Sound and Vibration* 194.3 (1996), pp. 317–336.

[19] Ahmet Kahraman and G Wesley Blankenship. "Experiments on nonlinear dynamic behavior of an oscillator with clearance and periodically time-varying parameters." In: (1997).

[20] A Kahraman and GW Blankenship. "Effect of involute tip relief on dynamic response of spur gear pairs." In: (1999).

[21] A Kahraman and GW Blankenship. "Effect of involute contact ratio on spur gear dynamics." In: (1999).

[22] Caterina Natali, Mattia Battarra, Giorgio Dalpiaz, and Emiliano Mucchi. "A critical review on FE-based methods for mesh stiffness estimation in spur gears." In: *Mechanism and Machine Theory* 161 (2021), p. 104319.

[23] JH Kuang and YT Yang. "An estimate of mesh stiffness and load sharing ratio of a spur gear pair." In: *Advancing power transmission into the 21 st century* (1992), pp. 1–9.

[24] Y. Cai and T. Hayashi. "The Linear Approximated Equation of Vibration of a Pair of Spur Gears (Theory and Experiment)." In: *Journal of Mechanical Design* 116.2 (June 1994), pp. 558–564. ISSN: 1050-0472. DOI: 10.1115/1.2919414. eprint: https://asmedigitalcollection.asme.org/mechanicaldesign/article-pdf/116/2/558/5679841/558_1.pdf. URL: https://doi.org/10.1115/1.2919414.

[25] He Dai, Xinhua Long, Feng Chen, and Chao Xun. "An improved analytical model for gear mesh stiffness calculation." In: *Mechanism and Machine Theory* 159 (2021), p. 104262. ISSN: 0094-114X. DOI: https://doi.org/10.1016/j.mechmachtheory.2021.104262. URL: https://www.sciencedirect.com/science/article/pii/S0094114X21000203.

[26] M.H. Arafa and M.M. Megahed. "Evaluation of spur gear mesh compliance using the finite element method." In: *Proceedings of the Institution of Mechanical Engineers, Part C: Journal of Mechanical Engineering* 213.6 (1999). Cited by: 54, 569 – 579. DOI: 10.1243/0954406991522509. URL: https://www.scopus.com/inward/record.uri?eid=2-s2.0-0032721998.

[27] Niels Leergaard Pedersen and Martin Felix JÃ¸rgensen. "On gear tooth stiffness evaluation." In: *Computers & Structures* 135 (2014), pp. 109–117. ISSN: 0045-7949. DOI: https://doi.org/10.1016/j.compstruc.2014.01.023. URL: https://www.sciencedirect.com/science/article/pii/S0045794914000340.

[28] Timo Kiekbusch, Daniel Sappok, Bernd Sauer, and Ian Howard. "Calculation of the Combined Torsional Mesh Stiffness of Spur Gears with Two- and Three-Dimensional Parametrical FE Models." In: *Strojniški vestnik - Journal of Mechanical Engineering* 57.11 (2011), pp. 810–818. ISSN: 0039-2480. DOI: 10.5545/sv-jme.2010.248. URL: https://www.sv-jme.eu/article/calculation-of-the-combined-torsional-mesh-stiffness-of-spur-gears-with-two-and-three-dimensional-parametrical-fe-models/.

[29] Jiaxing Zhan, Mohammad Fard, and Reza Jazar. "A CAD-FEM-QSA integration technique for determining the time-varying meshing stiffness of gear pairs." In: *Measurement* 100 (2017), pp. 139–149. ISSN: 0263-2241. DOI: https://doi.org/10.1016/j.measurement.2016.12.056. URL: https://www.sciencedirect.com/science/article/pii/S0263224116307540.

[30] Christopher G. Cooley, Chunguang Liu, Xiang Dai, and Robert G. Parker. "Gear tooth mesh stiffness: A comparison of calculationÂ approaches." In: *Mechanism and Machine Theory* 105 (2016), pp. 540–553. ISSN: 0094-114X. DOI: https://doi.org/10.1016/j.mechmachtheory.2016.07.021. URL: https://www.sciencedirect.com/science/article/pii/S0094114X16301628.

[31] Sandeep Vijayakar. "A combined surface integral and finite element solution for a three-dimensional contact problem." In: *International journal for numerical methods in engineering* 31.3 (1991), pp. 525–545.

[32] L. Vedmar and B. Henriksson. "A General Approach for Determining Dynamic Forces in Spur Gears." In: *Journal of Mechanical Design* 120.4 (Dec. 1998), pp. 593–598. ISSN: 1050-0472. DOI: 10.1115/1.2829320. eprint: https://asmedigitalcollection.asme.org/mechanicaldesign/article-pdf/120/4/593/5685384/593_1.pdf. URL: https://doi.org/10.1115/1.2829320.

[33] Anette Andersson and Lars Vedmar. "A dynamic model to determine vibrations in involute helical gears." In: *Journal of Sound and Vibration* 260.2 (2003), pp. 195–212.

[34] Lehao Chang, Geng Liu, and Liyan Wu. "A robust model for determining the mesh stiffness of cylindrical gears." In: *Mechanism and Machine Theory* 87 (2015), pp. 93–114. ISSN: 0094-114X. DOI: https://doi.org/10.1016/j.mechmachtheory.2014.11.019. URL: https://www.sciencedirect.com/science/article/pii/S0094114X14003012.

[35] Alberto Gabrielli, Mattia Battarra, and Emiliano Mucchi. "A Critical Analysis of Finite-Element Modeling Procedures for Radial Bearing Stiffness Estimation." In: *Mathematical Problems in Engineering* 2021 (2021).

[36] TLH Walford and BJ Stone. "The measurement of the radial stiffness of rolling element bearings under oscillating conditions." In: *Journal of Mechanical Engineering Science* 22.4 (1980), pp. 175–181.

[37] JJJSG Kraus, JJ Blech, and SG Braun. "In situ determination of rolling bearing stiffness and damping by modal analysis." In: (1987).

[38] AB Jones. "A general theory for elastically constrained ball and radial roller bearings under arbitrary load and speed conditions." In: (1960).

[39] Tedric A Harris and Michael N Kotzalas. *Advanced concepts of bearing technology: rolling bearing analysis*. CRC press, 2006.

[40] MF While. "Rolling element bearing vibration transfer characteristics: effect of stiffness." In: (1979).

[41] Arvid Palmgren. "Ball and roller bearing engineering." In: *Philadelphia: SKF Industries Inc* (1959).

[42] EP Gargiulo. "A simple way to estimate bearing stiffness." In: *Machine design* 52.17 (1980), pp. 107–110.

[43] Hua Zhao. "Analysis of load distributions within solid and hollow roller bearings." In: (1998).

[44] Ludwik Kania. "Modelling of rollers in calculation of slewing bearing with the use of finite elements." In: *Mechanism and machine theory* 41.11 (2006), pp. 1359–1376.

[45] Alain Daidié, Zouhair Chaib, and Antoine Ghosn. "3D simplified finite elements analysis of load and contact angle in a slewing ball bearing." In: (2008).

[46] Marek Krynke, Ludwik Kania, and Eugeniusz Mazanek. "Modelling the contact between the rolling elements and the raceways of bulky slewing bearings." In: *Key Engineering Materials*. Vol. 490. Trans Tech Publ. 2012, pp. 166–178.

[47] Hua Wang, Peiyu He, Bitao Pang, and Xuehai Gao. "A new computational model of large three-row roller slewing bearings using nonlinear springs." In: *Proceedings of the Institution of Mechanical Engineers, Part C: Journal of Mechanical Engineering Science* 231.20 (2017), pp. 3831–3839.

[48] László Molnár, Károly Váradi, Gábor Bódai, Péter Zwierczyk, and László Oroszváry. "Simplified modeling for needle roller bearings to analyze engineering structures by FEM." In: *Periodica Polytechnica Mechanical Engineering* 54.1 (2010), pp. 27–33.

[49] Ruben Lostado, Roberto Fernandez Martinez, and Bryan J Mac Donald. "Determination of the contact stresses in double-row tapered roller bearings using the finite element method, experimental analysis and analytical models." In: *Journal of Mechanical Science and Technology* 29.11 (2015), pp. 4645–4656.

[50] Roberto Fernandez Martinez, Ruben Lostado Lorza, Ana A Santos Delgado, and Nelson O Piedra Pullaguari. "Optimizing presetting attributes by softcomputing techniques to improve tapered roller bearings working conditions." In: *Advances in Engineering Software* 123 (2018), pp. 13–24.

[51] Necdet Demirhan and Bahattin Kanber. "Stress and displacement distributions on cylindrical roller bearing rings using FEM." In: *Mechanics Based Design of Structures and Machines* 36.1 (2008), pp. 86–102.

[52] Xu Hao, Xinxin Gu, Xianwen Zhou, Xin Liao, and Qingkai Han. "Distribution characteristics of stress and displacement of rings of cylindrical roller bearing." In: *Proceedings of the Institution of Mechanical Engineers, Part C: Journal of Mechanical Engineering Science* 233.12 (2019), pp. 4348–4358.

[53] A. Fernandez del Rincon, A. Diez-Ibarbia, M. Iglesias, and F. Viadero. "Gear rattle dynamics: Lubricant force formulation analysis on stationary conditions." In: *Mechanism and Machine Theory* 142 (2019), p. 103581. ISSN: 0094-114X.

[54] S. Theodossiades, O. Tangasawi, and H. Rahnejat. "Gear teeth impacts in hydrodynamic conjunctions promoting idle gear rattle." In: *Journal of Sound and Vibration* 3-5.303 (2007), pp. 632–658.

[55] S. Theodossiades and H. Tangasawi O.and Rahnejat. "Lightly loaded lubricated impacts: idle gear rattle." In: *Journal of Sound and Vibration* 3-5.308 (2007), pp. 418–430.

[56] Renato Brancati, Ernesto Rocca, and Riccardo Russo. "An analysis of the automotive driveline dynamic behaviour focusing on the influence of the oil squeeze effect on the idle rattle phenomenon." In: *Journal of Sound and Vibration* 303.3-5 (2007), pp. 858–872.

[57] Paulo Flores. "Kinematics and dynamics of mechanical systems with lubricated revolute joints: the infinitely-short journal-bearing approach." In: (2007).

[58] Cheon Gill-Jeong. "Analysis of the nonlinear behavior of gear pairs considering hydrodynamic lubrication and sliding friction." In: *Journal of Mechanical Science and Technology* 23.8 (2009), pp. 2125–2137.

[59] Raynald Guilbault, Sébastien Lalonde, and Marc Thomas. "Nonlinear damping calculation in cylindrical gear dynamic modeling." In: *Journal of Sound and Vibration* 331.9 (2012), pp. 2110–2128.

[60] M.P. Koster. *Vibrations of cam mechanisms: consequences of their design*. English. Commerciele uitgave van het proefschrift, 1973, verschenen o.d.t.: Vibrations of cam mechanisms and their consequences on the design. Technische Hogeschool Eindhoven, 1974. ISBN: 0-333-17732-0.

[61] Necdet Demirhan and Bahattin Kanber. "Stress and displacement distributions on cylindrical roller bearing rings using FEM." In: *Mechanics Based Design of Structures and Machines* 36.1 (2008), pp. 86–102.

[62] Marius Băţăuş, AN Maciac, IM Oprean, and Nicolae Vasiliu. "Real time simulation of complex automatic transmission models." In: *Proceedings of" Virtual Powertrain Creation* (2010).

[63] R.G. Parker, S.M. Vijayakar, and T. Imajo. "NON-LINEAR DYNAMIC RESPONSE OF A SPUR GEAR PAIR: MODELLING AND EXPERIMENTAL COMPARISONS." In: *Journal of Sound and Vibration* 237.3 (2000), pp. 435–455.

[64] Sandeep Vijayakar. "A combined surface integral and finite element solution for a three-dimensional contact problem." In: *International Journal for Numerical Methods in Engineering* 31.3 (1991), pp. 525–545.

[65] Tugan Eritenel and Robert G. Parker. "Three-dimensional nonlinear vibration of gear pairs." In: *Journal of Sound and Vibration* 331.15 (2012), pp. 3628–3648.

[66] Chenxin Wang and Robert G. Parker. "Nonlinear dynamics of lumped-parameter planetary gears with general mesh phasing." In: *Journal of Sound and Vibration* 523 (2022), p. 116682.

[67] "Impact of planet mesh phasing on the vibration of three-dimensional planetary/epicyclic gears." In: *Mechanism and Machine Theory* 164 (2021), p. 104422.

[68] Chengzhi Shi and Robert G. Parker. "Vibration mode structure and simplified modelling of cyclically symmetric or rotationally periodic systems." In: *Proceedings of the Royal Society A: Mathematical, Physical and Engineering Sciences* 471.2173 (2015), p. 20140672.

[69] S. Theodossiades and S. Natsiavas. "NON-LINEAR DYNAMICS OF GEAR-PAIR SYSTEMS WITH PERIODIC STIFFNESS AND BACKLASH." In: *Journal of Sound and Vibration* 229.2 (2000), pp. 287–310.

[70] Steven W. Shaw and Richard H. Rand. "The transition to chaos in a simple mechanical system." In: *International Journal of Non-Linear Mechanics* 24.1 (1989), pp. 41–56.

[71] In: *Nonlinear Oscillations*. John Wiley and Sons, Ltd, 1995, pp. I–XIV.

[72] Alexandre Carbonelli, J. Perret-Liaudet, and Emmanuel Rigaud. In: Dec. 2014.

[73] Dongil Shin and Alan Palazzolo. "Nonlinear analysis of a geared rotor system supported by fluid film journal bearings." In: *Journal of Sound and Vibration* 475 (2020), p. 115269.

[74] Sha Wei, Qinkai Han, Xing-Jian Dong, Z.K Peng, and Fulei Chu. "Dynamic response of a single-mesh gear system with periodic mesh stiffness and backlash nonlinearity under uncertainty." In: *Nonlinear Dynamics* 89 (July 2017).

[75] A Al-Shyyab and A Kahraman. "Non-linear dynamic analysis of a multi-mesh gear train using multi-term harmonic balance method: period-one motions." In: *Journal of Sound and Vibration* 284.1-2 (2005), pp. 151–172.

[76] A. Al-shyyab and A. Kahraman. "Non-linear dynamic analysis of a multi-mesh gear train using multi-term harmonic balance method: sub-harmonic motions." In: *Journal of Sound and Vibration* 279.1 (2005), pp. 417–451.

[77] Hilali, Youssef, Braikat, Bouazza, Lahmam, Hassane, and Damil, Noureddine. "An implicit algorithm for the dynamic study of nonlinear vibration of spur gear system with backlash." In: *Mechanics & Industry* 19.3 (2018), p. 310.

[78] Bruno Cochelin, Noureddine Damil, and Michel Potier-Ferry. *Méthode asymptotique numérique*. Methodes numériques. Hermes Lavoissier, 2007, p. 297.

[79] "Effect of gear topology discontinuities on the nonlinear dynamic response of a multi-degree-of-freedom gear train." In: *Journal of Sound and Vibration* 516 (2022), p. 116495.

[80] Rüdiger Seydel. "From Equilibrium to Chaos: Practical Bifurcation and Stability Analysis." In: 1988.

[81] M. Peeters, R. Viguié, G. Sérandour, G. Kerschen, and J.-C. Golinval. "Nonlinear normal modes, Part II: Toward a practical computation using numerical continuation techniques." In: *Mechanical Systems and Signal Processing* 23.1 (2009). Special Issue: Non-linear Structural Dynamics, pp. 195–216.

[82] E. J. Doedel, W. Govaerts, and Yu. A. Kuznetsov. "Computation of Periodic Solution Bifurcations in ODEs Using Bordered Systems." In: *SIAM Journal on Numerical Analysis* 41.2 (2003), pp. 401–435.

[83] F. Fontanela, A. Grolet, L. Salles, and N. Hoffmann. "Computation of quasi-periodic localised vibrations in nonlinear cyclic and symmetric structures using harmonic balance methods." In: *Journal of Sound and Vibration* 438 (2019), pp. 54–65.

[84] B. Zhou, F. Thouverez, and D. Lenoir. "A variable-coefficient harmonic balance method for the prediction of quasi-periodic response in nonlinear systems." In: *Mechanical Systems and Signal Processing* 64-65 (2015), pp. 233–244.

[85] AN Jean and HD Nelson. "Periodic response investigation of large order non-linear rotordynamic systems using collocation." In: *Journal of sound and vibration* 143.3 (1990), pp. 473–489.

[86] N.M. Krylov and N.N. Bogoliubov. *Introduction to Non-linear Mechanics*. Annals of Mathematics Studies. Princeton University Press, 1950.

[87] M. Nakhla and J. Vlach. "A piecewise harmonic balance technique for determination of periodic response of nonlinear systems." In: *IEEE Transactions on Circuits and Systems* 23.2 (1976), pp. 85–91.

[88] ZK Peng, ZQ Lang, SA Billings, and GR Tomlinson. "Comparisons between harmonic balance and nonlinear output frequency response function in nonlinear system analysis." In: *Journal of Sound and Vibration* 311.1-2 (2008), pp. 56–73.

[89] Bruno Cochelin and Christophe Vergez. "A high order purely frequency-based harmonic balance formulation for continuation of periodic solutions." In: *Journal of sound and vibration* 324.1-2 (2009), pp. 243–262.

[90] B. Cochelin. "A path-following technique via an asymptotic-numerical method." In: *Computers and Structures* 53.5 (1994), pp. 1181–1192.

[91] B. Cochelin, N. Damil, and M. Potier-Ferry. "Asymptotic–numerical methods and Pade approximants for non-linear elastic structures." In: *International Journal for Numerical Methods in Engineering* 37.7 (1994), pp. 1187–1213.

[92] Louis Guillot, Bruno Cochelin, and Christophe Vergez. "A generic and efficient Taylor series–based continuation method using a quadratic recast of smooth nonlinear systems." In: *International Journal for Numerical Methods in Engineering* 119.4 (2019), pp. 261–280.

[93] Louis Guillot, Bruno Cochelin, and Christophe Vergez. "A Taylor series-based continuation method for solutions of dynamical systems." In: *Nonlinear Dynamics* (2019).

[94] "Manlab - An interactive path-following and bifurcation analysis software." In: (). URL: http://manlab.lma.cnrs-mrs.fr/.

[95] Mehmet Bozca. "Torsional vibration model based optimization of gearbox geometric design parameters to reduce rattle noise in an automotive transmission." In: *Mechanism and Machine Theory* 45.11 (2010), pp. 1583 –1598. ISSN: 0094-114X.

[96] Emmanuel Rigaud and Joël Perret-Liaudet. "Investigation of gear rattle noise including visualization of vibro-impact regimes." In: *Journal of Sound and Vibration* 467 (2020), p. 115026. ISSN: 0022-460X.

[97] Wen-Bin Shangguan, Xue-Lai Liu, Yuming Yin, and Subhash Rakheja. "Modeling of automotive driveline system for reducing gear rattles." In: *Journal of Sound and Vibration* 416 (2018), pp. 136 –153. ISSN: 0022-460X.

[98] Jong-Yun Yoon and Byeongil Kim. "Gear rattle analysis of a torsional system with multi-staged clutch damper in a manual transmission under the wide open throttle condition." In: *Journal of Mechanical Science and Technology* 30.3 (2016), pp. 1003–1019.

[99] Renato Brancati, Ernesto Rocca, and Riccardo Russo. "Gear rattle reduction in an automotive driveline by the adoption of a flywheel with an innovative torsional vibration damper." In: *Proceedings of the Institution of Mechanical Engineers, Part K: Journal of Multi-body Dynamics* 233.4 (2019), pp. 777–791.

[100] Hugo Miyasato, Vinícius Simionatto, and Milton Dias Junior. "STUDY OF THE GEAR RATTLE PHENOMENA IN AUTOMOTIVE POWERTRAIN SYSTEMS." In: Oct. 2011.

[101] Axel Baumann and Bernd Bertsche. "Experimental study on transmission rattle noise behaviour with particular regard to lubricating oil." In: *Journal of Sound and Vibration* 341 (2015), pp. 195–205.

[102] A. Diez-Ibarbia, A. Fernandez del Rincon, P. Garcia, and F. Viadero. "Gear rattle dynamics under non-stationary conditions: The lubricant role." In: *Mechanism and Machine Theory* 151 (2020), p. 103929. ISSN: 0094-114X.

[103] Peter Fietkau and Bernd Bertsche. "Influence of tribological and geometrical parameters on lubrication conditions and noise of gear transmissions." In: *Mechanism and Machine Theory* 69 (2013), pp. 303 –320. ISSN: 0094-114X.

[104] A. A. Rust, F.K. Brandl, and G. E. Thien. "Investigations into gear rattle phenomena-key parameters and their influence on gearbox noise." In: *Proc. of IMechE Conference on Gearbox Noise and Vibration* (1990), pp. 113 –120.

[105] Chandramouli Padmanabhan, Todd E. Rook, and Rajendra Singh. "Modeling of Automotive Gear Rattle Phenomenon: State of the Art." In: *SAE Technical Paper*. SAE International, May 1995.

[106] *An Analytical Investigation of Rattle Characteristics of Powder Metal Gears*. Vol. Volume 10: 2019 International Power Transmission and Gearing Conference. International Design Engineering Technical Conferences and Computers and Information in Engineering Conference. Aug. 2019.

[107] Z. G. Chen, Y. M. Shao, and T. C. Lim. "Non-linear dynamic simulation of gear response under the idling condition." In: *International Journal of Automotive Technology* 13.4 (2012), pp. 541–552.

[108] Riccardo Russo, Renato Brancati, and Ernesto Rocca. "Experimental investigations about the influence of oil lubricant between teeth on the gear rattle phenomenon." In: *Journal of Sound and Vibration* 321.3 (2009), pp. 647 –661. ISSN: 0022-460X.

[109] Y. Guo, T. Eritenel, T.M. Ericson, and R.G. Parker. "Vibration and acoustic characterization of a gearbox system with spur gears, shafts, bearings, and a compliant housing." In: *Proceedings of ISMA 2014 - International Conference on Noise and Vibration Engineering and USD 2014 - International Conference on Uncertainty in Structural Dynamics*. 2014.

[110] Harry Walker et al. "Gear tooth deflection and profile modification." In: *Engineer* 166 (1938), pp. 409–412.

[111] Stephen L. Harris. "Dynamic Loads on the Teeth of Spur Gears." In: *Proceedings of the Institution of Mechanical Engineers* 172.1 (1958), pp. 87–112.

[112] Faydor L. Litvin and Alfonso Fuentes. *Gear Geometry and Applied Theory*. 2nd ed. Cambridge University Press, 2004. DOI: 10.1017/CBO9780511547126.

[113] Zaigang Chen and Yimin Shao. "Mesh stiffness calculation of a spur gear pair with tooth profile modification and tooth root crack." In: *Mechanism and Machine Theory* 62 (2013), pp. 63–74.

[114] Hui Ma, Xu Pang, Ranjiao Feng, and Bangchun Wen. "Evaluation of optimum profile modification curves of profile shifted spur gears based on vibration responses." In: *Mechanical Systems and Signal Processing* 70-71 (2016), pp. 1131–1149.

[115] Jorg Borner and Donald R. Houser. "Friction and Bending Moments as Gear Noise Excitations." In: *International Off-Highway and Powerplant Congress and Exposition*. SAE International, 1996.

[116] Menglei Sun, Chihua Lu, Zhien Liu, Yi Sun, Hao Chen, and Cunrui Shen. *Classifying, Predicting, and Reducing Strategies of the Mesh Excitations of Gear Whine Noise: A Survey*. 2020.

[117] Philippe Velex and Violaine Cahouet. "Experimental and numerical investigations on the influence of tooth friction in spur and helical gear dynamics." In: *J. Mech. Des.* 122.4 (2000), pp. 515–522.

[118] Donald R Houser, Manish Vaishya, and Jim D Sorenson. *Vibro-acoustic effects of friction in gears: an experimental investigation*. Tech. rep. SAE Technical Paper, 2001.

[119] M Vaishya and R Singh. "Analysis of periodically varying gear mesh systems with Coulomb friction using Floquet theory." In: *Journal of sound and vibration* 243.3 (2001), pp. 525–545.

[120] Manish Vaishya and Rajendra Singh. "Sliding friction-induced non-linearity and parametric effects in gear dynamics." In: *Journal of sound and vibration* 248.4 (2001), pp. 671–694.

[121] Ronald G Schlegel and Kenneth C Mard. "Transmission noise control-approaches in helicopter design." In: *Mechanical Engineering*. Vol. 89. 8. ASME-AMER SOC MECHANICAL ENG 345 E 47TH ST, NEW YORK, NY 10017. 1967, p. 55.

[122] DL Seager. "Conditions for the Neutralization of Excitation by the Teeth in Epicyclic Gearing." In: *Journal of Mechanical Engineering Science* 17.5 (1975), pp. 293–299.

[123] ROBERT G. PARKER. "A PHYSICAL EXPLANATION FOR THE EFFECTIVENESS OF PLANET PHASING TO SUPPRESS PLANETARY GEAR VIBRATION." In: *Journal of Sound and Vibration* 236.4 (2000), pp. 561–573.

[124] R. G. Parker and J. Lin. "Mesh Phasing Relationships in Planetary and Epicyclic Gears." In: *Journal of Mechanical Design* 126.2 (May 2004), pp. 365–370.

[125] Sripathi Vangipuram Canchi and Robert G Parker. "Vibration Resonances in a Planetary Gear Ring: Effects of Mesh Phasing and Contact Ratio." In: *International Design Engineering Technical Conferences and Computers and Information in Engineering Conference*. Vol. 48086. 2007, pp. 505–510.

[126] Yichao Guo and Robert G Parker. "Analytical determination of mesh phase relations in general compound planetary gears." In: *Mechanism and Machine Theory* 46.12 (2011), pp. 1869–1887.

[127] J. Sanchez-Espiga, A. Fernandez-del Rincon, M. Iglesias, and F. Viadero. "Influence of the phase in planetary gears load sharing and transmission error." In: *Advances in Mechanism and Machine Science*. Ed. by Tadeusz Uhl. 2019, pp. 1059–1067.

[128] Javier Sanchez-Espiga, Alfonso Fernandez-del Rincon, M Iglesias, and F Viadero. "Influence of errors in planetary transmissions load sharing under different mesh phasing." In: *Mechanism and Machine Theory* 153 (2020), p. 104012.

[129] Javier Sanchez-Espiga, Alfonso Fernandez-del Rincon, M Iglesias, and F Viadero. "Planetary gear transmissions load sharing measurement from tooth root strains: Numerical evaluation of mesh phasing influence." In: *Mechanism and Machine Theory* 163 (2021), p. 104370.

[130] V. Kartik and Donald Houser. "Analytical Predictions for the Transmission Error Excitation in Various Multiple-Mesh Gear-Trains." In: vol. 4. Jan. 2003.

[131] Gang Liu and Robert Parker. "Nonlinear dynamics of idler gear systems." In: *Nonlinear Dynamics* 53 (Sept. 2008), pp. 345–367.

[132] Robert White and Pravin Patil. "Phase Management as a Strategy to Reduce Gear Whine in Idler Gear Sets." In: (2020).

[133] Bjorn Ole Helgestad. "An Investigation of Noise Emission from an Axial Piston Hydralic Pump." PhD thesis. University of Birmingham, 1967.

[134] KA Edge and J Darling. "Cylinder pressure transients in oil hydraulic pumps with sliding plate valves." In: *Proceedings of the Institution of Mechanical Engineers, Part B: Management and engineering manufacture* 200.1 (1986), pp. 45–54.

[135] Jaroslav Ivantysyn and Monika Ivantysynova. *Hydrostatische Pumpen und Motoren: Konstruktion und Berechnung*. Vogel, 1993.

[136] Jaroslav Ivantysyn and Monika Ivantysynova. *Hydrostatic pumps and motors: principles, design, performance, modelling, analysis, control and testing*. Tech Books International, 2003.

[137] Raymond Charles Binder. *Advanced fluid mechanics*. Vol. 2. Prentice-Hall, 1958.